HEMOGLOBIN OXYGENATION OF A TWO-LAYER TISSUE-SIMULATING PHANTOM FROM TIME-RESOLVED REFLECTANCE

By

ROBERT HUNTER, B.SC., M.SC.

A Thesis
Submitted to the School of Graduate Studies
in Partial Fulfillment of the Requirements
for the Degree
Doctor of Philosophy

McMaster University

HEMOGLOBIN OXYGENATION OF TWO-LAYER PHANTOMS

DOCTOR OF PHILOSOPHY (2001)
(Physics)

MCMASTER UNIVERSITY
Hamilton, Ontario

TITLE: Hemoglobin Oxygenation Of A Two-Layer Tissue-Simulating Phantom From Time Resolved Reflectance

AUTHOR: Robert Hunter, B.Sc. Hon., M.Sc. (McMaster University, Canada)

SUPERVISOR: Dr. Michael S. Patterson

NUMBER OF PAGES: xii, 122

ABSTRACT

A dual wavelength time-resolved reflectance system was developed for monitoring hemoglobin saturation noninvasively. The ability of the system to determine the optical properties of tissue-simulating phantoms was examined. To quantify the accuracy of the technique in monitoring hemoglobin saturation, measurements were performed in a homogeneous phantom containing human erythrocytes in a scattering solution. The hemoglobin saturation of this phantom could be controlled and monitored with an alternate technique. After system validation in this simple model, a more realistic, two-layer phantom model was investigated. The top layer was chosen to simulate either skin or fat and the oxygenation of the bottom layer, which corresponded to muscle, was controlled. The thickness of the fat layer was varied from 1.5 to 10 mm to investigate the effects of increasing the top layer thickness. Time-resolved measurements of reflectance, performed through the top layer were analyzed with a simple homogeneous diffusion model to quantify the hemoglobin saturation of the bottom layer. These data were compared with simultaneous measurements of oxygenation made directly in the bottom layer. Errors in estimating hemoglobin saturation with this method ranged from 5 –11% depending on top layer thickness. Preliminary *in vivo* measurements were also undertaken which demonstrated promising results, although no comparative technique was used in these studies.

ACKNOWLEDGEMENTS

I am especially grateful to Dr. Michael Patterson for sharing his insight and providing encouragement and direction for this project over the years. I would also like to thank Dr. Tom Farrell for his extensive help with this thesis. Thanks also go to Dr. William Prestwich and Dr. Brian Pogue for their input. I also wish to express my thanks to Dr. Joe Hayward and Kevin Diamond for their assistance and general knowledge around the lab. I wish to acknowledge the machine shop and electronics shop for their help in the project. In addition, I am thankful to the many students for their contributions to this thesis. I am also indebted to Jon Dysart, my volunteer for the *in vivo* measurements. Finally, I would like to thank Julie and my family for their continued support over the years.

TABLE OF CONTENTS

LIST OF FIGURES

LIST OF TABLES

1 INTRODUCTION

1.1 Motivation

The use of light as a diagnostic tool has increased in recent years, due to a trend towards noninvasive techniques in medicine. The measurement of tissue optical properties can provide information regarding the physiological status of tissue. For example, the scattering properties of tissue may be useful in studying glucose concentration in tissue (Bruulsema *et al.* 1997). Measurement of absorption can provide information regarding exogenous chromophores, such as photosensitizing, or chemotherapeutic drugs or endogenous chromophores, such as hemoglobin. The study of tissue oxygenation through the monitoring of hemoglobin absorption is an important area of bio-optics research, as indicated by the large number of conference proceedings on the subject (*Optical Tomography and Spectroscopy of Tissue IV,* SPIE Proceedings, 2001, Vol. 4520 and *Advances in Optical Imaging and Photon Migration*, TOPS Conference Proceedings, 1998, Vol. 21).

Near infrared (NIR) light penetrates well into tissue, has no deleterious biological effect at low intensity and measurements can be performed rapidly, making it an excellent candidate as a monitoring tool. Quantification of hemoglobin concentration can be obtained through estimates of tissue absorption combined with a knowledge of the absorption spectra of oxy- and deoxyhemoglobin. Such oxygenation studies have been performed in the brain (Isobe *et al.* 2000 and Toronov *et al.* 2001), muscles in the extremities (Casavola *et al.* 2000 and Hicks *et al.* 1999) and in tumor tissue (Hull *et al.* 1999 and Liu *et al.* 2000). It is believed that low oxygen levels in the blood or poor cerebral blood flow may lead to brain damage in neonatal infants (Cope 1991). For patients with poor circulation in the extremities, such as those with peripheral vascular disease, complications range from a dull ache in the legs to gangrene; diagnosis of this condition may be improved through the use of NIR oxygenation measurements. Oxygen also plays an important role in the treatment of tumors with photodynamic therapy and with conventional radiotherapy. In photodynamic therapy, singlet oxygen ($^1O_2$) is thought to be the main cytotoxic species (Henderson and Dougherty 1992) and therefore, oxygen must be present for a successful treatment. It is well known that the effectiveness of radiation therapy depends upon the oxygen concentration in the treatment volume (Hall 1988). A method to monitor oxygenation in the tissue treated would be beneficial. These are three fields where a noninvasive technique for monitoring tissue oxygenation would prove useful.

1.2 Light propagation models

In order for light to be used as an effective diagnostic tool, it is important to understand light propagation in tissue. The problem of light transport is complicated by the fact that tissue is a highly scattering medium at optical wavelengths. Light transport has been modeled using Monte Carlo techniques, random walk models and diffusion theory. The diffusion theory is an approximation of the radiative transport equation, assuming an isotropic source term and a radiance that is almost isotropic. In these approaches photons are considered neutral particles whose only interactions are absorption and elastic scattering (Duderstadt and Hamilton 1976). Tissue is characterized by an absorption coefficient μ_a and a scattering coefficient μ_s, where this value represents the probability per unit pathlength of that interaction occurring. A "phase function" is also necessary to describe the angular dependence of scatter. The first moment of this distribution, the anisotropy parameter, g, is the mean cosine of the scattering angle and is usually sufficient to characterize the angular dependence of the scattering. Since different combinations of μ_s and g will produce similar light distributions, they are typically combined into one parameter, the reduced scattering coefficient μ_s', where $\mu_s' = (1-g)\mu_s$. Scattering in tissue is probably due to cells or large organelles and since these structures are comparable in size to the wavelength of light, the type of scattering is known as Mie scattering. A third parameter to characterize light transport in tissue is the index of refraction which determines the speed of light in the medium and is approximately 1.4 for tissue in the near infrared region.

Absorption of light in the near infrared region is dominated by specific chromophores, such as melanin, myoglobin, water and, most importantly, hemoglobin. The total absorption is assumed to be the sum of the absorption from each chromophore present. For most oxygenation experiments, it is assumed that the major chromophore that contributes to absorption is hemoglobin. By exploiting the differences in the absorption of oxyhemoglobin and deoxyhemoglobin at different wavelengths it is possible to determine the concentration of each molecular species. This, in turn, is indicative of the oxygenation of the tissue being investigated. The oxygenation is characterized by the hemoglobin saturation, SO_2 which is defined by:

$$SO_2 = \frac{[HbO_2]}{[HbO_2]+[Hb]} \tag{1}$$

where $[HbO_2]$ and [Hb] are the concentrations of oxyhemoglobin and deoxyhemoglobin, respectively. For tissue, the absorption coefficient in the wavelength range of interest (600 to 900 nm) varies from 0.01 to 0.05 mm^{-1} and the reduced scattering coefficient varies from 0.5 to 7 mm^{-1} (Cheong *et al.* 1990).

Although the Monte Carlo method is the most powerful and general technique for modeling light transport, its high computational expense limits its applicability. Diffusion theory solutions have been obtained for the reflectance from homogeneous and semi-infinite turbid media in the steady-state, frequency and time domains (Farrell *et al.* 1992, Patterson *et al.* 1991 and Patterson *et al.* 1989). Steady-state methods involve a continuous wave (cw) light source and measurement of the reflectance at multiple distances. Frequency domain measurements utilize an intensity modulated light source and examine changes in phase and amplitude of the light at single or multiple source-detector separations. Time domain techniques use a pulsed light source and the reflectance at one distance, measured as a function of time. All three approaches can provide estimates of the optical properties of the tissue being sampled through minimization of the differences between the forward diffusion theory solution and the observed reflectance. Each method has been used for *in vivo* tissue oxygenation measurements (Cubeddu *et al.* 1999, Liu *et al.* 1995a and Pogue *et al.* 1998 and 2000).

1.3 Time-resolved measurements

Time-resolved measurements have two main advantages over other modalities; they do not require an absolute reflectance measurement, nor do they need measurements at multiple distances to estimate μ_a and μ_s'. These methods use a short pulse of light, on the order of picoseconds, which is incident on the medium in a pencil beam geometry. The observed quantity, the diffuse reflectance, is collected at a specific source detector separation (ρ) as a function of time. Within the medium, the pulse undergoes multiple scattering events which broaden the pulse in the time domain, and absorption events which attenuate the pulse. A schematic picture of the time domain technique is presented in Figure 1.1. Since the pathlength is short for early times, absorption will have less influence on the collected signal when $\mu_a << \mu_s'$. These early arriving photons will have undergone few scattering events and will have penetrated only a few millimeters in the tissue. At later times, the light is highly diffuse and absorption will have the principle influence on pulse shape. These late-arriving photons will have penetrated deeper into the tissue, up to 10 mm or more, and will carry information primarily from deeper lying tissues. This is illustrated in Figure 1.2. The paths of three photons are shown, they have pathlengths d_1,d_2 and d_3 respectively where $d_1 < d_2 < d_3$. The photon that follows d_1 has undergone few scattering events and therefore has a shorter pathlength than the photon that follows d_2 or d_3. This photon will also reach the detector before the other photons; its time of flight will be d_1/c where c is the speed of light in the tissue. The other photons have traveled farther, have penetrated deeper into the tissue and arrive at times proportional to their pathlengths (d_2/c and d_3/c). A histogram of photon times-of-flight is thus constructed. The diffuse reflectance, i.e. this time histogram, can then be fit with a time dependent diffusion model and the differences between the predicted pulse shape and the observed data minimized by varying μ_a and μ_s'.

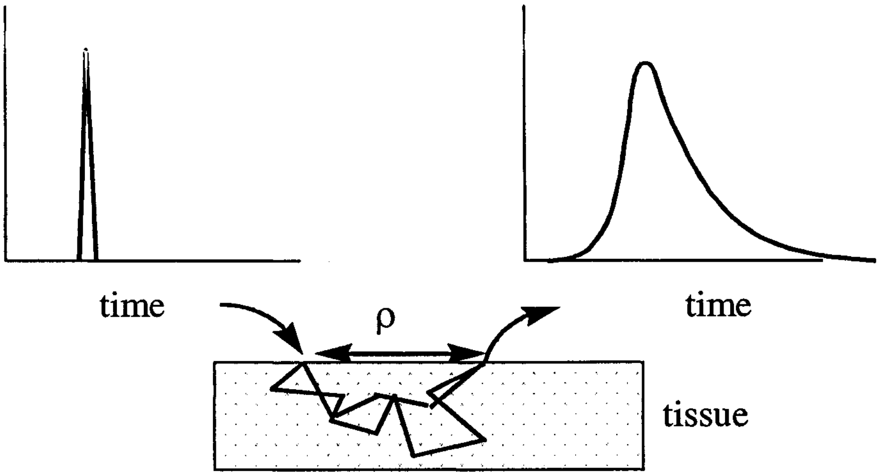

Figure 1.1: A pictorial representation of the time domain measurement system. A narrow pulse of light is broadened due to scattering and attenuated, due to absorption, as it travels through a turbid medium.

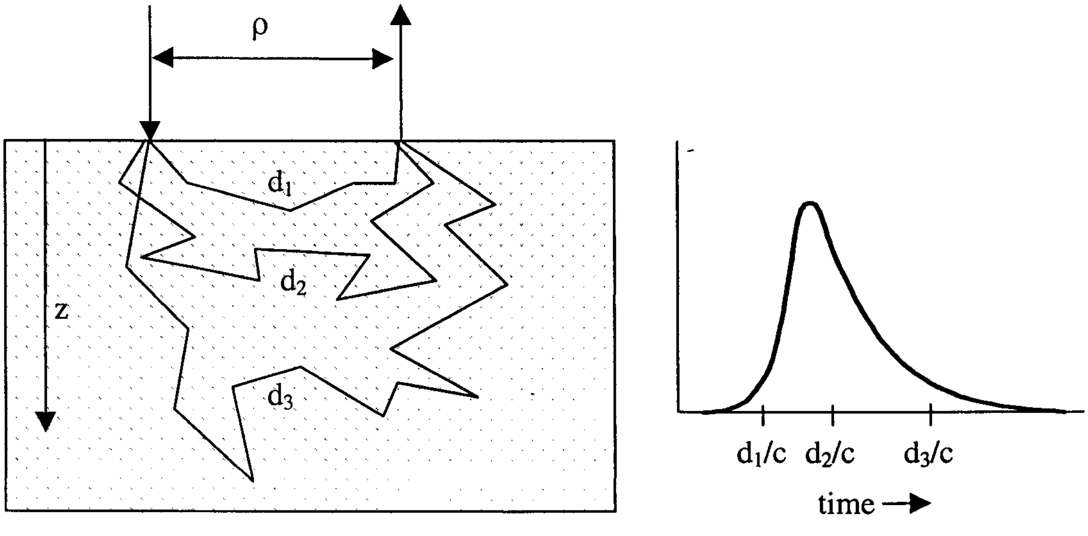

Figure 1.2: Schematic representation of the relationship between photon pathlength, penetration depth and time of flight through a turbid sample.

The technology for time domain measurements became readily available in the 1980's with the advent of picosecond light sources and fast photodetectors, such as microchannel plate photomultiplier tubes (MCP-PMT). Early oxygenation experiments using this technology were performed by Chance *et al.* (1988) and Delpy *et al.* (1988). A simple diffusion model that showed good agreement with the results was proposed by Patterson *et al.* (1989). Since then, more accurate models have been developed to take into account reflections at mismatched boundaries (Haskell *et al.* 1994 and Kienle and Patterson 1997).

The main disadvantage of time-resolved techniques compared to others is the complexity and expense of the equipment needed. Pulsed lasers and MCP-PMTs are costly and better suited to a lab environment than a clinic. Technology improvements are beginning to solve this problem. The main advantages of the time-resolved measurement technique over other methods include: (a) the ability to extract absorption information at a small ρ value, as would be used in an endoscope (Jacques and Flock 1991). (b) since time of flight determines penetration depth, this can be controlled by varying the detection time window (c) the measurements are less affected by boundary conditions than steady state measurements and (d) since single photon counting is used, they are excellent techniques when light levels are low, as is the case for measurements in tissue. The particular advantage that is to be exploited in this thesis is (b), the ability to control penetration depth. Since tissue is a complicated structure, the ability to localize the collected signal is essential if physiological information about the tissue is to be useful.

1.4 Layered tissue structure

Most of the models used to describe light transport assume that the medium is homogeneous. For investigations of tissue oxygenation, the models used are typically diffusion based or rely upon a modified Beer-Lambert law where the effective pathlength is modified to account for scattering effects. This is accomplished by the use of a differential pathlength factor (DPF) which assumes that absorption changes are small and homogeneously distributed (Delpy *et al.* 1988). A major assumption of these models is that tissue is homogeneous, while it is well known that tissue is very heterogeneous. Many areas of the body, such as the head, have a layered architecture to a first approximation. Results obtained from a homogeneous model applied to these situations must be interpreted with caution (Farrell *et al.* 1998). Alternatively, one must implement a new model that accounts for the structure of tissue.

If a homogeneous model is used to analyze results obtained from a tissue measurement, the optical properties returned may not be accurate. They could be representative of either of the layers present, or an average of the two layers, or not representative of either layer. This will depend on the source-detector separation used, the measurement method, the thickness of the top layer and the optical properties of the layers. Using source-detector separations in the range 1.5-4.5 cm, Franceschini *et al.* (1998) determined that when the top layer was less than 0.4 cm thick, the optical properties returned from a homogeneous model were similar to those of the bottom layer. For a top layer thicker than 1.3 cm, the model returned properties representative of the top layer. They used a frequency domain measurement system with a wavelength of 750 nm and gelatin layered phantoms with 100 different sets of optical properties to obtain these results.

To overcome the difficulties associated with using a homogeneous model to analyze data from a layered sample, much effort has been put into developing new models. A two-layer diffusion theory model has been developed (Kienle *et al.* 1998) and random walk and Monte Carlo methods have been used (Hielscher *et al.* 1996 and Nossal *et al.* 1988). Monte Carlo methods, although accurate and general, have a high computational expense which limits their applicability in a clinical setting (Kienle and Hibst 1995). The two-layer diffusion model has met with some success, but it is generally necessary to have knowledge of the top layer thickness *a priori* (Kienle and Glanzmann 1999). A hybrid Monte Carlo-diffusion theory approach has also been employed by Alexandrakis *et al.* (2000) to combine the speed of the diffusion calculations and the increased accuracy of Monte Carlo methods at distances close to the source. Researchers have also used a simple empirical correction curve to account for overlying fat layers (Niwayama *et al.* 2000). The curve relates reflected intensity to optical properties, source-detector separation and a constant proportional to the fat layer thickness. It was determined from experiments and simulations.

Steinbrick *et al.* (2001) developed a technique to determine absorption changes from the distribution of times of flight of photons. They extended the concept of the mean partial pathlength, the average pathlength of photons in the layer under consideration, to the time domain. The time-dependent mean partial pathlength expresses the sensitivity of the measured time-resolved reflectance to absorption changes in that layer. They used their model, along with a single distance time domain method, to determine absorption changes successfully with depth resolution in a layered phantom. This method also showed promising *in vivo* results.

Under many conditions, it may not be necessary to have a model that accurately recovers five parameters (top and bottom layer absorption and reduced scattering and top layer thickness). In many clinical applications, the physiological status of only the bottom layer of tissue is of interest. This would be true for measurements of muscle oxygenation, where the top layer is skin and/or fat and the bottom layer is muscle, or for studies of tumor oxygenation where a subcutaneous tumor is the region of interest. As previously mentioned, late arriving photons provide more information about deeper layers since those photons have penetrated further into the tissue. Furthermore, the later portion of the time-resolved reflectance is more dependent on absorption and so, by examining this region of the curve it may be possible to obtain information about the bottom layer absorption, which can be used to determine bottom layer oxygenation. Also, by increasing the source-detector separation a greater fraction of photons that have penetrated into the bottom layer will contribute to the signal. This is suggested by the work of Farrell *et al.* (1998) who showed that it might be possible to determine the bottom layer absorption coefficient in a two-layer system if a suitable source-detector separation is used. At a source-detector separation of 20 mm, the homogeneous diffusion model recovered an absorption only 9% different from the true bottom layer absorption input to a Monte Carlo simulation of skin (thickness of 1.5 mm) on a semi-infinite fat layer. The goal of this research is to further investigate this problem and examine the limitations of using a homogeneous diffusion theory model to analyze data from a layered medium.

1.5 Clinical applications

Monitoring tissue oxygenation with NIR light was pioneered by Jobsis (1977). Although experimental research in the field of near infrared spectroscopy (NIRS) is still proceeding in areas such as devices (Fantini *et al.* 1995 and Yang *et al.* 1997), effect of layers (Kienle and Glanzmann 1999 and Pham *et al.* 2000) and correlation with other techniques (Conover *et al.* 2000, Ntziachristos *et al.* 1998 and Hull *et al.* 1998), many clinical studies have also been performed. Application of NIRS to four general areas will be briefly discussed: cerebral monitoring, peripheral vascular disease, muscle and tumor oxygenation.

Much of the clinical research using NIRS has involved cerebral oxygenation studies, especially in neonatal or young infants. Light penetrates well into the gray matter of the brain in both adults and neonates (Chance *et al.* 1998). The very thin soft tissue and bone of the neonate head allow for excellent penetration, and neurological injuries that occur in newborns often involve problems with cerebral perfusion and oxygen delivery. Furthermore, the portability of NIRS devices allows for the use of the instrument in the operating room or at the bedside without patient immobilization. Studies have shown the ability of NIRS to detect changes in fetal cerebral perfusion and oxygenation during labour by transvaginal placement of optodes on the fetal head

(Peebles *et al.* 1994, Aldrich *et al.* 1994 and 1996). This may prove to be clinically feasible to detect hypoxia or ischemia during high risk deliveries. Studies in preterm and term infants measured cerebral blood volume (CBV) and cerebral blood flow (CBF). This information may be useful in the management of apneic events or during endotracheal suctioning (Mosca *et al.* 1997). Infants with hydrocephalus have been monitored with NIRS and have been shown to have increased CBV, oxyhemoglobin and cytochrome aa_3 (du Plessis *et al.* 1995). Research on the oxygenation changes in the newborn immediately following birth has been performed on normal neonates and those with complications and has demonstrated differences in cerebral oxygenation between the two groups (Isobe *et al.* 2000). In the future, NIRS may prove to be an important tool to study the effects of asphyxia and subsequent interventions involving preterm and term infants.

NIRS is also used to study adult brain function. The detection of cranial hematomas, up to a depth of 3-4 cm, with NIRS has been verified by x-ray CT (Robertson *et al.* 1997). Levy *et al.* (1995) used NIRS to study cerebral oxygenation, specifically to detect ischemia during ventricular fibrillation, and compared the results with an electroencephalogram. More recently, due to decreased acquisition times and better signal localization, NIRS has been used to investigate brain activity. Studies involving motor (Toronov *et al.* 2001, Hirth *et al.* 1997 and Obrig *et al.* 1997) and visual (Villringer and Chance 1997 and Meek *et al.* 1998) stimulations confirmed by positron emission tomography (Deiber *et al.* 1991) and functional magnetic resonance imaging (Chance *et al.* 1998) showed significant responses, i.e. increased absorption from blood, at the activated brain area. The latest results, for example Toronov *et al.* (2001), provide spatial maps of oxy- and deoxyhemoglobin concentrations with an acquisition time of 160 ms per map. This safe, portable and affordable method is developing into a useful instrument for the study of cerebral hemodynamics in diseased brain tissue and during applied stimuli.

Peripheral vascular disease is a progressive occlusive disease of the arteries that supply the extremities. It not only has direct effects on health and function but is associated with increased incidence of cardiovascular disease. Detection of peripheral vascular disease (PVD) is another potential application of NIRS since traditional methods of detecting PVD, such as pain assessment, grading ankle pulses and measurement of arm-ankle systolic pressure, have poor sensitivity in the case of mild disease (McCully *et al.* 1997). NIRS provides a non-invasive, real-time, inexpensive and portable technique for monitoring tissue oxygenation to detect PVD and the results of intervention. Recovery of oxygen saturation following oxygen challenge has been shown to be slower in patients with PVD (McCully *et al.* 1994 and Cheatle *et al.* 1991) and this can be exploited through the use of different protocols (exercise, venous occlusion and tilting table) to differentiate between healthy and diseased individuals (Casavola *et al.* 1999a and McCully *et al.* 1994). A review of the success of PVD detection using NIRS was performed by McCully *et al.* (1997) and he found that NIRS was successful in 77% of patients with most failures occurring in obese patients. There was also reasonable agreement between NIRS measurements and clinical assessment and a relationship between the measurement and risk factors for cardiovascular disease.

Monitoring oxygenation in muscle may aid in the detection of PVD, but can also be used to study blood flow and oxygen consumption in the arm or leg of healthy individuals to investigate muscle physiology during and after exercise. Initial studies (Chance *et al.* 1988, Ferrari *et al.* 1991 and 1992) demonstrated the feasibility of this approach and since then, researchers in the field of sports medicine have used the technique to study oxygen availability and utilization in muscle (McCully and Hamaoka 2000, De Blasi *et al.* 1997, Boushel and Piantadosi 2000 and Hicks *et al.* 1999). Szmedra *et al.* (2001) used NIRS to study the effect of posture during alpine skiing on muscle blood volume and oxygen desaturation. Although results have been promising with studies involving exercise (Hicks *et al.* 1999), tilting table protocol (Casavola 1999b) and venous occlusion (Casavola 2000), it has been noted that results from this method must be interpreted with caution (McCully and Hamaoka 2000 and Boushel and Piantadosi 2000).

Another potential clinical application of NIRS is the study of tumor hypoxia. It is well known that hypoxic tumors are more radio-resistant than normal tissue (Gray *et al.* 1953) and although there are many studies using other techniques, the benefits of NIRS in this field have yet to be realized. A murine model was used to study tumor oxygenation changes during respiratory challenges which may provide insight into tumor vascular development and hence have prognostic value in the future (Liu *et al.* 2000). NIRS was compared to cryospectrophotometry in estimating hemoglobin saturation in a rodent tumor model and was found to have good sensitivity and specificity, despite its lack of spatial resolution (Conover *et al.* 2000). Phantom and preliminary *in vivo* measurements were performed by McBride *et al.* (2001) to map oxygen saturation in breast tissue. Although phantom studies showed promising results, it was concluded that four wavelengths were necessary to quantify hemoglobin saturation, due to the background absorption of water and lipids and the complexity of the ill-posed image reconstruction problem. Nioka *et al.* (2000) traced oxygenation changes in metastatic tumors during radiation treatment and concluded that this may be a useful technique for monitoring the effectiveness of radiation therapy (Hull *et al.* 1999).

The use of NIR monitoring of tissue oxygenation is being investigated in four different areas: cerebral monitoring, peripheral vascular disease, muscle function and tumor oxygenation. This field will keep expanding as the trend towards non-invasive diagnostic techniques in medicine continues.

1.6 Thesis proposal

Although the use of NIRS in clinical settings has increased in recent years due to the advantages of the technique, research into the interpretation of the NIRS signal must continue. Discrepancies in results have been observed, and the simple model used to describe light transport in tissue may be the primary factor. The limitations of a homogeneous model have been identified by various authors (Farrell *et al.* 1998, Kienle *et al.* 1998 and Pham *et al.* 2000). The aim of the thesis is to use a time-resolved system (that is capable of measuring optical properties of homogeneous turbid media accurately) and identify the limitations of the system and a homogeneous model in determining hemoglobin saturation in a layered measurement geometry.

By using a large source-detector separation and examining primarily late arriving photons, it may be possible to use this system to study oxygenation in the bottom layer of a two-layer system. Although a two-layer phantom model is still a simplification of the actual tissue architecture, it may provide a suitable representation of tissue under certain anatomical condition, for example, an overlying fat layer on muscle, or skin on top of a subcutaneous tumor. The application of a simple homogeneous diffusion theory model to data from a two-layer measurement was examined through the use of mathematical models, Monte Carlo simulations and experiments. The performance of the experimental system was characterized and optimized for homogeneous media. Initial measurements were performed in tissue simulating liquid phantoms with known optical properties. Deoxygenation experiments, where the quantity of interest was primarily hemoglobin saturation, were carried out in a homogeneous geometry and then in a two-layer phantom. The performance of the simple model was studied by analyzing two-layer diffusion theory calculations of reflectance with a homogeneous model. Experimental verification was performed through the use of a simpler two-layer experiment that involved changing bottom layer absorption by increasing the ink concentration, simulating hemoglobin saturation changes. These experiments were performed for different top layers, i.e. representing skin or fat, and different top layer thicknesses to determine the limitations of this experimental apparatus when used with a homogeneous diffusion model. Finally, a direct test of the success of the system in recovering bottom layer oxygenation parameters was performed using a two-layer phantom with blood in the bottom layer.

2 THEORY AND DATA ANALYSIS

For all the experiments discussed in this thesis, the time-resolved reflectance data were fitted to a time-dependent semi-infinite diffusion model. This provided an estimate of the absorption coefficient which could then used to calculate hemoglobin concentration and saturation. Saturation results were compared to saturation calculated from pO_2 measurements (see section 3.2) or saturation derived from cw reflectance. The reflectance from the cw system was analyzed using a modified Beer's Law and provided an estimate of SO_2 based on the shape of the normalized spectrum.

2.1 Time-resolved Measurements

The time-resolved reflectance data were fitted to semi-infinite diffusion theory using a non-linear least squares fitting algorithm. The observed experimental pulse was a convolution of the true signal and the impulse response of the detector and electronics. The most straightforward manner in which to deal with the instrument response would be a deconvolution in the time domain. It would also be possible to convolve the theoretical reflectance with the measured instrument response at each iteration of the fitting algorithm and compare this to the experimental data. This process can be time-consuming because it is necessary to perform a convolution with each fitting iteration, so instead a Fourier transform was applied to the data. The Fourier transform of the instrument response can then be divided out from the spectrum and the data can be fit directly in the frequency domain. Therefore, before each experiment, an instrument response function (IRF) was measured by aligning the source and detector fibers which could then be accounted for in the fitting procedure.

The neutral particle transport equation can be used to model light propagation in tissue. This equation can be solved numerically, or under certain conditions, analytically. The diffusion equation assumes that the source is isotropic and the radiance is almost isotropic. For uniform tissues and homogeneous geometries, it is possible to produce a time-dependent analytical solution for the reflectance due to a point source (Patterson *et al.* 1989). This model does have limitations due to the assumptions made. Diffusion theory solutions are not valid under the following conditions: (1) when absorption and scattering coefficients are comparable. In general, it is best to have $\mu_a < 0.1\ \mu_s'$ which is true for most biological tissues in the NIR. (2) the source and detector are close together i.e. to be valid, $\mu_s'\rho >> 1$ (3) at times close to the ballistic transport limit and (4) near air-tissue boundaries.

The application of the correct boundary condition has received much attention (Farrell *et al.* 1992, Haskell *et al.* 1994 and Kienle and Patterson 1997). Three boundary condition have been employed: the zero boundary condition, the extrapolated boundary conditions and the partial current boundary condition (Haskell *et al.* 1994). All describe a relationship between the incoming and outgoing photon currents. The most practical compromise of speed and accuracy is the extrapolated boundary condition which accounts for mismatches at the boundary and can be solved analytically.

For this analysis a modified extrapolated boundary condition was applied as described by Haskell *et al.* (1994). The expression for the time-resolved reflectance involves the fluence rate, Φ (ρ,z,t) and the flux, R_f (ρ,t), where ρ is the source-detector separation, z is the depth into the medium perpendicular to the boundary and t is the time. The model also assumes that all photons are isotropically scattered at a mean depth z_o within the medium. The expressions are given by Kienle (Kienle and Patterson 1997) as:

$$\Phi(\rho,z,t)=\frac{c}{(4\pi Dct)^{3/2}}\exp(-\mu_a ct)\left\{\exp\left[-\frac{(z-z_o)^2+\rho^2}{4Dct}\right]-\exp\left[-\frac{(z+z_o+2z_b)^2+\rho^2}{4Dct}\right]\right\} \quad (2)$$

and

$$R_f(\rho,t)=\frac{t^{-5/2}}{2(4\pi Dc)^{3/2}}\exp(-\mu_a ct)\left\{z_o\exp\left[-\frac{r_1^2}{4Dct}\right]+(z_o+2z_b)\exp\left[-\frac{r_2^2}{4Dct}\right]\right\} \quad (3)$$

where $D = 1/[3(\mu_a + \mu_s')]$ is the diffusion coefficient, c is the speed of light in the medium, $z_o = 1/(\mu_a+\mu_s')$, $r_1^2 = z_o^2 + \rho^2$, $r_2^2= (z_o + 2z_b)^2 + \rho^2$ and the value of z_b is given by equation (4):

$$z_b=\frac{1+R_{eff}}{1-R_{eff}}2D \quad (4)$$

where R_{eff} is the fraction of photons that are internally diffusely reflected at the boundary (Kienle and Patterson 1997).

The time-resolved reflectance is given by equation (5):

$$R(\rho,t)=\frac{1}{4\pi}\int_{2\pi}\left[\Phi(\rho,z,t)+3D\frac{\delta\Phi(\rho,z,t)}{\delta z}\cos\theta\right]\times[1-R_{fres}(\theta)]\cos\theta\, d\Omega \quad (5)$$

where $R_{fres}(\theta)$ is the Fresnel reflection coefficient. Because the source and detector fibers were mounted in a black plastic probe, it was assumed that the boundary conditions were matched i.e. $R_{eff} = 0$ and, in this situation, equation (5) reduces to (Haskell *et al.* 1994):

$$R(\rho, t) = 0.25\Phi(\rho, z = 0, t) + 0.5R_f(\rho, t) \tag{6}$$

As previously stated, a fast Fourier transform was applied to the time-resolved data and the experimental phase and modulation were calculated as functions of frequency. This proved to be more efficient since the Fourier transform of the instrument response function could be divided out from each spectrum prior to fitting. The theoretical phase and modulation were calculated from the real and imaginary parts of the Fourier transform of the reflectance, determined from equation (6) (Haskell *et al.* 1994, Kienle and Patterson 1997) and were defined as:

$$\text{Phase lag} = k_{imag} r_1 - \arctan(\text{IMAG} / \text{REAL}) \tag{7}$$

$$\text{Modulation} = (\text{REAL}^2 + \text{IMAG}^2)^{1/2} / \text{DC} \tag{8}$$

where DC is the DC reflectance ($\omega = 0$), ω is the frequency and k_{imag} is defined by:

$$k_{imag} = (1.5\, \mu_a\, \mu_s')^{1/2}\ \{[(1 + (\omega/(\mu_a c))^2]^{1/2} - 1\}^{1/2} \tag{9}$$

and REAL and IMAG are weighted by the appropriate factors from equation (6) and are given by Haskell *et al.* (1994) as:

$$\begin{aligned}\text{REAL} = {} & \frac{\exp(-k_{real} r_1)}{r_1} - \cos[k_{imag}(r_2 - r_1)]\frac{\exp(-k_{real} r_2)}{r_2} + \left(k_{real} + \frac{1}{r_1}\right)\frac{z_o{}^2}{r_1}\frac{\exp(-k_{real} r_1)}{r_1} + \left(k_{real} + \frac{1}{r_2}\right) \\ & \times \frac{(2z_b + z_o)z_o}{r_2}\cos[k_{imag}(r_2 - r_1)]\frac{\exp(-k_{real} r_2)}{r_2} + k_{imag}\frac{(2z_b + z_o)z_o}{r_2}\sin[k_{imag}(r_2 - r_1)]\frac{\exp(-k_{real} r_2)}{r_2}\end{aligned}$$

$$(10)$$

$$\mathrm{IMAG}=\sin[k_{imag}(r_2-r_1)]\frac{\exp(-k_{real}r_2)}{r_2}+k_{imag}\frac{{z_o}^2}{r_1}\frac{\exp(-k_{real}r_1)}{r_1}+k_{imag}\frac{(2z_b+z_o)z_o}{r_2}\cos[k_{imag}(r_2-r_1)]$$
$$\times\frac{\exp(-k_{real}r_2)}{r_2}-\left(k_{real}+\frac{1}{r_2}\right)\frac{(2z_b+z_o)z_o}{r_2}\sin[k_{imag}(r_2-r_1)]\frac{\exp(-k_{real}r_2)}{r_2}\frac{\exp(-k_{real}r_2)}{r_2} \tag{11}$$

and $k_{real} = (1.5\ \mu_a\ \mu_s')^{1/2}\ \{[(1 + (\omega/(\mu_a c))^2]^{1/2} + 1\}^{1/2}$ (12)

The differences between experimental and theoretical phase and modulation were minimized simultaneously by varying two parameters, the absorption and scattering coefficients. A grid-search was used to search the χ^2 space until a minimum was obtained. The fitting procedure returned a best estimate of μ_a, μ_s' and the final χ^2 value, as well as the transformed data and the best fit phase and modulation. The relative weighting factors for the fitting of phase and modulation were obtained empirically by fitting Monte Carlo data and experimental data, since an accurate estimate of the standard deviations of these quantities was not available.

For homogeneous measurements, the fitting range was limited by noise in the experimental data to be from 0 to 1 GHz. As previously mentioned, by limiting the time range of the fitting it should be possible to gain a better estimate of the bottom layer optical properties in a two-layer system. Analogous to this, high frequency data were not included in the fitting range when fitting reflectance from a layered sample. When analyzing two-layer data in the frequency domain, the range of frequencies fit was limited to about 600 MHz, as this range was found to provide the best estimate of bottom layer optical properties when fitting Monte Carlo data.

2.2 *Determining Hemoglobin Saturation*

To test the proposed method, reflectance measurements of a tissue-simulating phantom with variable hemoglobin saturation were performed and analyzed with the approach detailed above. This resulted in a series of absorption coefficients, one at each wavelength, that varied over time as the oxygenation state of the phantom varied. From two absorption coefficients at different wavelengths it was then possible to calculate the oxygenation of the hemoglobin in the sample under investigation. In order to determine the concentration of oxyhemoglobin and deoxyhemoglobin in the phantoms, two equations of the form:

$$\mu_a(\lambda) = [HbO_2]\ \varepsilon(\lambda)_{HbO2} + [Hb]\ \varepsilon(\lambda)_{Hb} + \mu_a(\lambda)_{background} \qquad (13)$$

were solved to provide estimates of [Hb] and [HbO_2] where $\mu_a(\lambda)$ is the absorption measured at wavelength λ, $\varepsilon(\lambda)_i$ is the specific absorption of chromophore i at wavelength λ and $\mu_a(\lambda)_{background}$ is the background absorption which should correspond to that of water in these experiments. In practice, a reflectance measurement was performed on the phantom prior to the addition of blood and the background absorption was obtained from that measurement. Hemoglobin saturation, as defined by equation (1) was calculated, as well as total hemoglobin concentration, [tHb]:

$$[tHb] = [HbO_2] + [Hb] \qquad (14)$$

The specific absorption values were chosen, in accordance with the findings of Hull *et al.* (1998), from the values of ε_{Hb} as determined by Cope (1991) and the values of ε_{HbO2} from

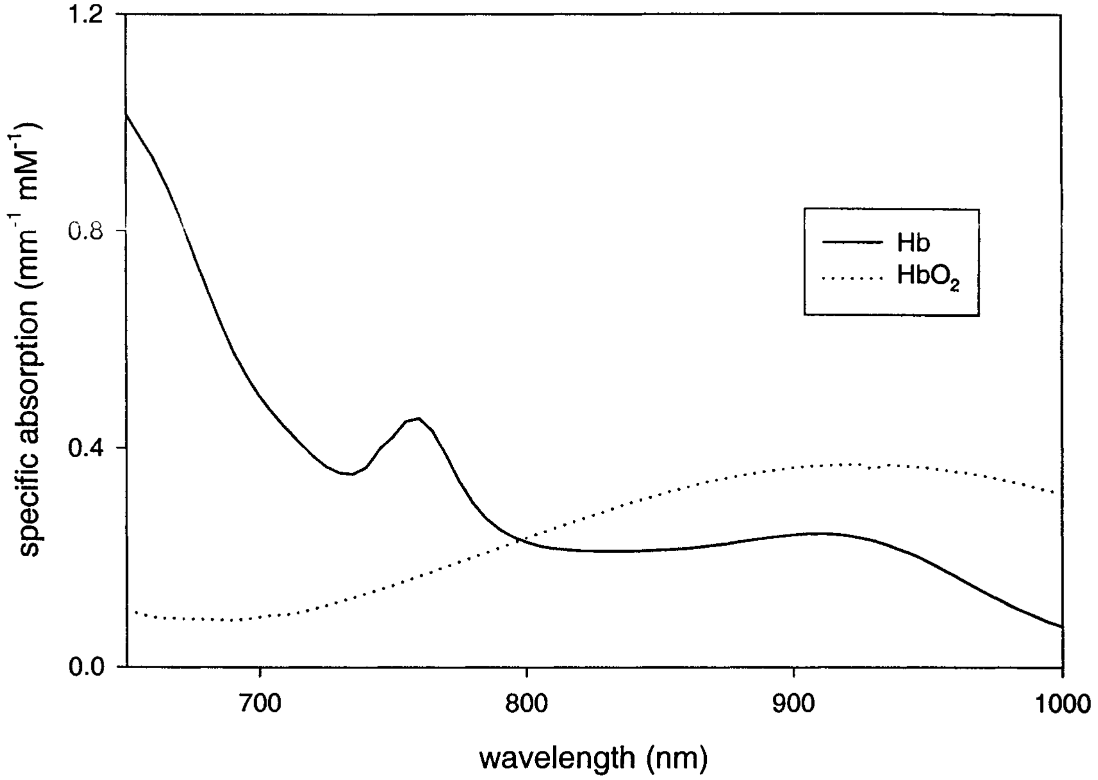

Wray *et al.* (1988). The absorption spectra of hemoglobin and oxyhemoglobin are shown in Figure 2.1.

***Figure 2.1**: The NIR absorption spectrum of oxyhemoglobin (Wray et al. 1988) and deoxyhemoglobin (Cope et al. 1991).*

2.3 *Continuous Wave Measurements*

The continuous wave measurement system collected reflectance over a range of wavelengths (700 to 850 nm) at a source-detector separation of 9 mm. In order to use this system to determine hemoglobin saturation without using the same technique as the time-resolved system i.e. fitting with diffusion theory and estimating absorption, the following approach was used. It is known that the reflectance, R, which is dependent on wavelength, is given by Beer's Law as:

$$R(\lambda) = k_1 \exp(-\mu_a \bar{x}) \qquad (15)$$

where k_1 is a constant depending on the source output and other instrument parameters and $\bar{x}$ is the effective pathlength.

Rewriting equation (13), we get:

$$\mu_a(\lambda) = \varepsilon(\lambda)_{HbO2} (SO_2) [tHb] + \varepsilon(\lambda)_{Hb} (1 - SO_2) [tHb] + \mu_{a(background)} \qquad (16)$$

As above, the values of ε_{Hb} were taken from Cope (1991) and the values of ε_{HbO2} from Wray *et al.* (1988). Since the pathlength is dependent on wavelength, due to the spectral dependence of the scattering coefficient, it is scaled by a wavelength correction factor, such that $\bar{x} = x(1 - n\lambda)$, where n is an empirically determined constant and has a value of about 8×10^{-4} nm^{-1} when λ is in nanometers. The natural logarithm of (15) gives the following expression:

$$\log(R) = \log k_1 - \varepsilon_{HbO2} (SO_2) [tHb] \bar{x} - \varepsilon_{Hb} (1 - SO_2) [tHb] \bar{x} - \mu_{a(background)} \bar{x} \qquad (17)$$

If the initial state is assumed to correspond to complete oxygenation ($SO_2 = 1$), the initial spectrum, R_o, has the form:

$$\log(R_o) = \log k_2 - [tHb]\, \varepsilon_{HbO2}\, \bar{x} - \mu_{a(background)}\, \bar{x} \quad (18)$$

where k_2 is the constant term,k_1, for the initial state. The difference of (17) and (18) gives:

$$\log(R/R_o) = k_3 - \varepsilon_{HbO2}\, (SO_2)\, [tHb]\, \bar{x} - \varepsilon_{Hb}\, (1- SO_2)\, [tHb]\, \bar{x} + [tHb]\, \varepsilon_{HbO2}\, \bar{x} \quad (19)$$

which reduces to:

$$\log(R/R_o) = (\varepsilon_{HbO2} - \varepsilon_{Hb})\, (1- SO_2)\, [tHb]\, \bar{x} + k_3 \quad (20)$$

Each spectrum was normalized by dividing by the initial spectrum, and the natural logarithm of this ratio was fitted to the difference of the absorption spectra of oxyhemoglobin and deoxyhemoglobin, yielding the term $(1- SO_2)\, [tHb]\, \bar{x}$. The constant term, k_3, would be zero if there were no fluctuations during an experiment, but it was allowed to vary to account for temporal variations in the source output and detector efficiency. It was assumed that the phantom began in a saturated state ($SO_2 = 1$) and progressed during the experiment to a deoxygenated state ($SO_2 = 0$). This was confirmed by measurements of pO_2 as discussed in section 4.3.1. Therefore, the final value of $(1- SO_2)\, [tHb]\, \bar{x}$ yields $[tHb]\, \bar{x}$, and this value can be used to estimate SO_2 at any other time. The technique also assumes the effective pathlength of light does not change as the absorption coefficient changes. The accuracy of this approach is investigated in detail in section 4.3. However, the fits to the data were good, as shown in Figure 2.2, indicating the validity of this method. The isobestic point can also be observed at about 800 nm. Data and fits from three different time points are displayed in Figure 2.2, corresponding to a fully oxygenated, an intermediate and a deoxygenated state from a typical experiment. By the analysis of the cw spectra, a time-course of SO_2 was constructed, which was compared to SO_2 calculated with the time domain system. Of course, this method could not be used for *in vivo* measurements due to the fact that it requires measurements to be taken when SO_2 is known to be both zero and one. This is not necessary for the time-resolved measurements.

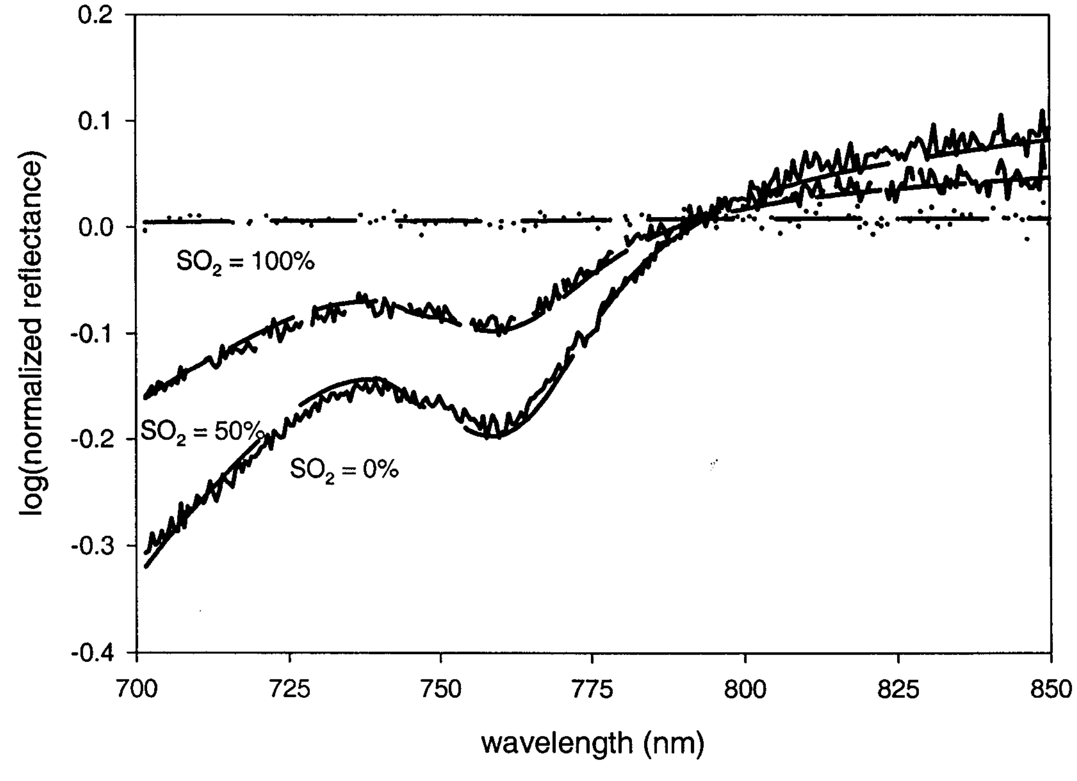

Figure 2.2: Reflectance spectra collected from direct cw measurement on a blood and Intralipid phantom during a deoxygenation experiment. The log (base e) of the normalized data are plotted as a function of wavelength for three cases (SO_2 = 100, 50 and 0%). Also shown is the best fit of equation (20) to each data set.

3 EXPERIMENTAL METHODS

The aim of this research was to investigate the performance of the time-resolved measurement system in determining the oxygenation of various tissue-simulating phantoms. This section will describe the set up of the time-resolved measurement system used throughout this thesis. In order to compare the results obtained from a time-resolved measurement, it is necessary to have an independent measure of oxygenation. In the initial experiments, this was provided by an oxygen electrode which measured the partial pressure of oxygen in the phantom. Subsequent measurements were compared to hemoglobin saturation determined with a direct spatially-resolved continuous wave measurement. The cw apparatus involved in these measurements is detailed in this section. Finally, the tissue-simulating phantoms used in the experiments will be discussed.

3.1 Time-resolved reflectance system

The technique of time-correlated single photon counting works under the assumption that by timing many single photons, a histogram of events versus time can be produced which, if many events are recorded, becomes representative of the desired probability distribution. For each event the time delay is measured and a count is added to the channel corresponding to the measured delay. This is repeated until a large sample has been accumulated (O'Conner and Phillips 1984). The source used has typically been a mode-locked dye laser and the detector, which must have a fast response time, is usually a photomultiplier tube (PMT).

The temporal resolution of the system is limited by the electronics and the PMT. The distribution of distances over which the photoelectrons and secondary electrons in the PMT must travel results in a variation in arrival times of the photoelectrons at the PMT anode and a transit time spread of up to 800 ps, depending on the PMT used. Thus, the observed signal is distorted by this effect and it becomes necessary to account for this temporal spreading when analyzing the data.

The instrumentation used in these experiments is shown in Figure 3.1. The lasers are pulsed diode lasers that have a pulse width < 50 ps (Hamamatsu Picosecond Light Pulser PLP-01 Users Manual). The first laser (PLP-01, LDH075, Hamamatsu Photonics K.K., Hamamatsu, Japan) emitted a train of pulses at 750 nm with a peak power of 40 mW. The other laser (PLP-01, LDH082, Hamamatsu Photonics K.K., Hamamatsu, Japan) emitted at 810 nm and had a peak power of 150 mW. The output of each laser was approximately 1 pJ per pulse. The laser pulse frequency was 10 MHz and the typical time resolution obtained was 400 ps as measured by the full-width at half maximum (FWHM) of the instrument response function. An IRF was measured prior to each set of measurements by aligning the source and detector fibers and collecting a time-resolved pulse for each wavelength. A typical IRF is shown in Figure 3.2. The probe used allowed for precise alignment of the source and detector fibers in this position and for the placement of additional filters so that the PMT was not saturated during the measurement of the instrument response function. The laser outputs were coupled with a 400 μm fiber optic combiner (Fibersense and Signals, Concord, ON) with losses of about 0.4 dB. The signal was then split into three fibers, the first fiber received about 80% of the combined power and delivered light through a 400 μm fibre to the sample, the second 10% was used as a reference pulse while the remaining 10% of the signal was routed to a PMT to provide a stop signal. The use of this optical trigger provided more stable operation than the electronic trigger available from the laser diode driver.

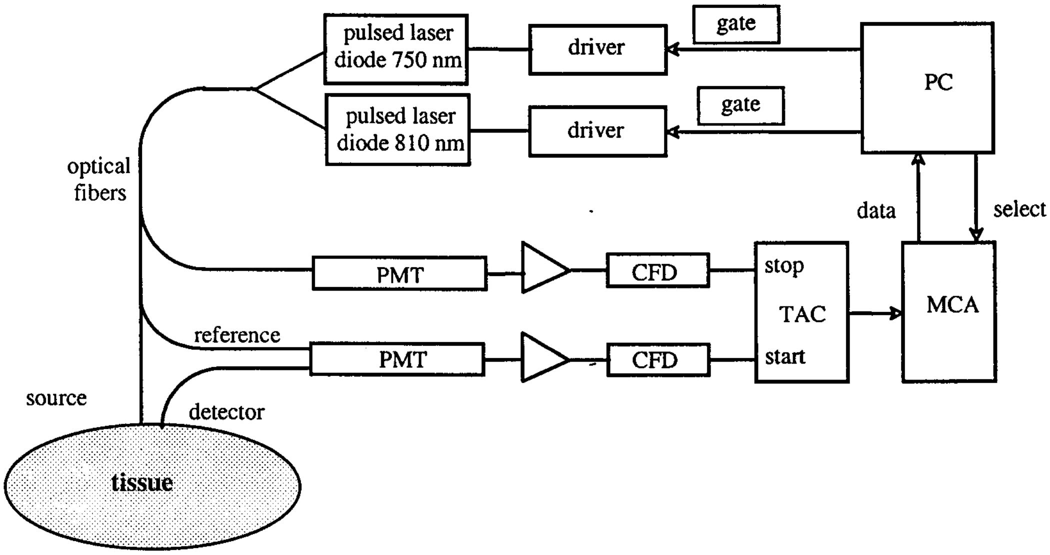

Figure 3.1: Schematic diagram of the dual wavelength time correlated photon counting system.

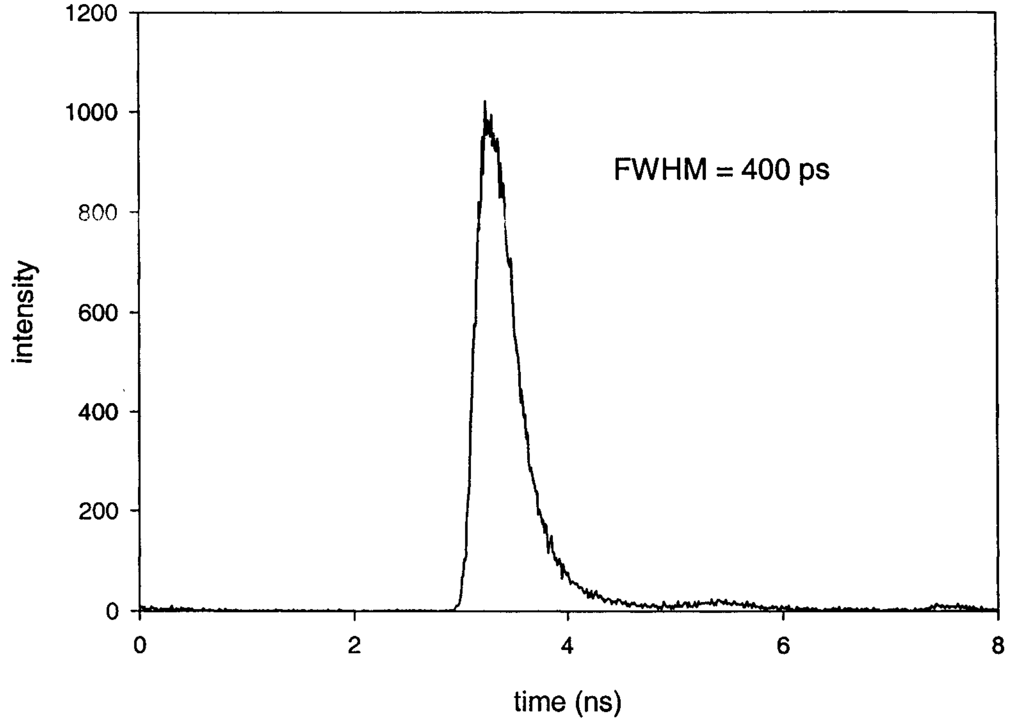

Figure 3.2: Typical instrument response function.

The light diffusely reflected from the phantom was collected with a 3 mm fiber bundle and coupled to a filter wheel. The reference signal, which allowed for the detection of time shifts due to drifts in the instrumentation, was sent through an attenuator (Oz Optics, Nepean, ON) and also transmitted through the filter wheel which was equipped with a range of neutral density filters. Both the attenuator and filter wheel allowed for control of the amount of light to ensure that single photon counting levels, which are essential to the technique, were obtained. These signals, which were separated in time due to different fiber lengths, were both incident on the photomultiplier tube (Metal Package PMT R5600U Series, Hamamatsu Photonics K.K.). The PMT was operated at 800 V and data collection time varied according to the situation but was on the order of one minute. The amplified detector output was fed through the constant fraction discriminator (CFD; TC 454, Tennelec/Nucleus, Oakridge, TN) and provided the start pulse for the time-amplitude converter (TAC; TC 864, Tennelec/Nucleus). The third optical signal was coupled to another PMT (Oriel Instruments Stratford, CT) amplified, sent through the CFD, delayed (TC 412A Delay, Tennelec/Nucleus) and acted as the stop pulse for the TAC. The system was operated in reverse mode, i.e., the trigger signal actually stopped the TAC because the counting electronics would be unable to reset between successive events for high source repetition rates. By allowing the sample signal to be the start pulse, the number of start pulses was reduced, providing more time for the electronics to reset. The TAC output, which was proportional to the temporal separation between start and stop pulses was sent to a multi-channel analyzer (MCA) where each bin was representative of a time window and PCA II software (Oxford Instruments, Oakridge, TN) was used to display the time histogram.

A black plastic probe was designed to hold the source fiber in place and fix the collection fiber bundle at a given separation from the source, typically 20 mm. The probe was constructed such that the black surface would minimize reflections and so that both fibers would be held in contact with the phantom or tissue surface. The probe was approximately 3 × 6 cm and formed an indexed-matched totally absorbing boundary between the fibers and the phantom for the reflectance measurements.

The lasers employed in these experiments were semiconductor diode lasers. For any diode head only one emission wavelength was available. The entire apparatus, including drivers was small, weighed less than 5 kg and could be run from a standard 120 V outlet. Although these lasers do not offer the pulse width, power or tunability of a Ti:Sapphire laser, they are much less expensive. Ti:Sapphire lasers are also large and not easily portable and require cumbersome cooling and power supplies. Although in a lab setting dye lasers have advantages over diode lasers, in a clinical environment the size and portability of the diode laser makes it more feasible.

The need for compact equipment with high accuracy and sensitivity has grown with the increasing popularity of optical techniques in clinical settings. This is also true for photodetectors such as photomultiplier tubes. The most common detector used for time correlated photon counting is probably the microchannel plate photomultiplier tube (MCP-PMT) which has excellent time response, sensitivity (which has low wavelength dependence over a specific range) and the ability to count photons with low noise. Semiconductor sensors can be used in place of MCP-PMTs but they do not have the excellent resolution nor do they have signal to noise ratios as high as MCPs. A compromise solution by Hamamatsu is the R5600U series of PMTs which employ a metal package instead of the glass envelope; they are small yet offer good sensitivity and resolution. They are smaller than a standard tube and their resolution, as measured by the FWHM of the IRF, can be as low as 275 ps compared to about 30 ps for a MCP-PMT, or about 2 ns for a standard side window PMT, under similar conditions. These miniature tubes use stacked thin electrodes (metal channel dynodes) to form an eight stage electron multiplier within a metal cylinder of 15 mm diameter and 10 mm height, about one-tenth the size of standard types. In addition to being compact, these tubes also cost less than ten percent of the price of an average MCP-PMT. These photomultiplier tubes have sufficient resolution to perform time-resolved reflectance measurements and are well suited to a clinical environment.

In order to perform simultaneous reflectance measurements at two wavelengths with the photon counting system described above, which only had one detector, it was necessary to implement an electronic control circuit that managed the lasers and the multi-channel analyzers. The multiplexing electronics allowed virtually simultaneous two wavelength measurements with a single detector; the two lasers were alternately enabled at a rate of 20 Hz. The circuit also controlled the two multi-channel analyzers to ensure that one MCA always collected data corresponding to the same laser.

3.2 Oxygen electrode

In the initial, single-layer oxygenation experiments, the performance of the system in measuring hemoglobin saturation was compared to the hemoglobin saturation calculated from a direct measurement of oxygen partial pressure in the phantom. The oxygen partial pressure in the phantom was monitored with a Clark style oxygen electrode (Diamond General, model 730, Ann Arbor, MI). This apparatus was calibrated using an air-saturated sample of a scattering solution and a sample deoxygenated with $Na_2S_2O_4$. The partial pressure of oxygen was then determined from the electrode current assuming a linear response (Hull *et al.* 1998). The results were corrected for changes in temperature; a temperature calibration was done in an Intralipid phantom. The pO_2 was monitored in an air saturated sampled and a calibration curve of current versus temperature was obtained by performing a linear fit to the data. In the phantom, the electrode was placed about 1 cm below the surface of the liquid towards the edge of the container so it did not interfere with the reflectance measurements.

By plotting the SO_2 measured by the time-resolved system against the pO_2 measured by the oxygen electrode it is possible to obtain an experimental hemoglobin-oxygen dissociation curve which can be compared to the well known dissociation curve (Stryer 1995), as shown in Figure 3.3. The hemoglobin-oxygen dissociation curve can be expressed as:

$$SO_2 = \frac{pO_2{}^n}{p_{50}^n + pO_2{}^n} \qquad (21)$$

where pO_2 is the oxygen partial pressure, p_{50} is the pressure at which hemoglobin is 50% saturated and n is the Hill coefficient (Stryer 1995). These two empirical parameters have typical values $n = 2.46 \pm 0.05$ and $p_{50} = 25.95 \pm 1.43$ mm Hg (Zwart *et al.* 1984). These values were determined at pH = 7.4 and at a temperature of 37°C. When phantom measurements were performed, these conditions were duplicated. Knowledge of the phantom volume and amount of red blood cells added made it possible to calculate the total hemoglobin concentration in the phantom as well.

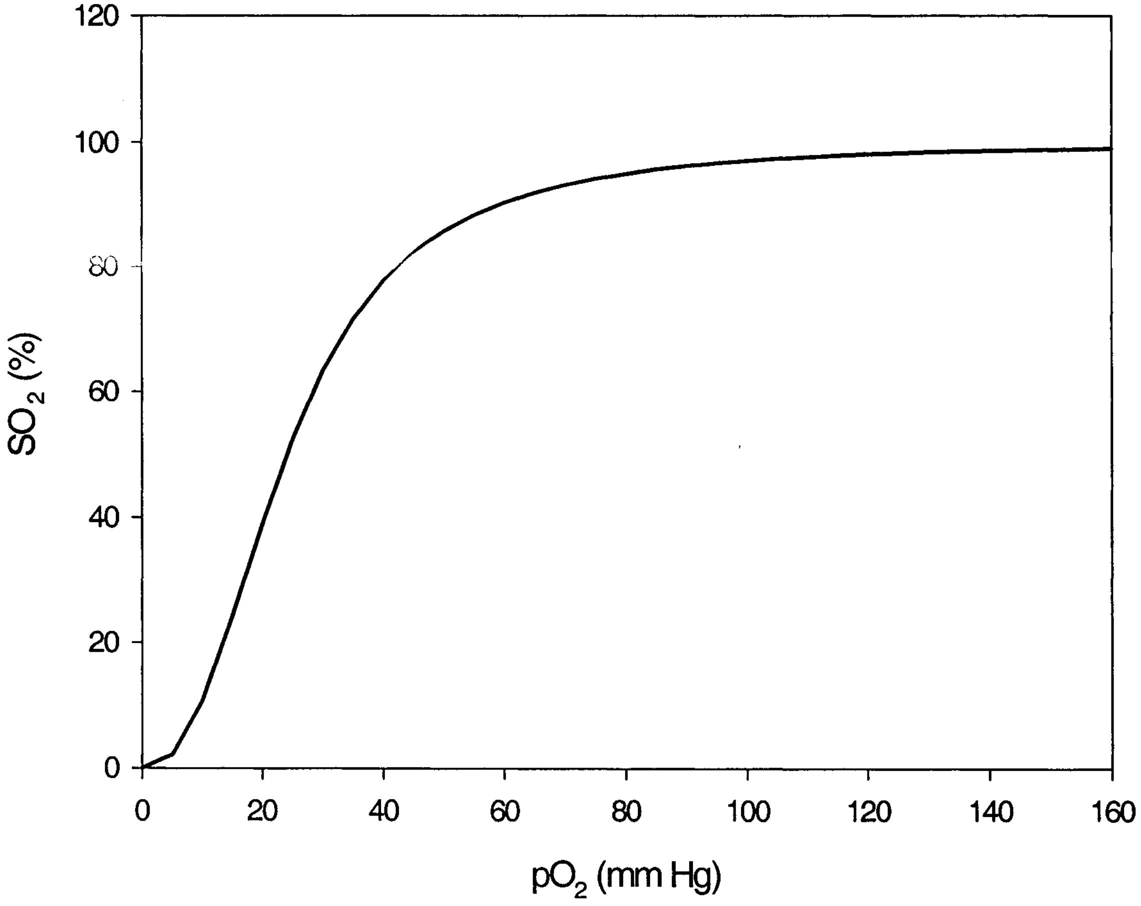

Figure 3.3: Hemoglobin-oxygen dissociation curve as described by equation (21) for typical values of n and p_{50} (Stryer 1995). Values were taken from Zwart et al. (1984) to be: n = 2.46 ± 0.05 and p_{50} = 25.95 ± 1.43 mm Hg.

3.3 Continuous-wave measurement system

The oxygen electrode introduced many difficulties into the experimental procedure. Problems with stability, temperature calibration and reproducibility lead to a change in the experimental protocol. Instead of measuring pO_2 and relying on the known hemoglobin dissociation curve, SO_2 was measured directly using a cw optical technique. This was first tested in a homogeneous phantom and then employed in the two-layer experiments. The direct measurement used a continuous wave system that has been described elsewhere (Bruulsema *et al.* 1997) and is shown diagrammatically in Figure 3.4. It consisted of a broadband quartz-tungsten-halogen (QTH) light source (Oriel Instruments) which delivered light through a fiber optic probe to the sample. The probe consisted of a source fiber with core diameter 200 μm and 15 detector fibers with diameters of 200 μm situated at distances from 1 to 10 mm from the source. Variable optical attenuators (Oz Optics) were used to limit light intensity, if necessary. The collected light was then dispersed by a spectrometer (Kaiser Systems, Ann Arbor, MI) and each detector fiber was imaged onto a two-dimensional thermoelectrically cooled CCD (Roper Scientific, Trenton, NJ). Hence, spectral and spatial information were obtained simultaneously over a useful range of about 600 to 900 nm. The data were collected by a PC and Windows based spectroscopy software. The response for each detector was corrected for differences in fiber transmission, CCD sensitivity and spectrometer optics. For these measurements, the steady-state reflectance was collected at a source-detector separation of 9 mm over a range of wavelengths from 700 to 850 nm. During an experiment, reflectance spectra were stored every minute and the data collection time was on the order of seconds. In this way, the changing reflectance spectra at different time points were stored for subsequent analysis as described in section 2.3.

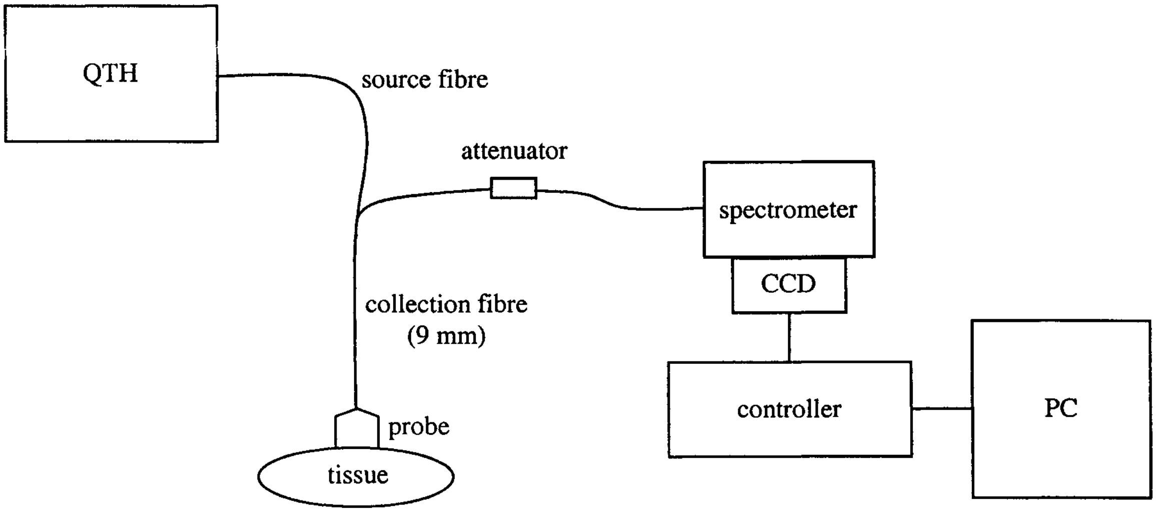

Figure 3.4: Schematic of continuous wave measurement system.

3.4 Phantom preparation

The experiments performed in this study relied on tissue-simulating liquid phantoms. Intralipid, at low concentrations, has been shown to provide scattering properties similar to tissue in the NIR region (van Staveren *et al.* 1991). This solution formed the basis for all the phantoms used. A concentration of 1% Intralipid results in a reduced scattering coefficient of about 1 mm^{-1} at 750 nm. A solution of polystyrene spheres in water also produces a phantom with a scattering coefficient similar to tissue. Using Mie theory, the expected scattering coefficient can be calculated explicitly. The index of refraction of these liquid phantoms was assumed to be that of water, n = 1.33 (van de Hulst 1980), since they were typically 99% water by volume. Absorption could be added to the phantom by the addition of different absorbers, such as Higgins Ink (Eberhard Faber, Inc. Lewisburg, TN), manganese *meso*-tetra(4-sulphanatophenyl) porphine (MnTPPS; Porphyrin Products, Logan, UT) or hemoglobin.

The expected absorption coefficient could be derived as a function of concentration for the different absorbers from measurements performed on a spectrophotometer. Absorbance measurements were performed on dilute solutions of the absorber (either ink or MnTPPS) to determine the relationship between absorption and concentration. This was done at both wavelengths used in experiments for a wide variety of absorption values. These measurements give a reasonable estimate of the expected absorption coefficient, but they assume that scattering is not present in the transmission measurement.

The phantoms utilized in the oxygenation experiments were designed to simulate the optical properties of tissue and were based on the protocol of Hull *et al.* (1998). A scattering solution of Intralipid-20% in 0.9% saline buffered to pH = 7.4 with Tris base (Boehringer Mannheim, Indianapolis, IN) formed the basis of the phantom. The concentration of Intralipid was varied to obtain a suitable scattering coefficient. Red blood cells were prepared from blood drawn from healthy human volunteers. Whole blood was centrifuged, typically three times at 1000 rpm for 10 minutes, or until the supernatant was clear. Red blood cells were then added to the phantom in a concentration similar to that expected in muscle, 1.6% by volume. During the experiment, a small amount of dry bakers' yeast was added to the phantom to consume oxygen over a course of about 60–90 minutes. The temperature of the phantom was increased from room temperature to 37 ± 2 °C to activate the yeast and maintained throughout the experiment. A magnetic stir rod was used to ensure the liquid was stirred continuously.

For the two-layer experiments, the same phantom described above was used to simulate a semi-infinite bottom layer and its scattering properties were chosen to simulate muscle. The top layer was designed to simulate either skin or fat by changing the Intralipid concentration and through the addition of ink. Optical properties were chosen in accordance with the work of other researchers (Farrell *et al.* 1998, Kienle and Glanzmann 1999), as shown in Table 1. The stated optical properties refer to a wavelength of 750 nm. The thickness of the skin layer was fixed at 1.5 mm and the fat layer thickness varied from 1.5 to 10 mm; this range of values is representative of what may be encountered clinically.

Tissue type	μ_a (mm^{-1})	μ_s' (mm^{-1})
Fat	0.003	1.0
Muscle	variable	0.5
Skin	0.02	1.5

Table 1: Optical properties chosen to represent different tissue types. Optical properties are approximate and represent the average at the two wavelengths used.

The experimental set-up for the two-layer measurements is shown in Figure 3.5. The fiber optic probe from the time domain system was suspended in the top layer and attached to a z-translator stage; this allowed the distance between the probe face and the surface of the bottom layer to be varied which effectively changed the top layer thickness. The top and bottom layers were separated by a clear, thin membrane (thickness ~ 10 μm) which did not significantly affect the reflectance measured (Hyde *et al.* 2001). Measurements made on a homogeneous phantom were compared to those made directly on the membrane and those made above the membrane when the top and bottom layers had equivalent optical properties. All measurements returned the same estimates of the optical properties of the sample as shown in Table 2. The standard deviations were calculated from ten measurements. The probe from the continuous-wave system was suspended within the bottom layer of the phantom, far enough from the time-resolved probe such that it did not interfere with that measurement. The light from the cw source was also blocked when a measurement was not being performed, so that the light did not interfere with the time-resolved measurement.

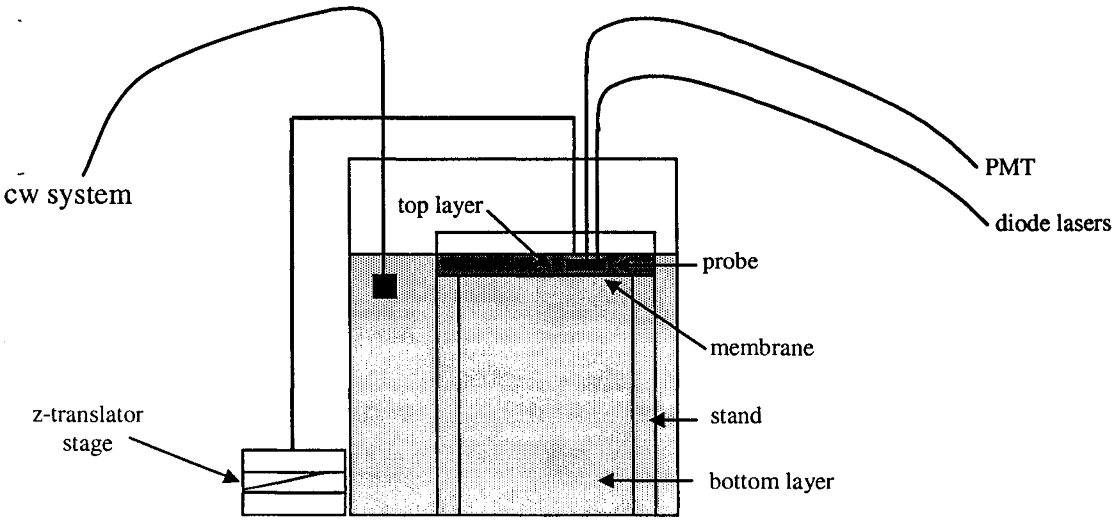

Figure 3.5: Experimental set-up of the Intralipid-blood-yeast phantom used in the two-layer oxygenation measurements. The probe from the time-resolved system is suspended in the top layer and its height above the bottom layer can be controlled. The probe from the cw system measured reflectance directly in the bottom layer of the phantom.

Experimental Set up	750 nm		810 nm	
	μ_a (mm^{-1}) $\pm\ \sigma(\mu_a)$	μ_s' (mm^{-1}) $\pm\ \sigma(\mu_s')$	μ_a (mm^{-1}) $\pm\ \sigma(\mu_a)$	μ_s' (mm^{-1}) $\pm\ \sigma(\mu_s')$
Single layer	0.0030 (1×10^{-4})	1.22 (0.01)	0.0029 (1×10^{-4})	1.15 (0.01)
Two-layer (t = 0 mm)	0.0033 (1×10^{-4})	1.23 (0.01)	0.0030 (1×10^{-4})	1.17 (0.02)
Two-layer (t = 1.5 mm)	0.0034 (1×10^{-4})	1.26 (0.01)	0.0030 (1×10^{-4})	1.17 (0.02)

Table 2: Effect of membrane on time-resolved reflectance measurements.

In some experiments, instead of deoxygenating the blood/yeast/Intralipid phantom as described above, absorption changes typical of those expected in an experiment were simulated in the bottom layer through the addition of ink. Estimates of absorption and therefore saturation determined through the top layer could be compared to those obtained with the top layer thickness set to zero (the probe directly on the thin membrane). These experiments were much simpler to perform than the actual deoxygenation experiments and provided an estimate of the expected measurement accuracy.

4 MEASUREMENTS IN HOMOGENEOUS PHANTOMS

Prior to performing measurements in two-layer phantoms, it was necessary to study the performance of the system in simple homogeneous media. System performance was quantified by the accuracy of the recovered optical properties. Factors affecting system performance were investigated through a variety of experiments. Once the system was optimized, the ability to measure absorption and scattering was characterized. This was accomplished through the use of tissue-simulating phantoms with known optical properties. Deoxygenation experiments using the blood-yeast-Intralipid mixture described in section 3.4 were performed. Time-resolved measurements of hemoglobin saturation were compared, first with data obtained from an oxygen electrode, and subsequently, to continuous wave measurements.

4.1 System optimization

Although system optimization had previously been performed (Hunter 1998), changes to the system and the fitting routine dictated that further experiments were necessary. System changes were introduced to improve the detectable light levels; a PMT was introduced in place of a photodiode to detect the reference pulse and the laser repetition frequency was increased to 10 MHz. To optimize the experimental apparatus, three sets of experiments were undertaken. In order to examine the effect of collection time and counting statistics on the reproducibility of measured optical properties, the variation in estimated properties as a function of collection time was determined. The stability of the system over time was also studied. When there were changes in stability, i.e. when the position of the reference pulse varied, the effect of correcting the data to account for this was examined.

The fitting program to estimate optical properties from diffusion theory was also characterized. It was necessary to weight the phase and modulation data appropriately; this weighting was studied with theoretical and experimental data. The effect of varying the range of frequencies fit on the estimated optical properties was also determined.

4.1.1 Experimental optimization

The effect of counting statistics on optical properties estimated by the model was investigated by performing ten consecutive measurements, each at a fixed data collection time, over the range 15 to 120 seconds. The data from this experiment are shown in Table 3 below. The measurements were performed on a 1% solution of Intralipid in water with no added absorber. The values of the fitted optical properties agreed with each other within experimental uncertainty and the standard deviation of the optical properties, determined from the ten measurements, decreased as the collection time increased. The number of counts in the peak channel ranged from 500 to 4000 for the range of collection times used. Although counting statistics improved with increased collection time, a practical compromise between time and statistics must be obtained. For this reason, during an oxygenation experiment a collection time of 30 seconds was typically used.

Collection time (s)	μ_a (mm^{-1}) $\pm\ \sigma(\mu_a)$	μ_s' (mm^{-1}) $\pm\ \sigma(\mu_s')$
15	0.0031 (0.0005)	1.09 (0.14)
30	0.0029 (0.0004)	1.04 (0.09)
60	0.0033 (0.0004)	1.14 (0.09)
120	0.0032 (0.0002)	1.12 (0.06)

Table 3: Short term stability of time-resolved system. Measurements were performed on a 1% Intralipid phantom at a wavelength of 750 nm.

The next investigation performed was the study of measurement stability. Since deoxygenation experiments using yeast take up to an hour (Hull *et al.* 1998), it was necessary to study the stability of the system over this time period. If there were temporal drifts in the system, it might be possible to correct for them through the use of the reference pulse which should remain fixed through an ideal experiment. Measurements on a solid phantom were performed every ten minutes over the course of an hour and the variation in the optical properties was observed. The average values and standard deviations in the optical properties were: $\mu_s' = 1.04 \pm 0.02$ mm^{-1} and $\mu_a = 0.0218 \pm 0.0008$ mm^{-1}. The standard deviations observed were much smaller than the absorption changes observed in a deoxygenation experiment. Long term stability was determined on the same phantom over the course of a week to be within about 10%. The average optical properties estimated from this experiment were: $\mu_s' = 0.9 \pm 0.1$ mm^{-1} and $\mu_a = 0.021 \pm 0.002$ mm^{-1}.

The effect of shifting the data during the fitting procedure in accordance with the shifts observed in the reference pulse was also investigated. The shifts were detected by recording the centroid of the reference pulse from each experiment and comparing to the centroid of the reference pulse from the IRF measurement; this will remain constant in an ideal experiment. The variations observed in this pulse are due to the experimental apparatus can be applied to the pulse from the sample. There was a direct correlation observed between the applied shift and the optical properties returned by the fitting routine, especially in the scattering coefficient, as expected. Since the fitting was performed in the frequency domain, shifting the experimental data will affect only the phase information not the modulation. If f(t) is the signal in the time domain which becomes F(s) in the frequency domain, then a time shift of δ has the following effect:

$$f(t) \rightarrow F(s)$$

$$f(t-\delta) \rightarrow F(s)e^{-i\omega s\delta}$$

resulting in a phase shift of $\omega s\delta$. The applied shifts introduced the expected changes in phase in the experimental data. If a large correction was required, it was noted that a poor estimate of the optical properties was returned. A large shift was often accompanied by a decrease in count rate and indicative of another problem, such as an influx of background light or the presence of bubbles on the probe surface. Such a data point was typically omitted from the analysis. If the time shift was ignored, a less accurate estimate of the optical properties was returned.

4.1.2 Weighting factors for fitting procedure

The fitting procedure iteratively minimized the weighted differences between observed and theoretical phase and modulation to provide an estimate of the optical properties of the sample. For such a fitting routine, each data point should be weighted by the inverse of its variance. These variances were not known for the results of analytical or Monte Carlo simulations however. The effect of the relative phase and modulation weights was investigated by fitting diffusion theory calculations of reflectance, Monte Carlo data and experimental results. From the analysis of simulated data, it was observed that the most accurate optical properties were obtained when the modulation was weighted by a factor between 200 and 1000, compared to phase, depending on the particular frequency range used. This large weighting factor is due to the fact that modulation varies from 1 to 0 and the phase change typically observed is on the order a few hundred degrees at high frequencies. This provided a starting point for the investigation of the correct weighting for the experimental data.

When fitting experimental data, the correct technique is to weight the phase and modulation according to their respective variances. These were not possible to calculate for any single experiment, so empirical weighting factors were used. To study the effect of different weighting factors, various tissue-simulating phantoms were used. Measurements were performed at source-detector separations of 20 and 30 mm at 750 nm and the modulation weight was varied in the fitting procedure. The measurements were repeated and the standard deviations in phase and modulation were calculated. However, the standard deviations depended on the frequency, generally increasing with higher frequencies, so the standard deviations were obtained as a function of frequency. Measurements were performed using two different solutions of polystyrene spheres in water and a solution of Intralipid with $CuPS_4$ added as an absorber.

The variation of optical properties with modulation weight is shown in Figure 4.1 (a-c). For each experiment, the optical properties estimated differed between the two distances measured. The optical properties were found to agree at both distances when the modulation weight was 0.999, although the results are still not correct. The phase weight and modulation weights were set to sum to a value of one, hence the phase weight was 0.001 and the relative weight was 1000:1. Figure 4.2 (a-c) shows the dependence of the ratio of variances, (the relative weighting factor) for different frequencies for the measurements performed at 20 mm. The ratio of the experimental variances, i.e. the correct relative weight depends upon the frequency chosen but is in the range 0 to 200, comparable to that observed with the theoretical data. However, as higher frequency data (up to 1 GHz) is included in the fitting range, it becomes necessary to increase the relative weights closer to the 1000:1 ratio. This produces better results, since it weights the modulation more as the variance in the phase is increasing rapidly with increasing frequency. If the frequency range is limited i.e. for the two-layered measurements, the optimum weighting factor is lower (200:1) since the variance in phase is less.

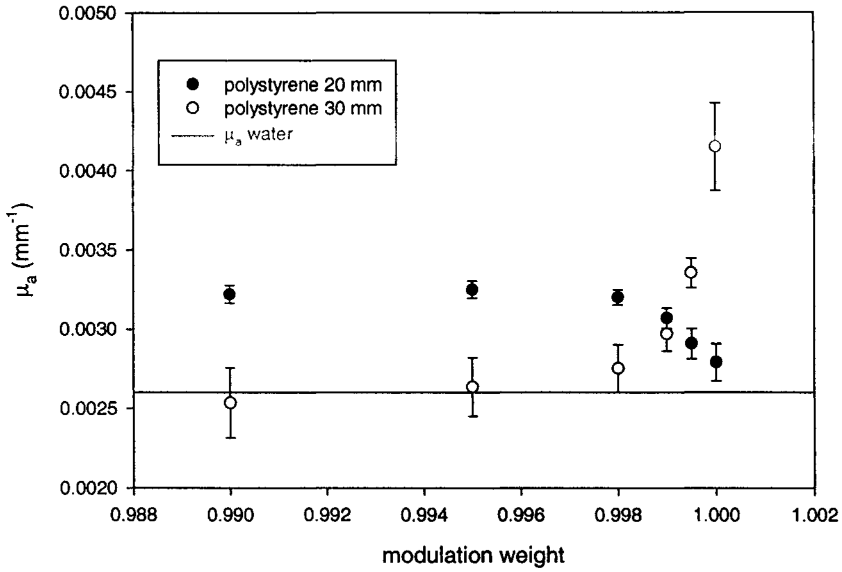

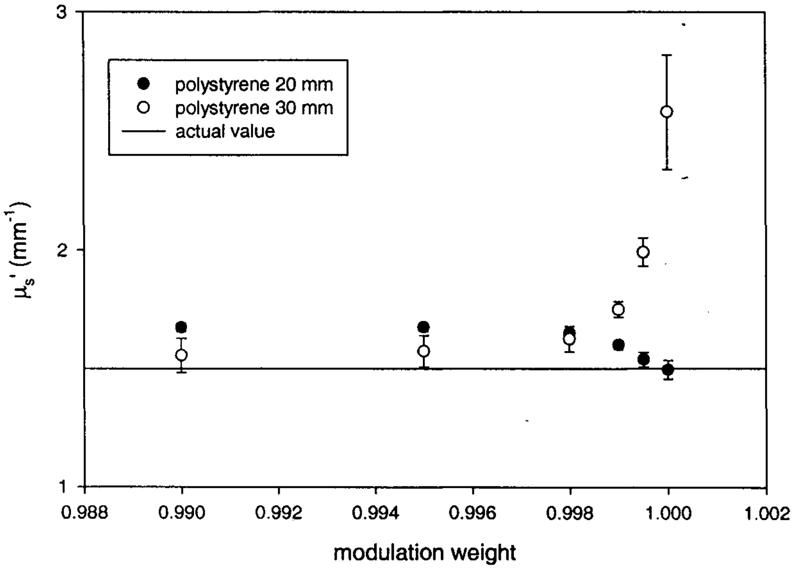

***Figure 4.1a**: Variation of scattering and absorption coefficients with modulation weight for* ρ *values of 20 and 30 mm. Results from measurements of polystyrene spheres with* $\mu_s' = 1.5$ *mm*$^{-1}$.

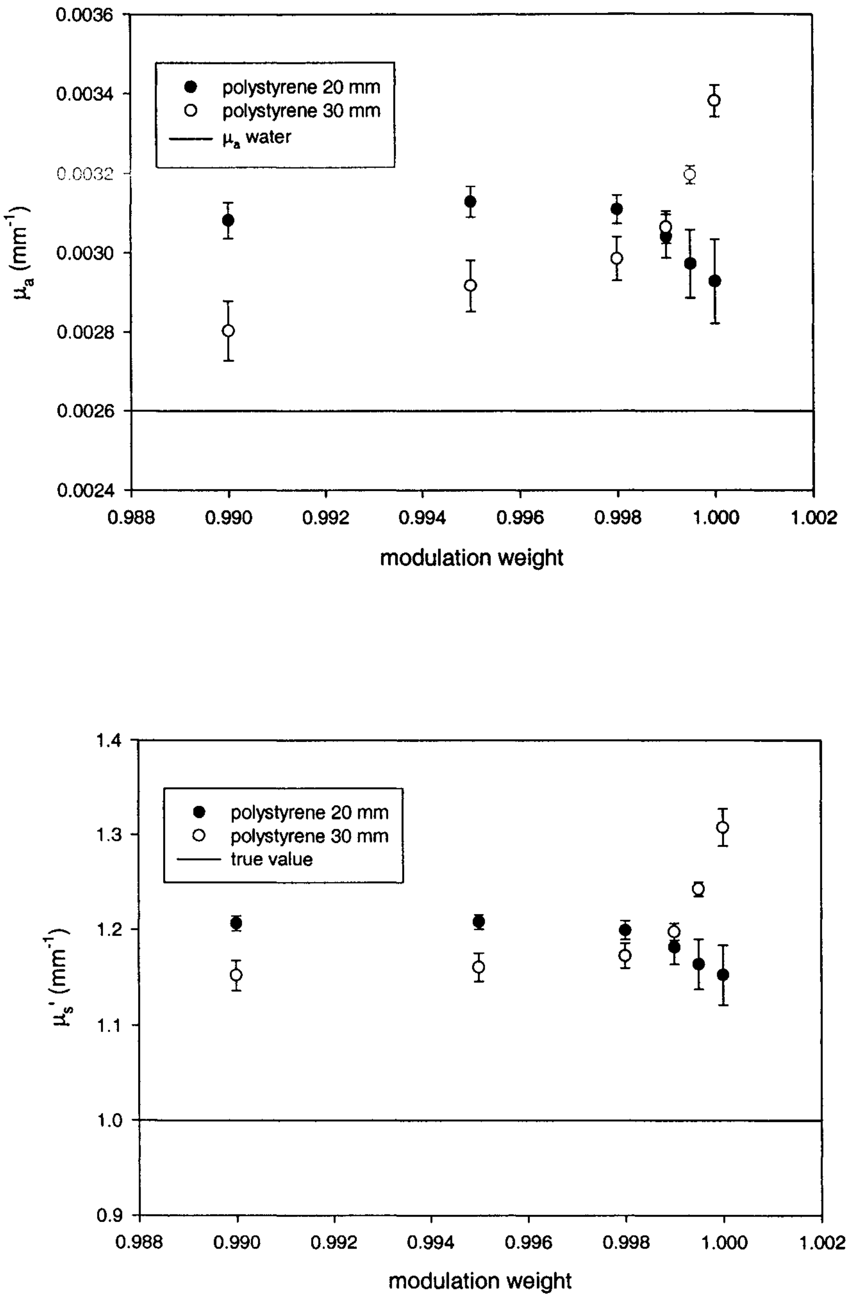

***Figure 4.1b**: Variation of scattering and absorption coefficients with modulation weight for ρ values of 20 and 30 mm. Results from measurements of polystyrene spheres with $\mu_s' = 1.0\ mm^{-1}$.*

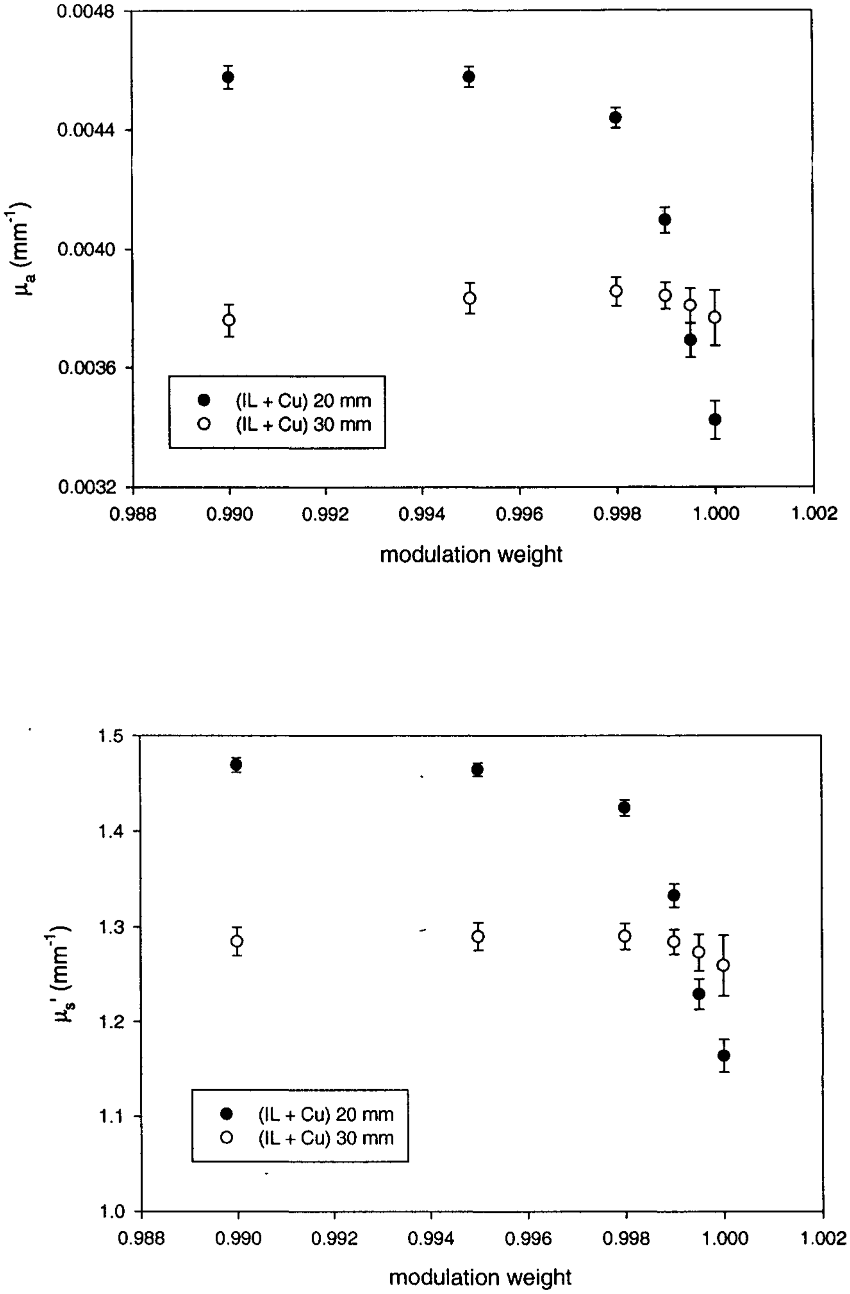

***Figure 4.1c**: Variation of scattering and absorption coefficients with modulation weight for ρ values of 20 and 30 mm. Results from measurements of 1% Intralipid with $CuPS_4$ added.*

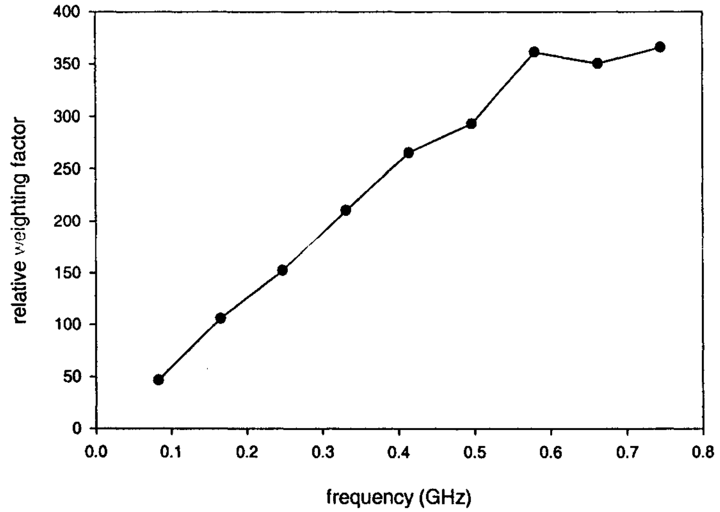

Figure 4.2a: *Variation of relative weighting factor versus frequency for the polystyrene spheres in water ($\mu_s' = 1.5\ mm^{-1}$).*

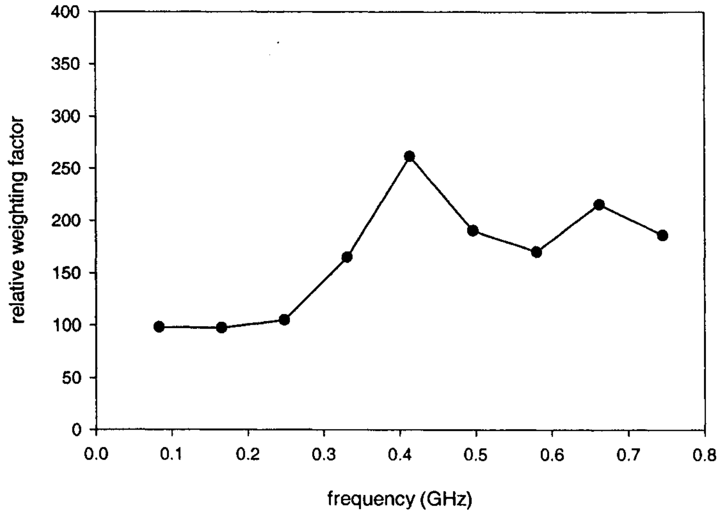

Figure 4.2b: *Variation of relative weighting factor versus frequency for the polystyrene spheres in water ($\mu_s' = 1.0\ mm^{-1}$).*

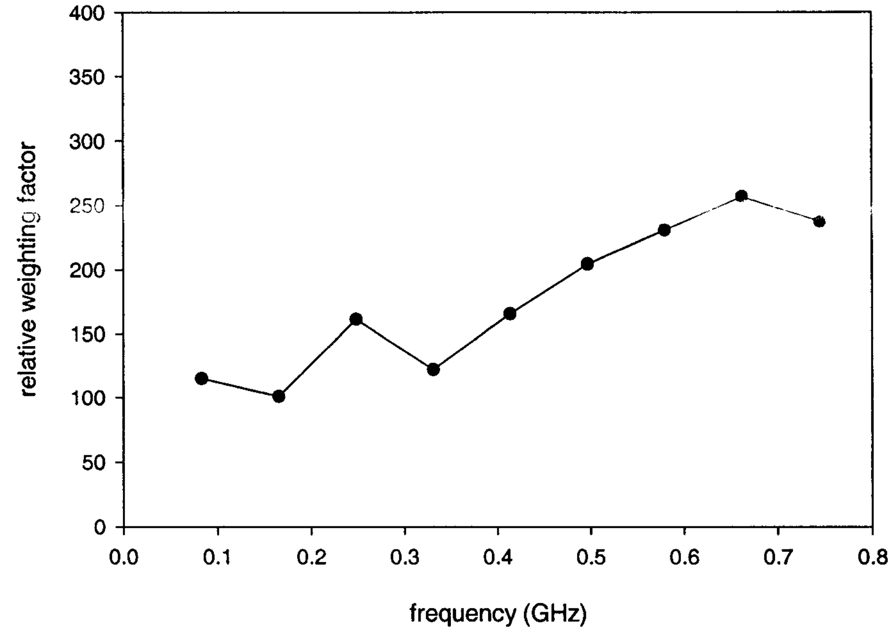

Figure 4.2c: Variation of relative weighting factor versus frequency for the 1% Intralipid in water with $CuPS_4$ added.

4.1.3 Effect of varying frequency range

To improve the speed of fitting, the Fourier transform of the time-resolved data was fitted in the frequency domain, but this made it more difficult to determine the optimal fitting range. In the time domain, the early times, where diffusion theory is not valid, are easily excluded from the fitting range. This region is less evident in the frequency domain but will correspond to higher frequency data points. The optimum fitting range for homogeneous data was investigated using simulated data (Monte Carlo and diffusion theory) and experimental data. The fitting range began at the first (frequency = 0) point, i.e. the DC point and contained all the points up to some maximum frequency, which was a variable parameter in the fitting procedure.

Diffusion theory and Monte Carlo simulations were used to produce time resolved reflectance profiles that were then analyzed with the diffusion theory model. A source-detector separation of 20 mm and optical properties: $\mu_s' = 1.0$ mm^{-1} and $\mu_a = 0.01$ mm^{-1} were used. When fitting forward generated diffusion theory calculations of reflectance with a diffusion theory model in the frequency domain, it was determined that the most accurate results were obtained by fitting to a very high frequency, typically 5 GHz. Errors obtained were less than 1% in either optical property ($\mu_s' = 1.0004$ mm^{-1} and $\mu_a = 0.01003$ mm^{-1}). Small errors were observed regardless of the fitting range used, within a range of 2-10 GHz for the maximum frequency fit. Since the data did not have noise added and the model should be exact, such small errors were not surprising. However, when Monte Carlo data was fitted over different fitting ranges, a greater dependence on fitting range was observed. Counting statistics and noise were obtained that were typical of actual experiments. Errors of up to 20% in the optical properties were observed for some fitting ranges. At the optimum fitting range, (0 – 4 GHz), the errors in either the absorption or scattering coefficients were less than 5% ($\mu_s' = 1.039$ mm^{-1} and $\mu_a = 0.01046$ mm^{-1}).

Time-resolved reflectance measurements were performed on a dilute solution of Intralipid in water with and without added absorber. The fitting range was varied and the estimated optical properties from the fit were compared to the expected values. The scattering coefficient can be predicted based on an empirical relationship. The absorption of water is known to be 0.002 mm^{-1} at 810 nm and the absorber (MnTPPS) was quantified prior to the experiment by absorption spectrophotometry. The data are shown in Figure

4.3 (a-d) as are the expected optical properties. The optical properties were less accurate when the absorption value was low (the only absorption in 4.3a was due to water) than when it was higher (4.3c). The relative and absolute errors were both higher in Figure 4.3a than in 4.3c. The best results were obtained when frequencies up to 1 GHz were included in the fitting range. As the maximum frequency increased above 1 GHz there was little improvement in the estimated optical properties. Therefore, in typical homogeneous measurements, the maximum frequency fit was 1 GHz.

4.2 Characterization of system performance

The success of the time-resolved system in measuring changes in oxygenation is dependent on its accuracy in estimating the absorption properties of tissue, or a tissue-simulating phantom. The response of the system to changes in scattering, as well as absorption, was investigated in the following experiments. Changes in the reduced scattering or absorption coefficient were induced by increasing the concentration of scatterer or absorber. Measured changes in optical properties were then compared to the expected changes in optical properties which were calculated from theory or a direct measurement.

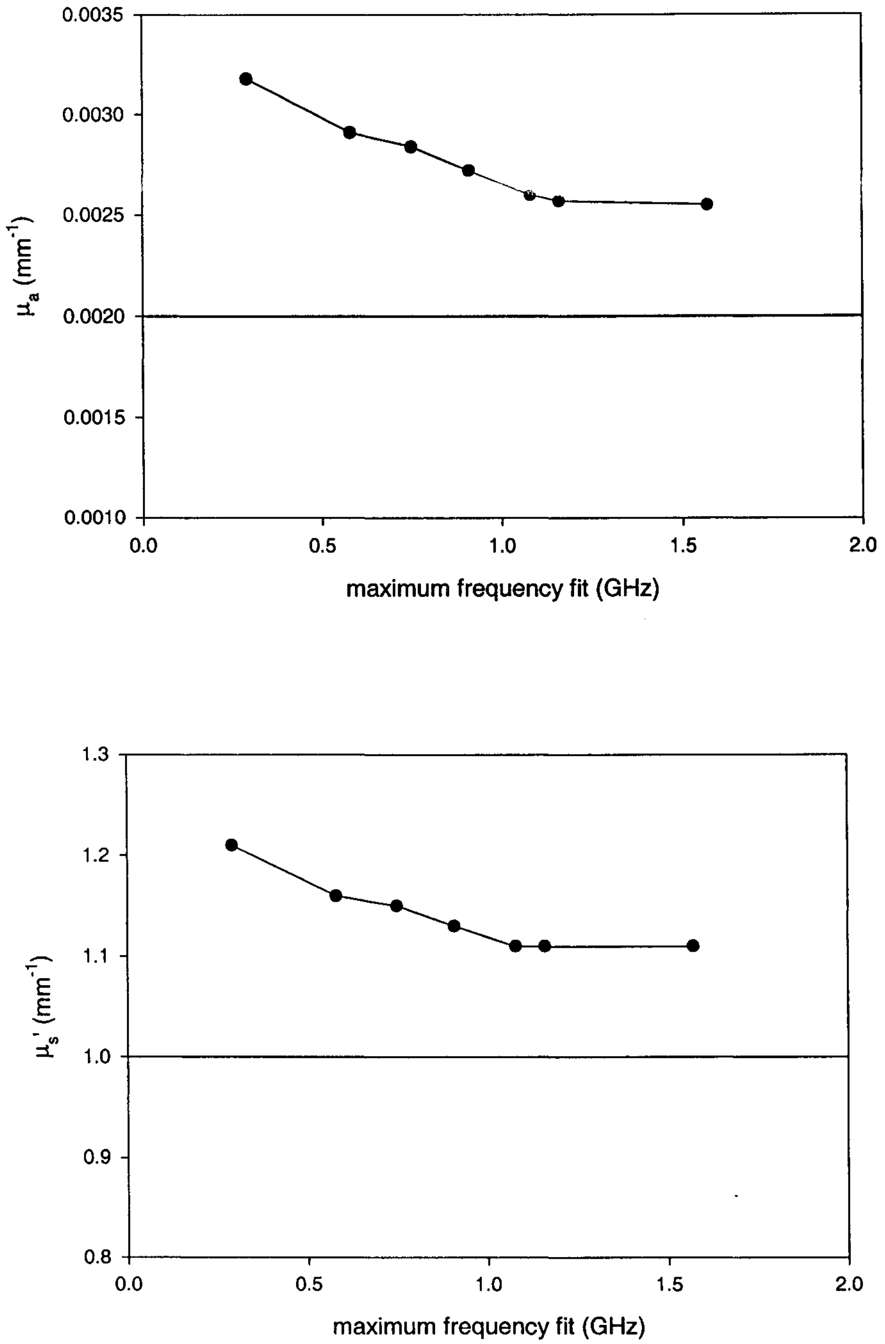

***Figure 4.3(a,b)**: Variation of absorption and scattering coefficients with fitting range. Results are shown for (a) absorption and (b) scattering for a 1% solution of Intralipid in water. The trend line and the expected values are also shown.*

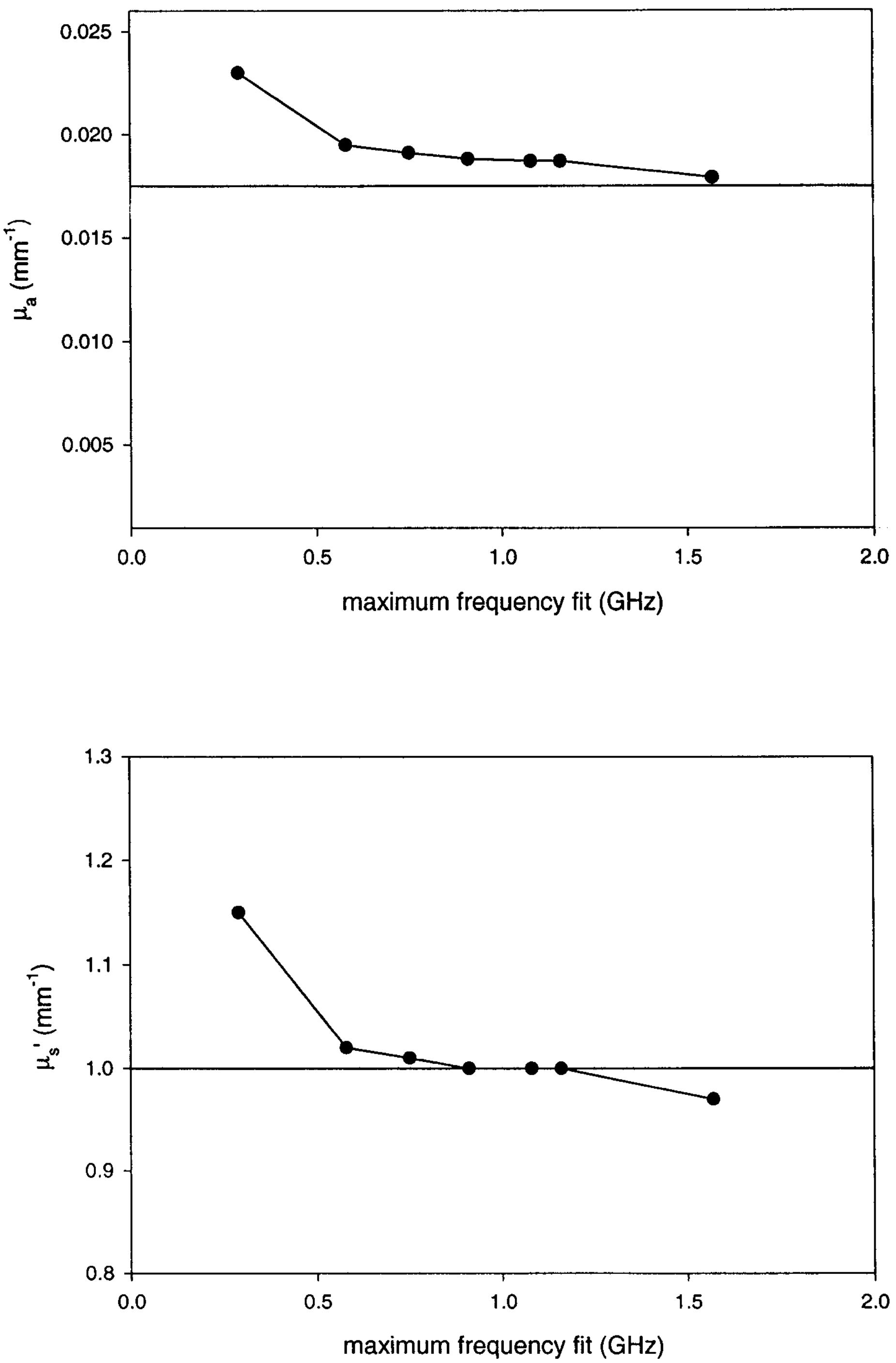

Figure 4.3(c,d): *Variation of absorption and scattering coefficients with fitting range. Results are shown for (c) absorption and (d) scattering for a 1% solution of Intralipid in water with a known amount of absorber added. The trend line and expected values are also shown.*

4.2.1 Measuring changes in μ_s'

Two sets of measurements using increasing concentrations of Intralipid were performed at a wavelength of 750 nm. The estimated optical properties were compared to the expected properties. The expected absorption was that of water at 750 nm, 0.0026 mm^{-1} and the reduced scattering coefficient was known from the empirical relationship: μ_s' = 1.0 (% Intralipid in water) at 750 nm. A range of concentrations from 0.5 to 1.5% were used. From the diffusion theory fit to the time-resolved data, scattering and absorption coefficients were estimated; six measurements were made at each concentration. Regression analysis was performed on the μ_s' versus concentration data and the equation of the best fit line was: μ_s' (mm^{-1}) = [1.18 ± 0.05 (% IL) + (0.05 ± 0.04)] mm^{-1}. The data from this experiment is plotted in Figure 4.4(a). The R^2 value obtained was 0.994 indicating a highly linear relationship. This was comparable to the equation derived from measurements performed with an independent frequency domain system in our lab (Hunter 1998): μ_s' (mm^{-1}) = [1.16 ± 0.04 (% IL) + (0.13 ± 0.03)] mm^{-1}. The average absorption coefficient determined from the measurements was 0.0020 ± 0.0002 mm^{-1}, comparable to the expected value of 0.0026 mm^{-1}. Although the measured scattering was slightly higher than expected, the relationship was highly linear. Deviations from the relationship are likely due to variations in batches of Intralipid. A different batch of Intralipid was analyzed in the same manner and the resulting best fit line was: μ_s' (mm^{-1}) = [0.96 ± 0.01 (% IL) + (0.11 ± 0.2)] mm^{-1} and R^2 = 0.995. The average μ_a value obtained was 0.0031 ± 0.0002 mm^{-1}, similar to the expected value of 0.0026 mm^{-1}. These data are shown in Figure 4.4(b).

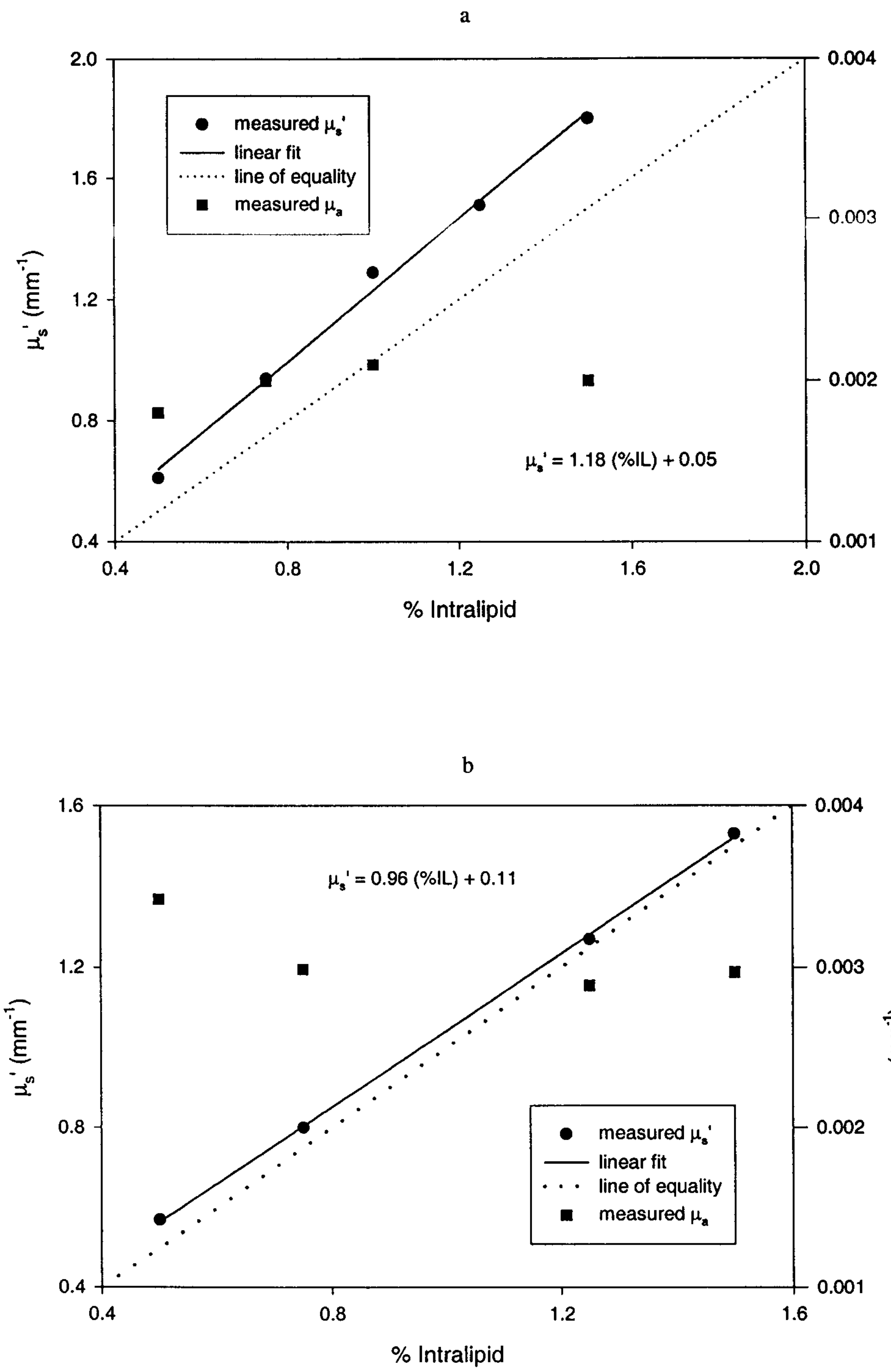

Figure 4.4: *Variation of scattering and absorption coefficients with Intralipid concentration. The best fit line and line of equality are also shown. Two separate experiments are shown in (a) and (b).*

Measurements were also performed on varying concentrations of polystyrene spheres in water. The reduced scattering coefficient can be calculated from Mie theory if the particle size and concentration are known. A graph of measured versus expected scattering coefficient is shown in Figure 4.5. The slope of the best fit line to the data was 1.06 and the R^2 value was 0.997. The average measured absorption coefficient value was $0.0033 \pm 0.0004\ mm^{-1}$, similar to the expected value of $0.0026\ mm^{-1}$ at 750 nm.

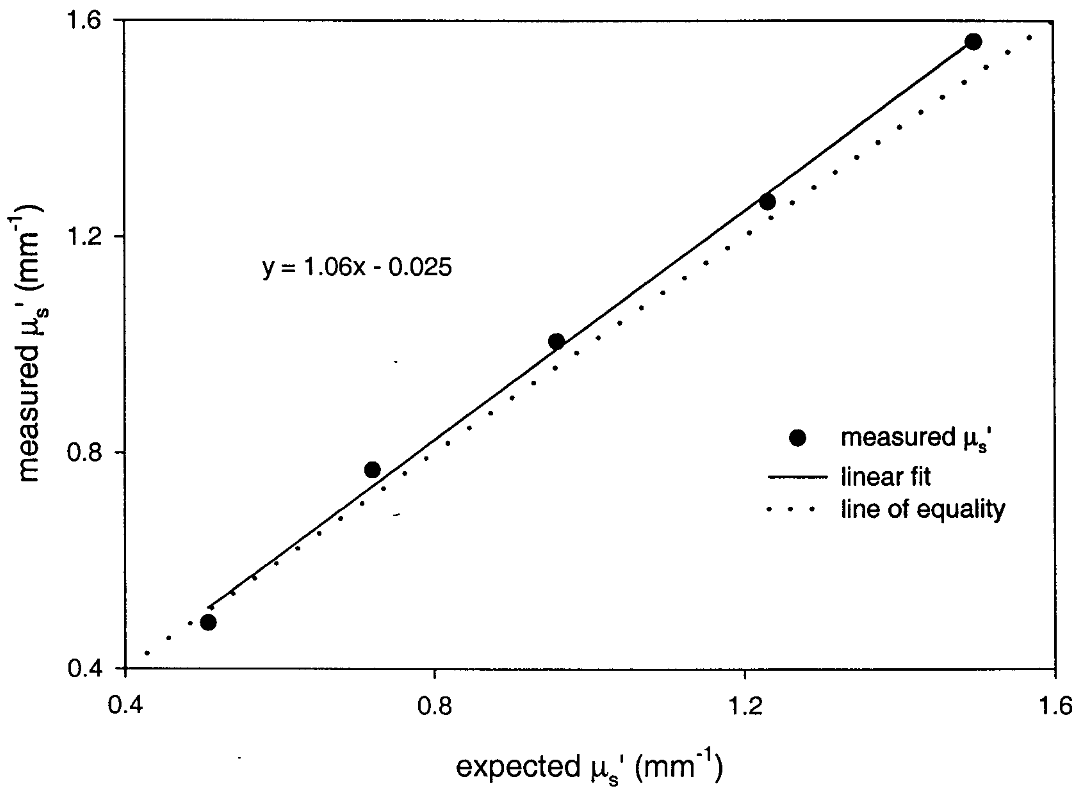

Figure 4.5: Measured versus expected scattering coefficient for a solution of polystyrene spheres in water. The expected value was calculated from Mie theory. The best fit line and line of equality are also shown.

The time-resolved measurement system can measure the reduced scattering coefficient of a tissue simulating phantom with an accuracy of about 10%. However, for hemoglobin saturation measurements, the ability of the system to monitor changes in absorption is the most important characteristic. This is investigated in the following two sections.

4.2.2 Measurements with Ink

The use of ink as an absorber for NIR measurements is a common technique (Madsen *et al.* 1992 and van Staveren *et al.* 1991). The expected absorption coefficient was determined from a direct transmission measurement using a spectrophotometer. A calibration curve relating μ_a to ink concentration was constructed for each measurement wavelength. Results from measurements performed at 810 nm will be reported here, but the results at 750 nm were similar. Increasing amounts of ink were then added to a dilute solution of Intralipid in water to produce known changes in the absorption coefficient of the phantom. Time-resolved measurements were performed and the best fit optical properties were obtained from diffusion theory. Measured and expected absorption coefficients were compared.

From the direct spectrophotometer transmission measurements, the following relationship was determined between absorption and Melan ink (MeL-Co, Orland, CA) concentration:

$$\mu_a = 0.92\ (\%\ \text{ink}) + 0.002\ \text{mm}^{-1} \qquad (22)$$

The ink experiment was performed three times with the following results from regression analysis of measured absorption coefficient versus ink concentration:

Trial	Slope (μ_a vs % ink)	constant	R^2
1	0.70 ± 0.04	0.0015 ± 0.0016	0.99
2	0.60 ± 0.05	0.002 ± 0.001	0.995
3	0.60 ± 0.04	0.0017 ± 0.0015	0.996

Table 4: Results of regression analysis of μ_a versus Melan ink concentration.

These results are lower than would be expected based on the transmission measurements.

A different brand of ink, Higgins Ink, was also measured using the same approach. The expected slope from the regression analysis was 3.1 ± 0.1, while the measured value was 2.95 ± 0.05. In both cases, the expected absorption from the transmission measurement was significantly higher than that predicted by the time-resolved measurements. A possible source of error in the transmission measurement is scattering by the ink particles. Any scattering will be misinterpreted as absorption, causing an incorrect overestimate of the absorption coefficient. Since ink particles can scatter light (Madsen *et al.* 1992), this method of determining μ_a does not have high accuracy. The use of a different absorber will be examined in the next section. However, in subsequent experiments ink is still used as an absorber when the absolute accuracy of the measurement is not essential.

4.2.3 Measurements with MnTPPS

An absorber that can be characterized more accurately than ink is manganese *meso*-tetra(4-sulphanatophenyl) porphine (MnTPPS). The absorption spectrum of this molecule was first measured with a spectrophotometer and the absorption coefficient versus concentration curve was generated as with the ink measurements. The absorbance spectrum is shown in Figure 4.6. The quantum yield of the molecule is low enough that it is considered non-fluorescing Since the molecule is unlikely to contribute to scattering, the predicted absorption coefficient from the transmission measurement should be more accurate than for ink. Two measurements were performed where the concentration of MnTPPS was increased in a tissue simulating phantom (~1 % Intralipid in water) and the optical properties were measured with the time-resolved system. The results from these measurements and the expected absorption coefficient values are shown in Figure 4.7; a summary of the regression analysis of these curves is presented in Table 5. These measurements were performed at 750 nm and for the first set of measurements, the average μ_s' was 1.16 ± 0.03 mm^{-1} while for the second set, μ_s' was 0.98 ± 0.05 mm^{-1}. Both measurements showed excellent linearity and there was good agreement between the measured and expected values. The expected intercept should be the water absorption coefficient value at 750 nm, which is 0.0026 mm^{-1}. The measurement values for this coefficient were 0.0050 and 0.0028 mm^{-1}. The first measurement estimated the slope of the absorption versus concentration curve more accurately, but predicted the intercept less accurately than the second measurement.

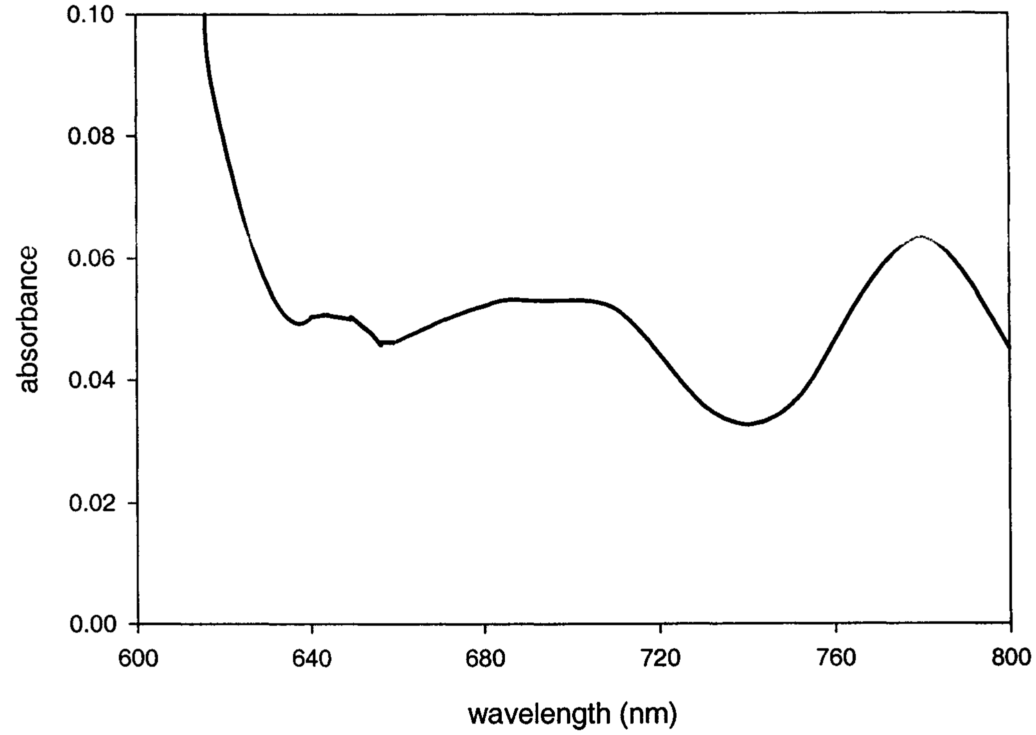

***Figure 4.6**: Absorbance spectrum of MnTPPS.*

Trial	Slope (μ_a vs % MnTPPS)	constant	R^2
Expected	1.82×10^{-4}	2.6×10^{-3}	1.0
Measurement 1	1.83×10^{-4}	5.0×10^{-3}	0.979
Measurement 2	2.02×10^{-4}	2.8×10^{-3}	0.996

Table 5: Results of regression analysis of μ_a versus MnTPPS concentration. The data are shown in Figure 4.7

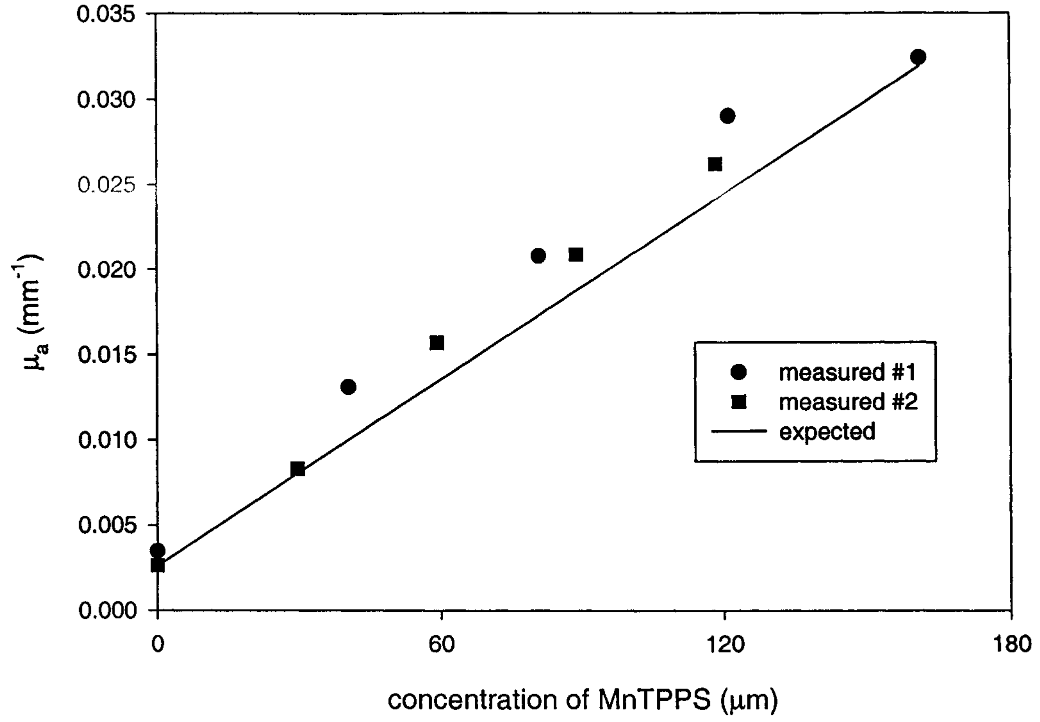

Figure 4.7: Measured and expected absorption coefficients for a solution of Intralipid in water with increasing amounts of MnTPPS added. The measurements were performed at 750 nm and the expected value was generated from direct transmission measurements in a spectrophotometer.

Although only the results from measurements performed at 750 nm were presented, similar accuracy was obtained at 810 nm. The time-resolved system and homogeneous semi-infinite diffusion model can quantify changes in the absorption coefficient of a homogeneous phantom. In the next section, the ability of the system to monitor oxygenation changes in this geometry was investigated.

4.3 Deoxygenation measurements in a homogeneous phantom

4.3.1 Measurements using oxygen electrode

Measurements were performed with the experimental set-up previously described. The sample used was the blood-yeast-Intralipid solution described in section 3.4 which was contained in a beaker and placed on a hot plate-stirrer. Light was delivered and collected with a black plastic probe that was suspended just below the surface of the liquid. The source-detector separation for the measurements was fixed at 20 mm. The entire apparatus was covered to prevent stray background light from entering the system.

In these experiments, the oxygen partial pressure in the phantom was monitored with an oxygen electrode. This apparatus was calibrated using an air-saturated sample of a scattering solution and a sample deoxygenated with $Na_2S_2O_4$ (Hull *et al.* 1998). The partial pressure of oxygen was then determined from the electrode current assuming a linear response.

Measurements were performed on the phantom in an air-saturated state and it was then deoxygenated through the activation of yeast at increased temperature for a period of up to 60 minutes. Time-resolved measurements of reflectance were collected simultaneously with measurements of pO_2 by the oxygen electrode over the course of the experiment at intervals of 60 seconds. The optical properties were estimated from the diffusion theory fit to the time-resolved reflectance data. The estimated μ_a values were used to determine the hemoglobin saturation as described in section 2.2. The experimental hemoglobin dissociation curves are produced by plotting SO_2 versus pO_2. These are shown in Figure 4.8 for three separate experiments. The expected results are also presented using the data of Zwart *et al.* (1984), $p_{50} = 25.95 \pm 1.43$ mm Hg and $n = 2.46 \pm 0.05$. From the best fit line of the data to equation (21), the p_{50} was determined to be 23.6 ± 3.5 mm Hg and the best fit n value was 2.32 ± 0.55. The root-mean-square error in hemoglobin saturation was defined as:

$$\text{rms error} = \sqrt{\frac{\sum_{N} (SO_{2\ \exp} - SO_{2\ \text{true}})^2}{N}} \tag{23}$$

where $SO_{2\ \exp}$ is the estimated hemoglobin saturation, $SO_{2\ \text{true}}$ is the true saturation calculated from pO_2 and N is the number of measurements. For these experiments, the rms error was 10.1%. The total hemoglobin concentration, [tHb], was typically about 50 μM (range of 45 to 60 μM) for these phantoms and calculated values of [tHb] from measured data were, on average, 11% lower than expected. Hence, the system is able to measure oxygenation in a simple homogeneous tissue-simulating phantom with an rms error of 10.1% in SO_2 and 11% in [tHb].

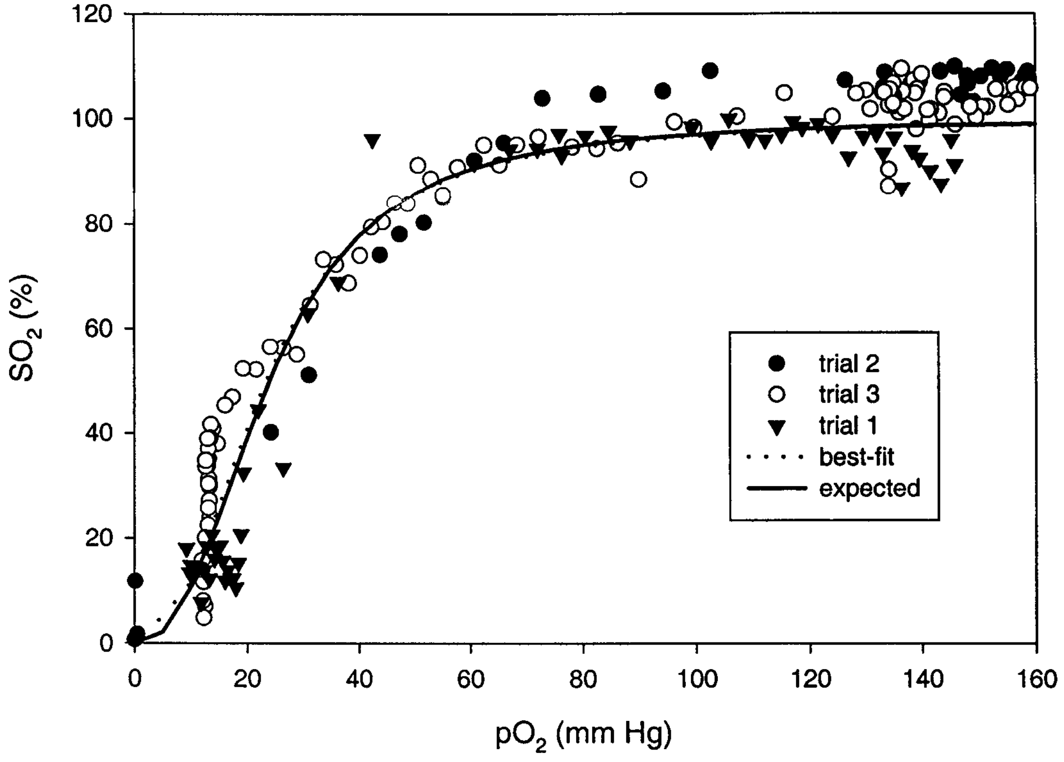

Figure 4.8: *The experimental and standard oxygen hemoglobin dissociation curves. Results from three separate experiments are shown. Best fit to all experimental data is also plotted (dotted line) as is the expected hemoglobin-oxygen dissociation curve (solid line).*

4.3.2 Validation of simple cw model

Due to difficulties with the oxygen electrode in terms of reproducibility, stability and ease of use, an optical method to monitor oxygenation was developed as detailed in sections 2.3 and 3.3. This instrument also measured SO_2 directly and did not rely on the hemoglobin oxygen dissociation curve to calculate SO_2 from the measured pO_2. The use of this cw optical technique simplified these experiments greatly.

In order to investigate the accuracy of the assumptions used in the cw data analysis described in section 2.3, diffusion theory calculations of steady state reflectance were analyzed. Data were generated from a spatially-resolved semi-infinite diffusion model (Farrell *et al.* 1992), for a source-detector separation of 9 mm. The diffuse reflectance was calculated at each wavelength from 700 to 850 nm, assuming a scattering coefficient of 0.5 mm^{-1} at 750 nm and wavelength dependent scattering as described by van Staveren *et al.* (1991). A total hemoglobin concentration of 50 μM was assumed and the absorption spectra of oxy- and deoxyhemoglobin were used to calculate a series of reflectance spectra corresponding to hemoglobin saturations ranging from 100 to 0%. The spectra predicted by diffusion theory from the μ_s' and μ_a values were normalized and analyzed with the simple Beer-Lambert model in the same manner as an experiment. The calculated hemoglobin saturation could then be compared to the true SO_2 used in the diffusion theory forward calculations. These data are shown in Figure 4.9, in which fit saturation is plotted against input saturation. The rms error in the experiment was only 1.9% and all values agreed to within 3% with the largest deviations occurring for the intermediate SO_2 values. Since this simple Beer-Lambert technique produced such accurate results, it was considered acceptable as a comparative technique or "gold standard" for monitoring SO_2 in a tissue-simulating phantom.

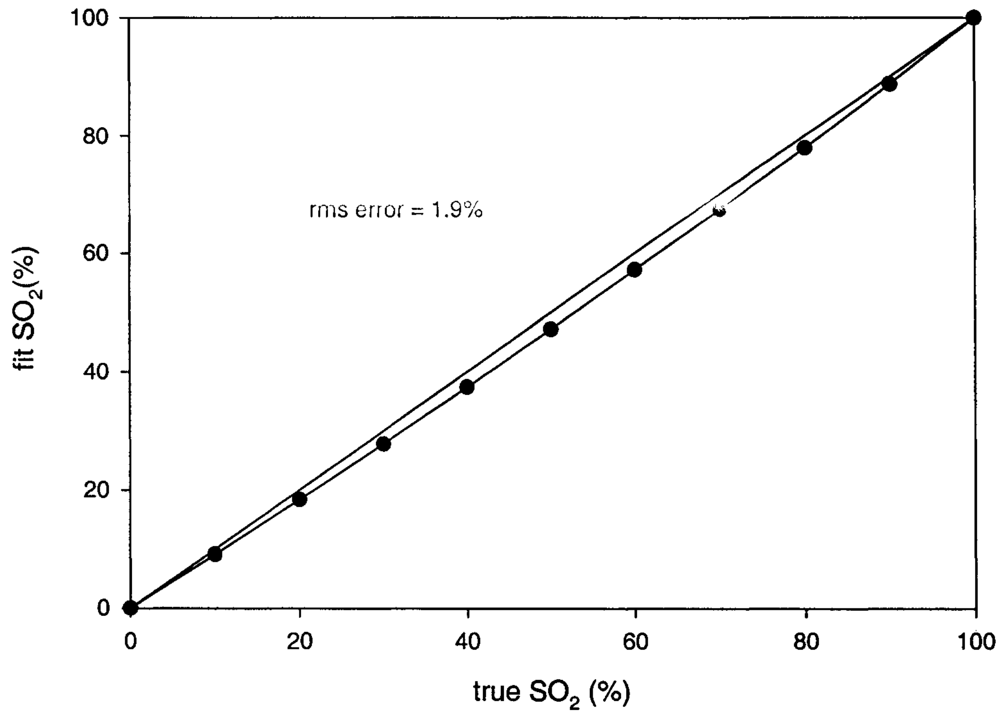

Figure 4.9: *Hemoglobin saturation estimated by application of a simple Beer-Lambert law to forward generated diffusion theory calculations for a homogeneous medium with scattering similar to muscle ($\mu_s' = 0.5\ mm^{-1}$) versus true saturation.*

4.3.3 Measurements correlated with cw system

The performance of the time-resolved system was then investigated in a homogeneous liquid phantom by comparison to the gold standard. The scattering coefficient of this phantom was 1 mm^{-1} at 750 nm and the concentration of hemoglobin was 39 μM. Deoxygenation of the phantom was performed and the reflectance was measured using the two optical techniques. The hemoglobin saturation was calculated for each method over the course of the experiment. The comparison of these two measurements is shown in Figure 4.10 and the corresponding rms error in the two-wavelength system was 4.2%. Good agreement was demonstrated between the two optical methods of measuring hemoglobin saturation in a homogeneous semi-infinite geometry. Although negative SO_2 values have no physical meaning, they result from errors in the estimated absorption coefficients. An overestimate of the μ_a value at 750 nm will result in an overestimate of [Hb] and SO2 values less than zero. It would be possible to constrain SO2 to the range 0 to 1, but this was not done to demonstrate the ability of the system to measure the full range of hemoglobin saturation values.

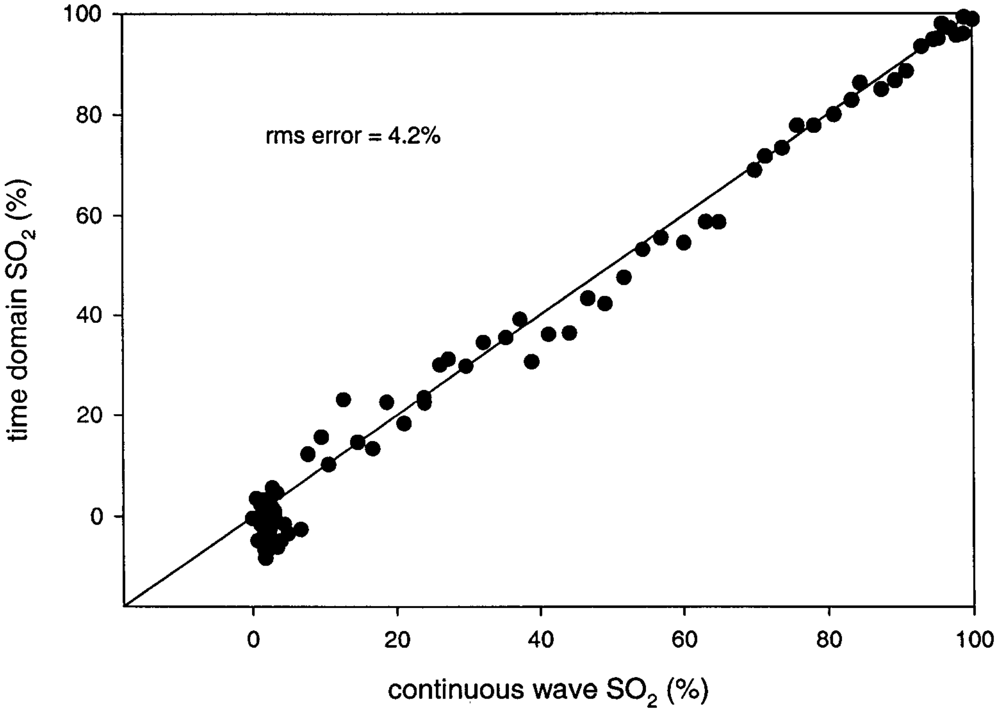

Figure 4.10: Hemoglobin saturation measured with time domain system plotted against that measured with continuous wave system. The line of equality is also shown. The measurement was performed in a homogeneous blood/yeast/Intralipid phantom.

5 MEASUREMENTS IN TWO-LAYER PHANTOMS

As previously discussed, a two-layer phantom may represent more accurately the actual architecture of tissue than the homogeneous model presented in the previous section. It may be possible to analyze time-resolved reflectance data from these measurements with a simple, homogeneous diffusion theory model and recover the bottom layer absorption and hence, hemoglobin saturation. Theoretical results are presented to show that this is possible in principle and to verify the accuracy of the diffusion theory model. Following a theoretical test of the model, an experimental verification of the measurement system was performed. Measurements in a layered geometry were performed where the absorption of the bottom layer was varied by the addition of ink to simulate hemoglobin saturation changes. Finally, experiments with the blood and Intralipid phantom described in section 3.4 were performed. The thickness and optical properties of the top layer were varied to represent different anatomical conditions.

5.1 Theoretical investigations

Previous research suggests that it may be possible to determine the absorption coefficient of the bottom layer in a two-layer system using a time domain technique and a suitable source-detector separation (Farrell *et al.* 1998). For example, at the ρ value used in these experiments, 20 mm, a homogeneous time-resolved diffusion theory model recovered the bottom layer absorption to within 9% for a two-layer Monte Carlo simulation of a 1.5 mm thick skin layer on a semi-infinite fat layer. Both Monte Carlo and forward generated diffusion theory calculations of reflectance will be studied to investigate the accuracy of this approach.

Photon transport through a two-layer structure was simulated using the Monte Carlo technique. The semi-infinite bottom layer had optical properties similar to that of muscle and the top layer had properties equivalent to either fat or skin. The principles of the Monte Carlo method are well known, therefore only specific details of these simulations are reported. The incident light was a pencil beam of photons normal to the skin surface. Photon histories were tracked until the photon escaped from the surface at a radial distance, ρ, from the source. Only those photons incident on a 1 mm wide annulus centered at 20 mm were scored. The time resolution was 4 ps and the scattering angle was sampled using the Henyey-Greenstein phase function with anisotropy factor of 0.9. Typically, 50 million individual histories were tracked.

Input optical properties were chosen to simulate different tissues and the bottom layer absorption was varied to simulate different hemoglobin saturation conditions. The bottom layer thickness was fixed to be large (2000 mm ~ semi-infinite) and the top layer thickness was variable. Also, it was necessary to simulate measurements at two wavelengths (750 and 810 nm) to be able to determine a simulated hemoglobin saturation. Although the scattering coefficient and the top layer absorption were chosen to be identical for the different wavelengths, the bottom layer absorption was wavelength dependent.

The first set of Monte Carlo data simulated a 1.5 mm skin layer (μ_a = 0.02 mm^{-1} and μ_s' = 1.5 mm^{-1}) over a semi-infinite muscle layer (μ_s' = 0.5 mm^{-1}). Six different values of μ_a in the bottom layer were simulated to produce data at two wavelengths corresponding to three different oxygenation states. The time-resolved reflectance data from the simulations were then analyzed with the homogeneous diffusion theory model. Best fit values of μ_a were used to calculate a value of SO_2 using the same technique as the oxygenation experiments equation (13). The results from this simulation are shown in Table 6 as actual and recovered hemoglobin saturation and concentration. The errors observed in estimating hemoglobin saturation in this two-layer system with a homogeneous model were less than 5% for a range of oxygenation conditions. The largest errors occurred at the intermediate SO_2 values. The success of this approach demonstrates that, in theory, bottom layer oxygenation can be estimated using a simple diffusion theory model for skin over muscle.

Oxygen Status	[tHb] (μM)		SO_2 (%)	
	actual	recovered	actual	recovered
oxygenated	45.1	46.5	100	99.2
intermediate	45.2	46.8	49.7	54.9
deoxygenated	45.3	47	10.1	13.0

Table 6: Results of fitting two-layer Monte Carlo data with homogeneous model.

The disadvantage of using Monte Carlo techniques to simulate experiments is that they are time consuming. To generate simulated data for a range of experimental conditions, it is necessary to perform many separate runs. Reflectance must be generated for every oxygenation state and for every anatomical situation (skin or varying fat layer thickness), as well as for each wavelength used. The high computational cost of this endeavor lead to an alternate approach. Since diffusion theory and Monte Carlo simulations should be in agreement at this large ρ value and it is quicker to generate forward diffusion theory predictions of reflectance, diffusion theory was as an alternative. It was necessary to confirm the agreement between diffusion theory and Monte Carlo results for these conditions.

The two-layer diffusion model used was developed by Kienle *et al.* (1998) and modified by Alexandrakis *et al* (1998). The results from the two-layer diffusion calculations were shown to be in good agreement with the Monte Carlo simulations in their research. There were errors at early times, as expected, due to inaccuracy of diffusion theory when photons are minimally scattered. The application of an extrapolated boundary condition improved their results in comparison with earlier work. Although good agreement between the calculated reflectances was observed, there were errors in the optical properties recovered by the two-layer model. In these studies, they were initially attempting to recover the optical properties of both the top and bottom layers and the top layer thickness. In the time-domain, the optical properties of both layers could be recovered from the model if the top layer thickness was known (Kienle *et al.* 1998).

The reflectance predicted by diffusion theory calculations and Monte Carlo simulations for a 5 mm fat layer over a semi-infinite muscle layer are shown in Figure 5.1 for a ρ value of 20 mm. Qualitatively, there is agreement between the two methods, although differences in the falling edges are evident. The agreement between Monte Carlo and diffusion theory at this ρ value was confirmed for other conditions. Although small differences were observed, the results were similar enough to justify the use of diffusion theory calculations of reflectance to study system performance.

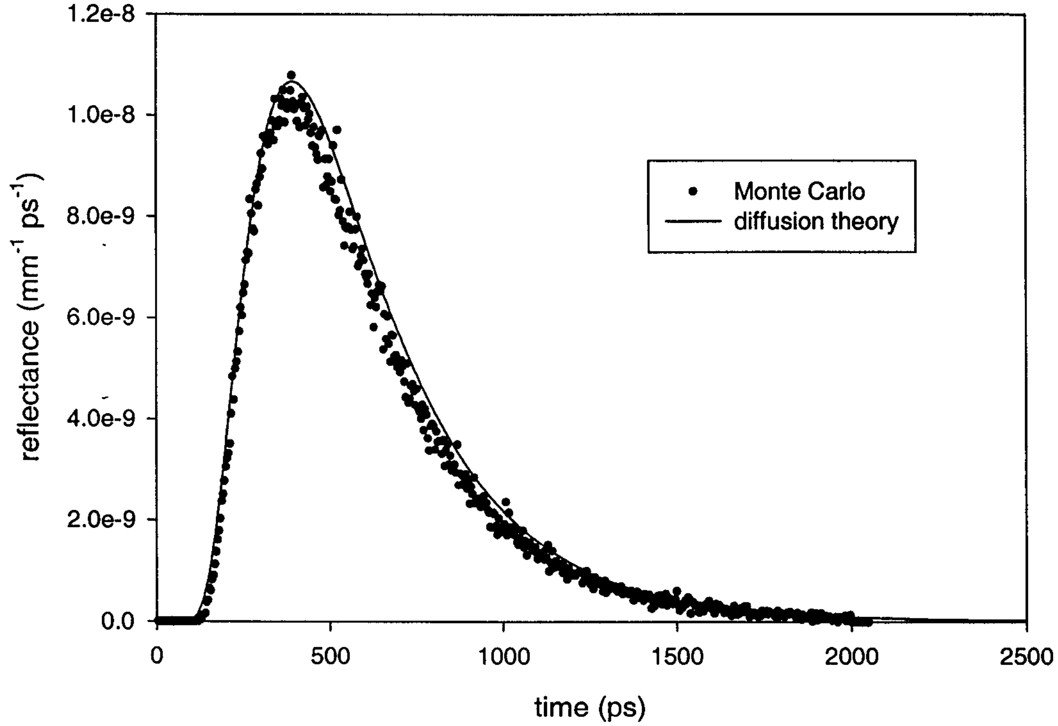

Figure 5.1: *Diffuse reflectance collected at 20 mm from a 5 mm fat layer on top of a semi-infinite muscle layer for both Monte Carlo calculations and two-layer diffusion theory results.*

5.2 Two-layer measurements with Ink

Experimental verification of the system performance was accomplished through the use of a two-layer tissue-simulating phantom. Bottom layer absorption was varied through the addition of ink to simulate deoxygenation. This simple protocol eliminated potential difficulties of using blood and deoxygenating with yeast and should provide an estimate of the errors expected. Measurements were performed on an Intralipid phantom where the semi-infinite bottom layer had a reduced scattering coefficient typical of muscle, 0.5 mm^{-1} and the addition of ink provided increased absorption. The top layer simulated fat, μ_a = 0.003 mm^{-1} and μ_s' = 1.0 mm^{-1} or skin, μ_a = 0.02 mm^{-1} and μ_s' = 1.5 mm^{-1}. The fat layer thickness was varied from 0 to 10 mm by changing the spacing between the probe and the membrane separating the two layers (see Figure 3.5), while the skin thickness was set to be either 0 or 1.5 mm. The measurement at 0 mm gave an estimate of the true bottom layer optical properties. It was confirmed that a measurement through the membrane gave a result identical to a measurement made directly in the bottom layer. Measurements were performed at both wavelengths at ρ = 20 mm. The amount of ink added to the bottom layer was selected to provide a range of absorption values similar to those anticipated during a deoxygenation experiment.

The optimum fitting range for homogeneous measurements was determined in section 4.1.3 to be about 0 to 1 GHz. However, to obtain maximum information from the bottom layer in a two-layer system, it was necessary to eliminate some of the high frequency information; in the time domain, this is analogous to preferentially examining only later times when the detected photons have traveled deeper into the tissue. To determine the optimum fitting range for the two-layer experiments, data were fitted over different ranges and compared to the measurement at 0 mm thickness. The data from this direct bottom layer measurement of μ_a were fitted over the range of 0 to 1 GHz, in accordance with the homogeneous results. The data from this experiment are plotted in Figure 5.2 as estimated absorption versus maximum frequency fit. As high frequency data was eliminated from the analysis the estimated μ_a was close to the homogeneous result. If the frequency range was further limited, too few data points are included in the fit. It was determined that the maximum frequency to fit for the two-layer measurements was between 0.5 and 0.6 GHz. This fitting range was used for all subsequent analyses.

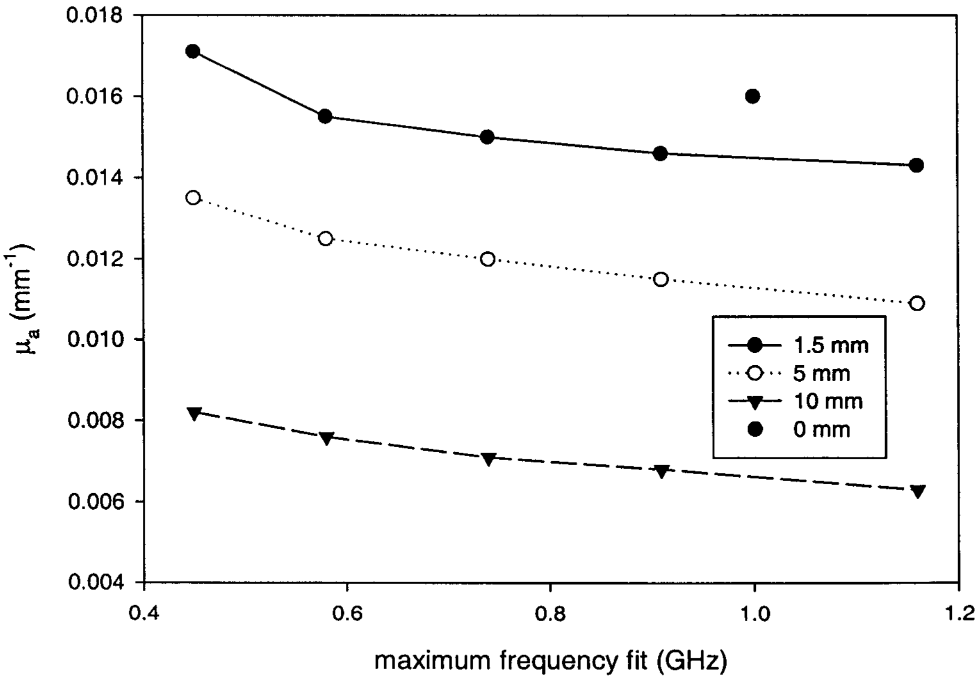

Figure 5.2: Variation of measured μ_a versus maximum frequency fit for two-layer experiment. The true value is assumed to be the absorption measured at 0 mm.

The results from these experiments are shown in Figure 5.3 and 5.4, as measured absorption through the top layer versus the absorption coefficient measured with the probe directly in contact with the membrane. The calculated scattering coefficient remained constant throughout all experiments to within about 10%. Figure 5.3 shows the results from the measurement of absorption through a skin layer at (a) 810 nm (b) 750 nm. The skin layer had little effect over the range of absorption coefficients measured. Regression analysis was also performed on the entire data set and is shown in Table 7. For the skin measurements, both the slope of the measured versus expected curve and the R^2 value were close to 1, indicating the accuracy of the measurement.

Measurement top layer / λ (nm)	slope	y-intercept (mm^{-1})	R^2
Skin / 810	1.03 ± 0.05	$(0.5 \pm 7) \times 10^{-4}$	0.998
Skin / 750	1.03 ± 0.05	$(-1 \pm 9) \times 10^{-4}$	0.999
Fat 1.5 mm / 810	0.91 ± 0.06	$(7 \pm 6) \times 10^{-4}$	0.977
Fat 1.5 mm / 750	0.97 ± 0.07	$(0.3 \pm 1.0) \times 10^{-3}$	0.972
Fat 5 mm / 810	0.65 ± 0.04	$(1.8 \pm 0.5) \times 10^{-3}$	0.977
Fat 5 mm / 750	0.69 ± 0.05	$(1.8 \pm 0.6) \times 10^{-3}$	0.978
Fat 10 mm / 810	0.30 ± 0.03	$(2.7 \pm 0.3) \times 10^{-3}$	0.958
Fat 10 mm / 750	0.32 ± 0.02	$(3.4 \pm 0.2) \times 10^{-3}$	0.985

Table 7: Results of regression analysis on measured versus actual μ_a for various experiments using ink to simulate absorption changes.

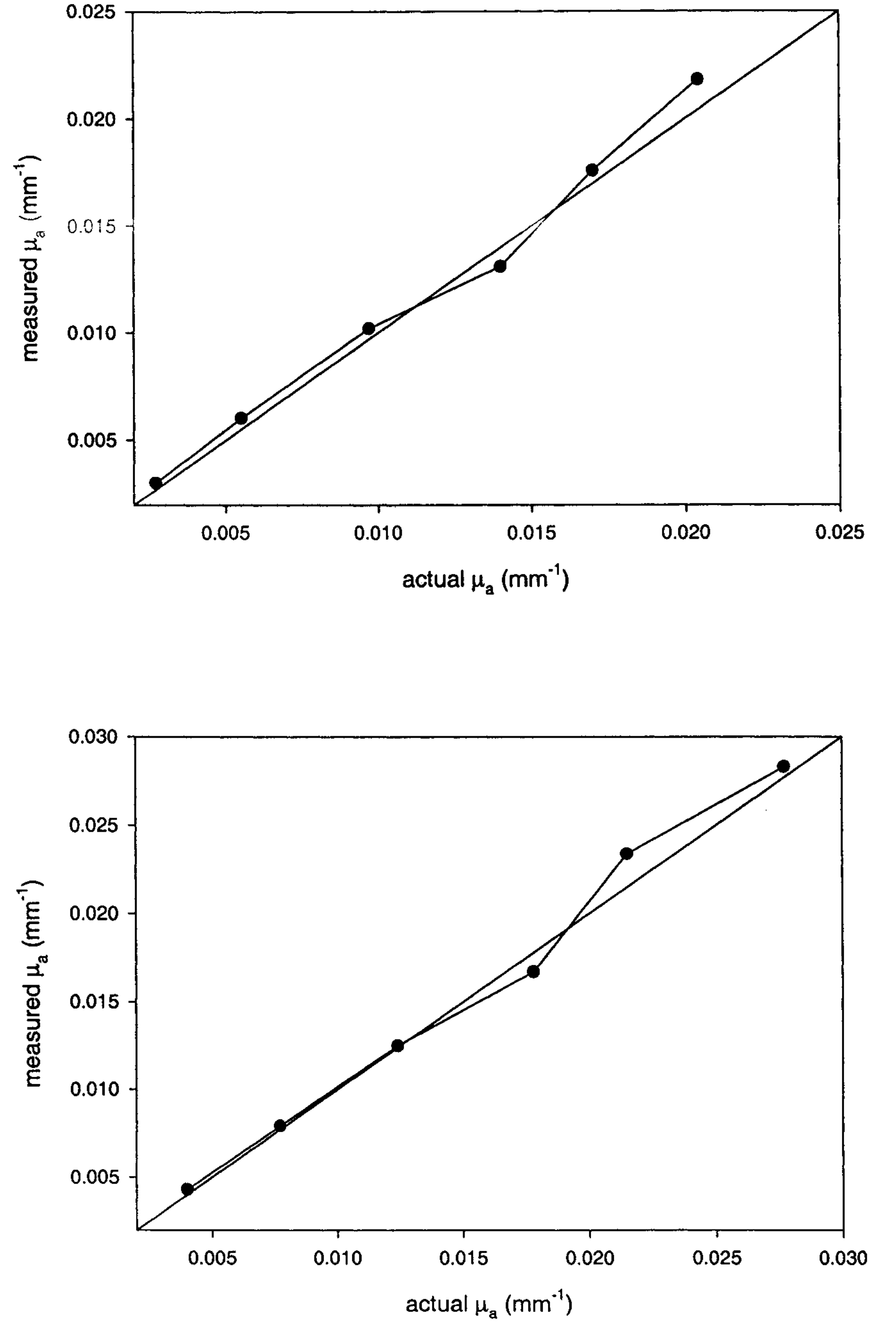

***Figure 5.3:** Measured μ_a through a 1.5 mm skin layer versus μ_a measured directly in the bottom layer for measurements at (810 nm) and (b) 750 nm.*

The measurements performed with increasing fat thickness are displayed in Figure 5.4 at (a) 810 nm and (b) 750 nm. For the thinnest layer (1.5 mm) there was good agreement between the μ_a value measured through the top layer and the actual value. However, as the top layer thickness increased, the measured absorption deviated from the true bottom layer absorption, as expected. From Table 7, the slope of the measured versus true curves decreased from 0.97 ± 0.07 to 0.30 ± 0.03 as the fat layer thickness increased. The slope would approach zero as the top layer thickness increased. Eventually, variations in the bottom layer would be completely obscured by the thick top layer. At 5 and 10 mm, the measured absorption decreased because more of the photons traveled only in the low absorbing top layer, resulting in a lower absorption recovered by the homogeneous model. Although the bottom layer absorption was underestimated by measuring through a 10 mm fat layer, the increase in absorption was still linear. Since the calculation of SO_2 is based on the ratio of μ_a values, it is possible that errors in saturation could be less than the errors in the absorption coefficients themselves. This conjecture is examined in the next section.

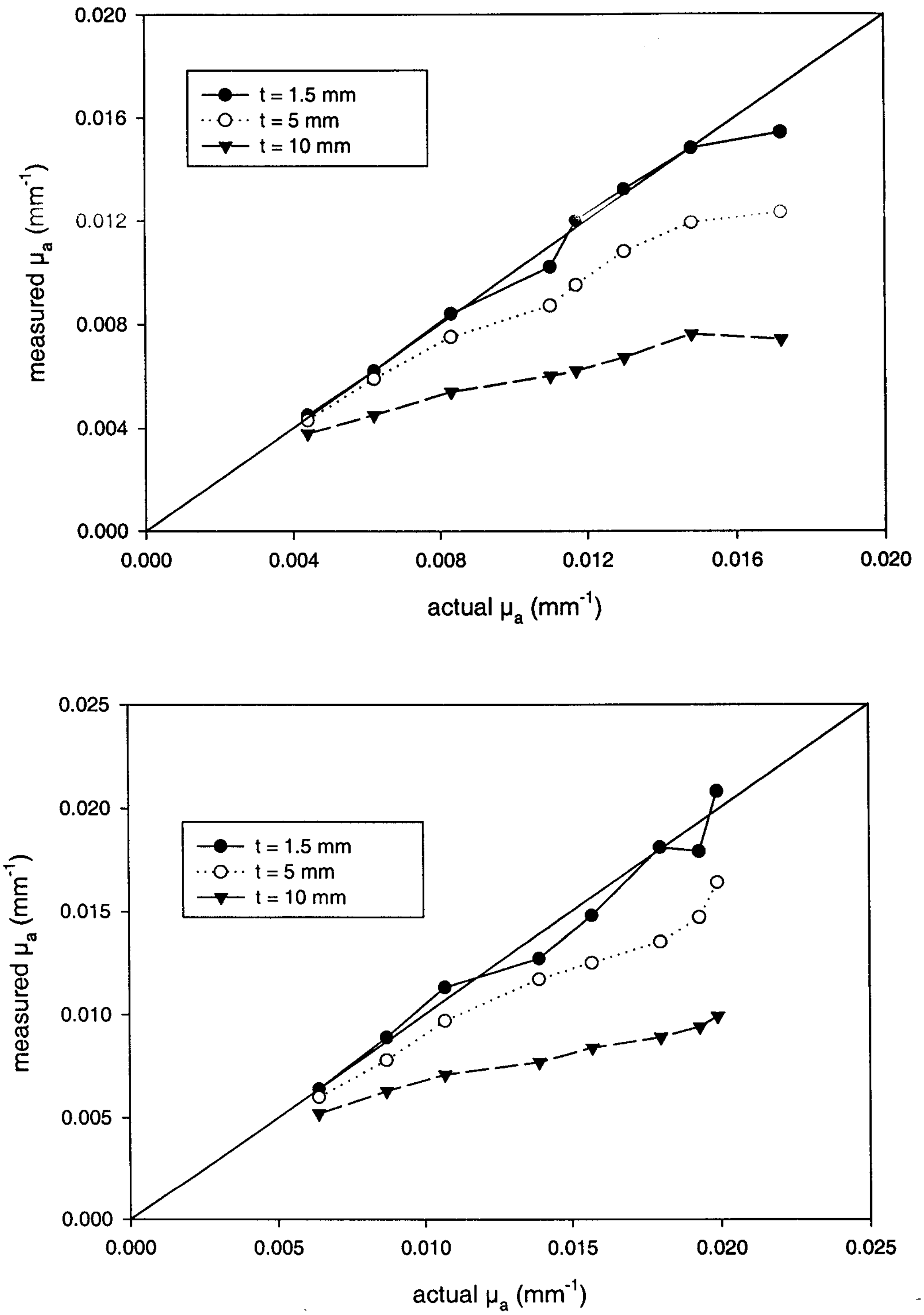

***Figure 5.4:** Measured μ_a through fat layer versus μ_a measured in the bottom layer for measurements at (a) 810 and (b) 750 nm. The thickness of the fat layer varied from 1.5 to 10 mm.*

5.3 Hemoglobin oxygenation experiments in a two-layer phantom

In order to interpret results obtained from actual two-layer oxygenation measurements, the accuracy of both the homogeneous model and the experimental apparatus were first investigated. The expected system performance in recovering bottom layer oxygenation was tested by using the experimental data, such as that shown in Figure 5.3 and 5.4, to predict measured saturation versus true saturation. At each wavelength and for each top layer (i.e. 1.5 mm skin, 1.5, 5, and 10 mm fat), a straight line was fitted to the measured μ_a versus true μ_a data. These linear fits could then be used to calculate the μ_a we would expect to measure for any true value of the bottom layer absorption coefficient. Thus for an arbitrary hemoglobin concentration and SO_2 in the bottom layer, we could calculate the true values of μ_a at 750 nm and 810 nm, the values we would expect to recover at the two wavelengths, and hence the SO_2 value we would recover. The accuracy of the system in determining bottom layer oxygenation can be estimated for various anatomical situations, over a range of saturation values and any hemoglobin concentration.

To study shortcomings in the homogeneous model alone for monitoring oxygenation changes in a semi-infinite layer with an overlying skin or fat layer, two-layer diffusion theory calculations of reflectance were generated using the model of Alexandrakis *et al.* (1998). Diffusion theory at this large source-detector separation was shown to be in agreement with two-layer Monte Carlo data (section 5.1). Since it is computationally more expensive to generate Monte Carlo data corresponding to different anatomical situations, wavelengths, and absorption values, diffusion theory was used.

Top layer optical properties were chosen to simulate either fat or skin and bottom layer scattering was chosen to be that of muscle. Absorption coefficients in the bottom layer were calculated for a range of oxygenation conditions and a hemoglobin concentration equivalent to that used in the corresponding deoxygenation experiment. The μ_a values at 750 and 810 nm were calculated from the known spectra of Hb and HbO_2 for a range of SO_2 values from zero to unity. The two-layer diffusion theory reflectance was then fit with the homogeneous diffusion model presented in section 2.1 over the same frequency range as the experimental data to obtain estimates of scattering and absorption. The absorption coefficients from the homogeneous fit were then used with equations (13) and (1) to generate hemoglobin saturation and equation (14) to obtain total hemoglobin concentration.

In this section the quantity of interest has been the absorption coefficient however, the behaviour of the reduced scattering coefficient can also be examined. For the ink experiments, as the top layer of fat increased from zero (presumably an estimate of the bottom layer scattering) to 10 mm, the μ_s' estimated from the homogeneous model increased from 0.65 ± 0.04 mm^{-1} to 0.91 ± 0.06 mm^{-1} at 750 nm. As the top layer thickness increased, the μ_s' value became more similar to the actual top layer scattering coefficient. The same effect was observed with the theoretical data where the estimated μ_s' value increased from 0.55 to 1.08 mm^{-1} as the top layer thickness varied from 1.5 to 10 mm of fat. Again the homogeneous model predicted a scattering similar to the bottom layer (0.5 mm^{-1}) when the top layer was thin and a μ_s' value comparable to the top layer value (1 mm^{-1}) with a thicker top layer. Fortunately, hemoglobin saturation is estimated from the absorption coefficient returned by the homogeneous model

Four oxygenation experiments using the blood-yeast-Intralipid phantom described in section 3.4 were performed corresponding to skin (1.5 mm) on muscle and fat on muscle, where the thickness of the fat layer was 1.5 mm, 5 mm or 10 mm. The time-resolved reflectance data were analyzed with the homogeneous diffusion model to provide estimates of μ_a and μ_s'. From the absorption coefficients estimated, the corresponding SO_2 values were calculated. Simultaneous continuous wave measurements of reflectance provided a value for the actual hemoglobin saturation determined from a measurement directly in the bottom layer of the two-layer phantom. These two values of SO_2 were then compared for the entire deoxygenation experiment. The accuracy of the time-resolved method was quantified by calculating the rms error in SO_2 and comparing the average value of [tHb] calculated to its known value.

Typical time courses of hemoglobin saturation as measured by the two methods are shown in Figure 5.5. The phantom used in this experiment was designed to simulate a 1.5 mm fat layer on top of a semi-infinite muscle layer. The agreement between the two values of SO_2 was excellent in this case. Initially, there is a slow decrease in SO_2 because the phantom is warming up and the yeast is becoming activated and due to the sigmoidal shape of the hemoglobin oxygen dissociation curve. Until the oxygen partial pressure drops below 80 mm Hg, there is little change in hemoglobin saturation (see Figure 4.8). The middle portion of the curve is fairly linear and it then plateaus at low SO_2 values. Once this plateau was reached, it was assumed that the phantom was fully deoxygenated. This had been previously confirmed by measurements with the oxygen electrode.

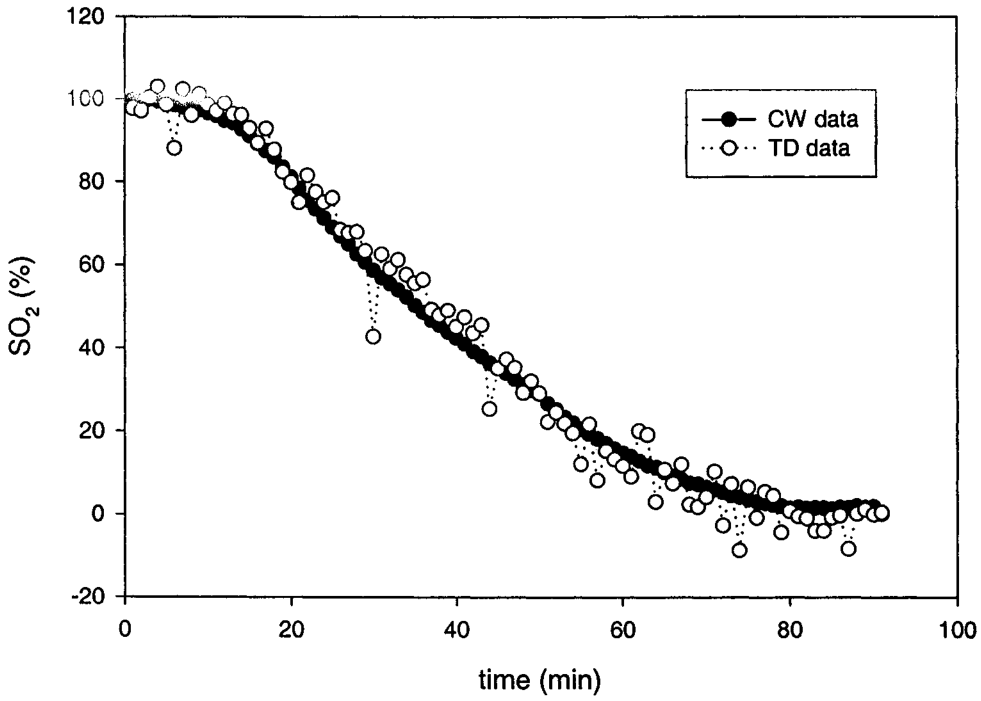

Figure 5.5: Time course of hemoglobin saturation as determined by time domain (TD) and continuous wave (CW) measurements for a phantom simulating 1.5 mm of fat on top of muscle.

For this experiment the time to deoxygenate the phantom was about ninety minutes and measurements were performed every minute. Before the blood and yeast were added to the Intralipid phantom, the baseline optical properties were measured in a single layer (homogeneous) geometry. This provided an estimate of the background absorption of the liquid phantom. The background absorption should be due to water alone, but at low μ_a values (0.002 to 0.0026 mm^{-1}) there are errors in the absorption coefficient as determined by the time-resolved system. The effect of this background estimate will be discussed in detail later.

Each graph in Figures 5.6 to 5.9 shows two predictions of the performance of the two wavelength system in measuring SO_2 and one direct test. To recap, the first prediction is based solely on diffusion theory calculations in which a two-layer model was used for forward calculation of the time-resolved reflectance, and a homogeneous model was used to recover μ_a and hence SO_2. The second prediction is based on experiments where the homogeneous model was used to estimate μ_a from measurements made on two-layer phantoms and the true value of μ_a was found from time-resolved measurements directly on the bottom layer. Both these methods assumed a hemoglobin concentration equivalent to that used in the actual experiment. Finally, the direct test of system performance was made in two-layer phantoms containing blood in the bottom layer. The true SO_2 value of this blood was known from the cw optical measurements performed directly on the bottom layer

Data summarizing the results from the simulations (theoretical and experimental) and the deoxygenation experiment for the case of a 1.5 mm skin layer over a muscle layer are displayed in Figure 5.6. The SO_2 measured by the time-resolved system is plotted versus the SO_2 determined by a direct bottom layer measurement. From the ink experiments, the SO_2 from the measurement through the top layer is compared to the direct measurement and for the simulation, the fit value of saturation is compared to the value determined from the known (input) absorption coefficient values. The rms error shown is for the actual deoxygenation experiment.

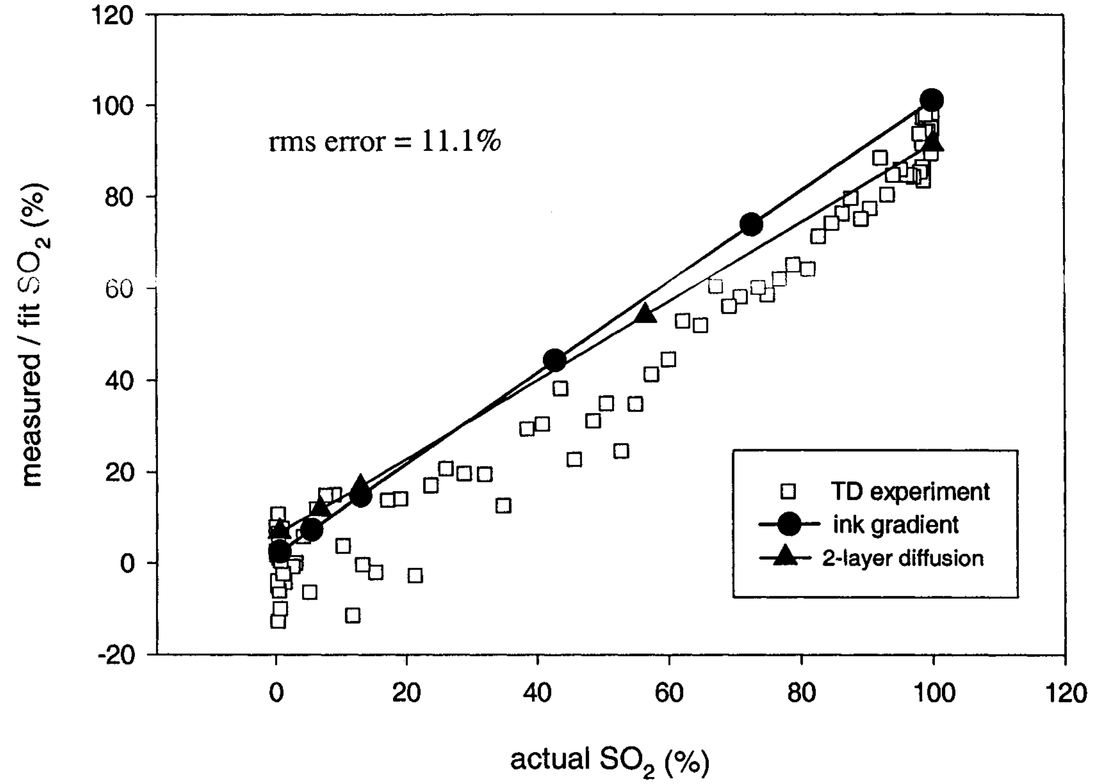

Figure 5.6: Measured or fit hemoglobin saturation plotted against actual SO_2 for skin on muscle experiment. Data from the deoxygenation experiment using the blood-yeast-Intralipid phantom, the simulated ink experiment and the two-layer diffusion theory simulation are shown. The rms error corresponds to the accuracy of the time-resolved measurement of SO_2 relative to the actual SO_2.

The experiment simulating skin on muscle (Figure 5.6) showed good correlation between the experimental SO_2 and the actual SO_2, for both ink and blood experiments, but there was a systematic underestimate of SO_2 in the blood experiments. The rms error in estimating the SO_2 with the time-resolved measurements compared to with the cw method with the two-layer blood phantom was 11.1%, while it was only 5.8% according to the diffusion theory predictions and 1.6% in the ink experiments. Although the skin layer is thin, it does have a high value of μ_s' and significant absorption, which affect the collected reflectance and produce the 11% error in hemoglobin saturation.

The presence of a 1.5 mm fat layer, which has both a lower μ_s' and a lower μ_a value than skin, will perturb the results less than the skin layer, as seen in Figure 5.7. The 1.5 mm fat layer showed the best results of all four data sets. The rms error in the SO_2 in this experiment was only 4.9% for the blood experiments. This is comparable to the error observed in the experiment with a homogeneous medium, which was 4.2% (section 4.3.3). The rms errors predicted by diffusion theory and the ink experiments were 0.6% and 1.2% respectively. High accuracy in estimating saturation can be obtained when measuring bottom layer absorption through a thin fat layer with this system.

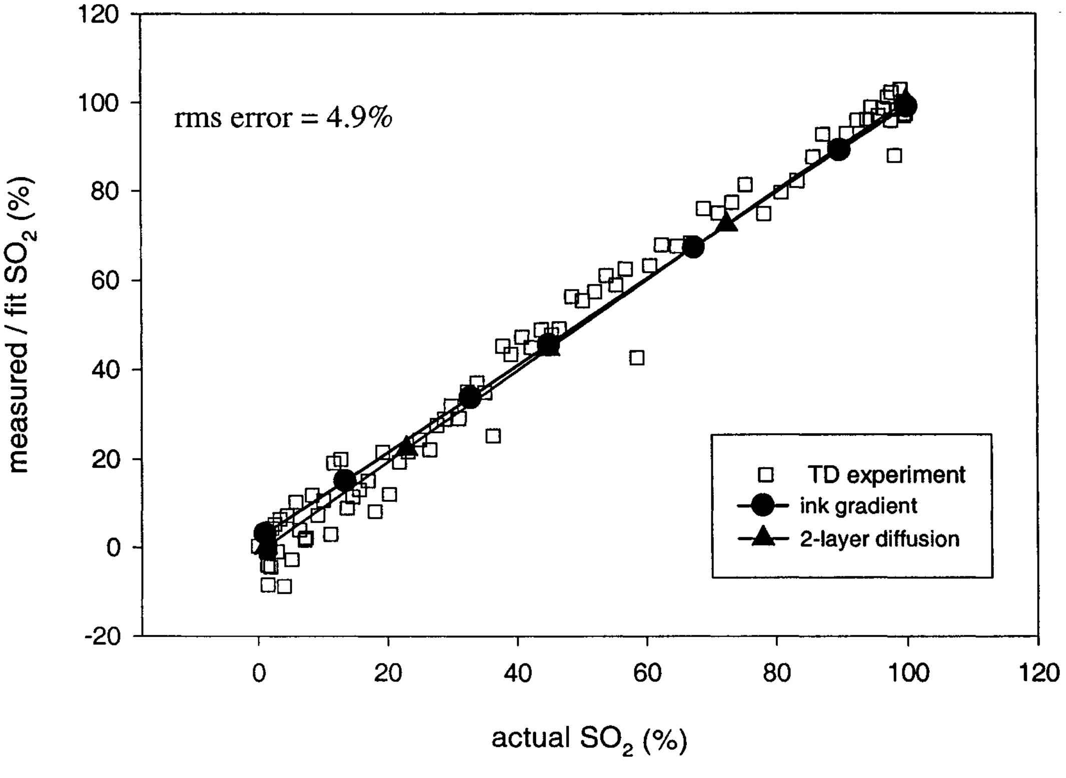

Figure 5.7: Measured or fit SO_2 plotted against actual SO_2 for 1.5 mm fat on muscle experiment. Data from the deoxygenation experiment using the blood-yeast-Intralipid phantom, the simulated ink experiment and the two-layer diffusion theory simulation are shown.

When the fat layer thickness increased to 5 mm (Figure 5.8), the diffusion theory calculations showed smaller errors than either experimental data set; the rms error was 3.0%. The error primarily resulted from measurements at low SO_2 values, the agreement was good when the phantom was well oxygenated. Again the results obtained from the two experiments were similar. The rms error in SO_2 when measuring the blood phantom was only 5.2%, only slightly larger than the errors obtained from the thinner fat layer or the homogeneous measurement. Even through a 5 mm thick fat layer, it was possible to estimate the hemoglobin saturation of the bottom (muscle) layer of the tissue-simulating phantom to within about 5%. The error slightly exceeded what would be expected according to the analysis of two-layer diffusion theory calculations of reflectance with the simple homogeneous diffusion model.

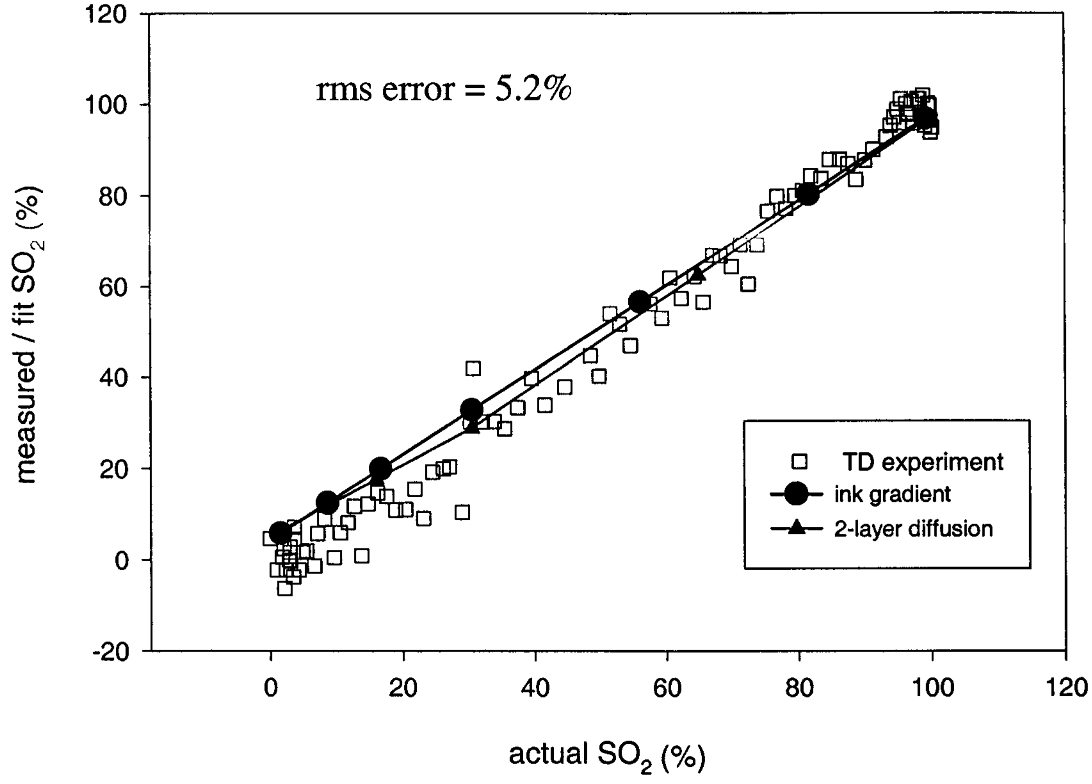

Figure 5.8: Measured or fit hemoglobin saturation plotted against actual SO_2 for 5 mm fat on muscle experiment. Data from the deoxygenation experiment using the blood-yeast-Intralipid phantom, the simulated ink experiment and the two-layer diffusion theory simulation are shown.

The system performance was poorest for the case simulating a 10 mm fat layer over a muscle layer, but the accuracy was considerably better for the experimental data than would be expected from diffusion theory (Figure 5.9). The experimental simulation and the blood-yeast-Intralipid phantom data showed similar accuracy. The rms error in hemoglobin saturation was 8.2% for the blood phantom as compared to 24.4% predicted by diffusion theory. The ink experiment predicted an rms error of 6.4%, comparable to what was found in the direct measurements. The agreement between theory and experiment was reasonable at high values of SO_2, but as the saturation decreased the differences increased; the absolute difference in saturation between measured and theoretical was about 30% at the lowest saturation. In this case, the experimental results were more accurate that the diffusion model predicted

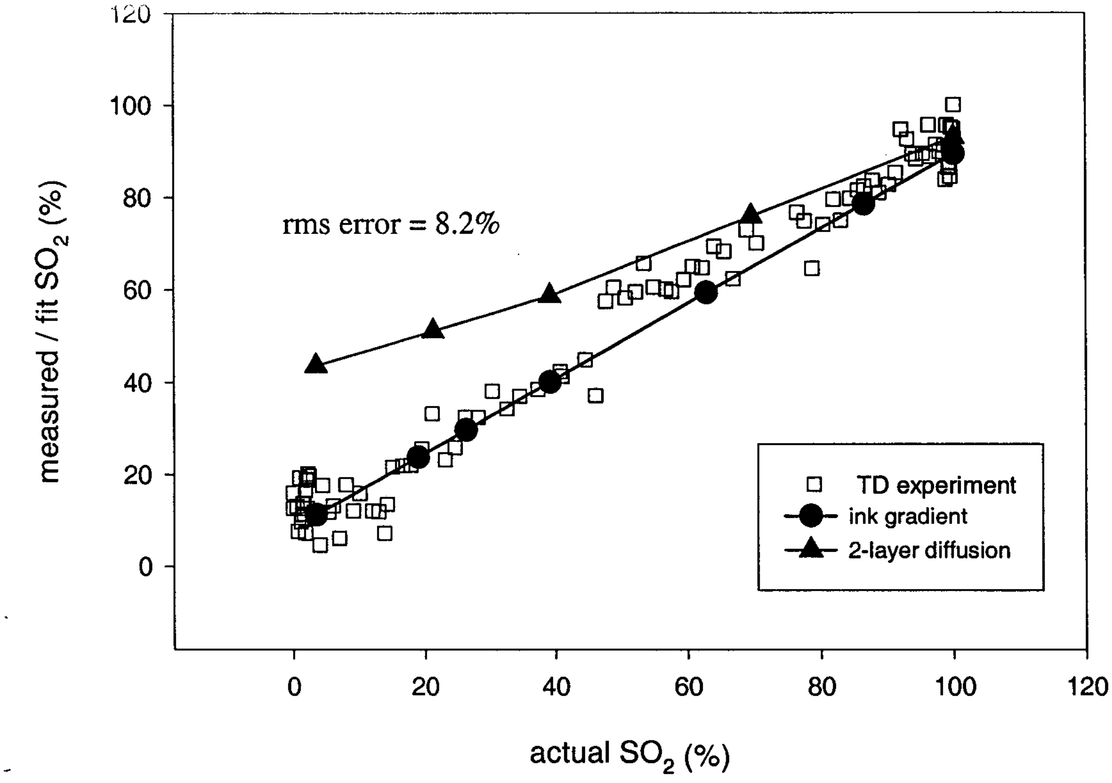

***Figure 5.9**: Measured or fit hemoglobin saturation plotted against actual SO_2 for 10 mm fat on muscle experiment. Data from the deoxygenation experiment using the blood-yeast-Intralipid phantom, the simulated ink experiment and the two-layer diffusion theory simulation are shown.*

A summary table of the rms errors in determining the hemoglobin saturation in the bottom layer of a two-layer system is shown below (Table 8). Results from all simulations and experiments are presented corresponding to each anatomical situation modeled. The rms errors from the experiments were similar in most cases. For the 1.5 mm layers (both skin and fat), the ink experiments produced results that were closer to the actual values than the experiments with blood in the bottom layer. The larger errors observed in the deoxygenation experiments could be due to the more complicated nature of the experimental procedure or due to the small errors associated with the cw technique itself. The cw technique had a 2% rms error when compared to theoretical data. The rms errors obtained from the analysis of two-layer diffusion theory calculations of reflectance showed some differences from the experiments. As mentioned, large differences were observed with the 10 mm thick fat layer. Although the other fat layer thicknesses showed better agreement with the experiment. For the 1.5 mm thick skin layer, the theoretical error was less than observed in the blood experiment but greater than that observed with the ink gradient measurements. The origin of these differences was unclear.

Top layer (bottom layer = muscle)	root-mean square error (%)		
	2-layer diffusion	ink gradient experiment	blood experiment
1.5 mm skin	5.8	1.6	11.1
1.5 mm fat	0.6	1.2	4.9
5 mm fat	3.0	2.9	5.2
10 mm fat	24.4	6.4	8.2

Table 8: Root-mean-square error in SO_2 from all the measurements and simulations performed.

For each experiment, it was also possible to calculate a measured and expected total hemoglobin concentration. For the simulated experiments, the [tHb] values were chosen to be equivalent to those used in the experiments and absorption coefficient values were determined accordingly. For the deoxygenation experiment, a knowledge of the volume of red blood cells added to the known phantom volume allowed for determination of true [tHb]. A comparison of the measured and true values is given in Table 9 for all experiments and all sites.

Measurement Method	True [tHb] (μM)	Measured [tHb] (μM)	% error in [tHb]
1.5 mm skin			
ink gradient experiment	37	38.6	4.3
2-layer diffusion	37	37.9	2.4
experimental	37	48	-23
1.5 mm fat			
ink gradient experiment	58	55.4	-4.5
2-layer diffusion	58	56.6	-2.4
experimental	58	54	-6
5 mm fat			
ink gradient experiment	51	38.1	-25.2
2-layer diffusion	51	52.1	2.2
experimental	51	39	-23.5
10 mm fat			
ink gradient experiment	55	22.5	-59.2
2-layer diffusion	55	32.2	-41.5
experimental	55	32	-42

Table 9: Measured and true total hemoglobin concentrations from the four experimental situations. Results from simulated and actual experiments are shown. The measured [tHb] represents the average over all time points.

For the estimation of total hemoglobin concentration, the most accurate results were obtained with the 1.5 mm fat layer. At a thickness of 5 mm, the theoretical error remained low but experimentally the error in [tHb] increased to about 24%. At 10 mm, all methods agreed that the [tHb] would be greatly underestimated. The value of [tHb] is dependent on the absorption sampled by the detected light, so it should decrease as the light travels further in the top layer (which has significantly less absorption than the bottom layer). A thicker, low absorbing top layer tends to mask the bottom layer absorption, causing the model to fit a lower value of absorption and hence underestimate [tHb] in the layer. From the blood-yeast-Intralipid deoxygenation experiments, the standard deviation in [tHb] from the time-resolved measurements was about 5 μM and the error in the true value was similar, 4 μM. Therefore, only the measurement through the 1.5 mm fat layer produced results that were in agreement with the actual value (58 ± 4 versus 51 ± 5 μM).

As expected, the best results, for both SO_2 and [tHb] were obtained with the 1.5 mm fat layer. For the situation corresponding to 5 mm of fat on muscle, the accuracy observed from the experimental data exceeded that expected from the diffusion theory calculations when measuring SO_2. However, the estimation of hemoglobin concentration was less accurate experimentally than it was according to the analysis of the theoretical calculations. The accuracy of the system in estimating SO_2 decreased further when the top layer thickness increased to 10 mm. However, even though the accuracy decreased, it did not deteriorate as much as would be expected from the theoretical results. These results are consistent with previous clinical results where it was observed that NIR light penetrates into fat on average a depth equal to half the source-detector separation when the fat thickness is between 4.0 and 10.0 mm (Homma *et al.* 1996). Therefore, for a source-detector separation of 20 mm, the average penetration depth would be about 10 mm and information from the bottom layer should be obtainable, as observed in these experiments. All measurements agreed that the hemoglobin concentration would be greatly underestimated for a 10 mm thick fat layer.

The rms error in estimating SO_2 in a homogeneous phantom was 4.2% when comparing time-resolved measurements to the cw technique. When two-layer measurements were performed, the error in estimating SO_2 increased from 5% to 8% when the fat layer thickness increased from 1.5 to 10 mm. The errors in estimating [tHb] also increased with increasing fat layer thickness up to about 40%. Since the estimate of SO_2 is dependent on the ratio of absorption coefficients measured, any linear change in absorption will provide a reasonable estimate of SO_2. The total hemoglobin concentration determined, however is dependent on the absolute value of the absorption coefficients measured and hence, will be less accurate as a thicker top layer masks the true bottom layer absorption. These experimental errors represent a best-case scenario since tissue is certainly more irregular and complex than the samples investigated here.

The background absorption for all the experiments described was measured in the phantom before the addition of red blood cells. This gave an accurate measurement of $\mu_a(\lambda)_{\text{background}}$ which should correspond to the absorption of water at the wavelength of interest for our phantom. However, the system typically overestimated the absorption of water at both wavelengths. Using the true wavelength dependent water absorption as a background (Hale and Querry 1973) produced less accurate results for these measurements. The data from the experiments with increasing fat layer thickness were

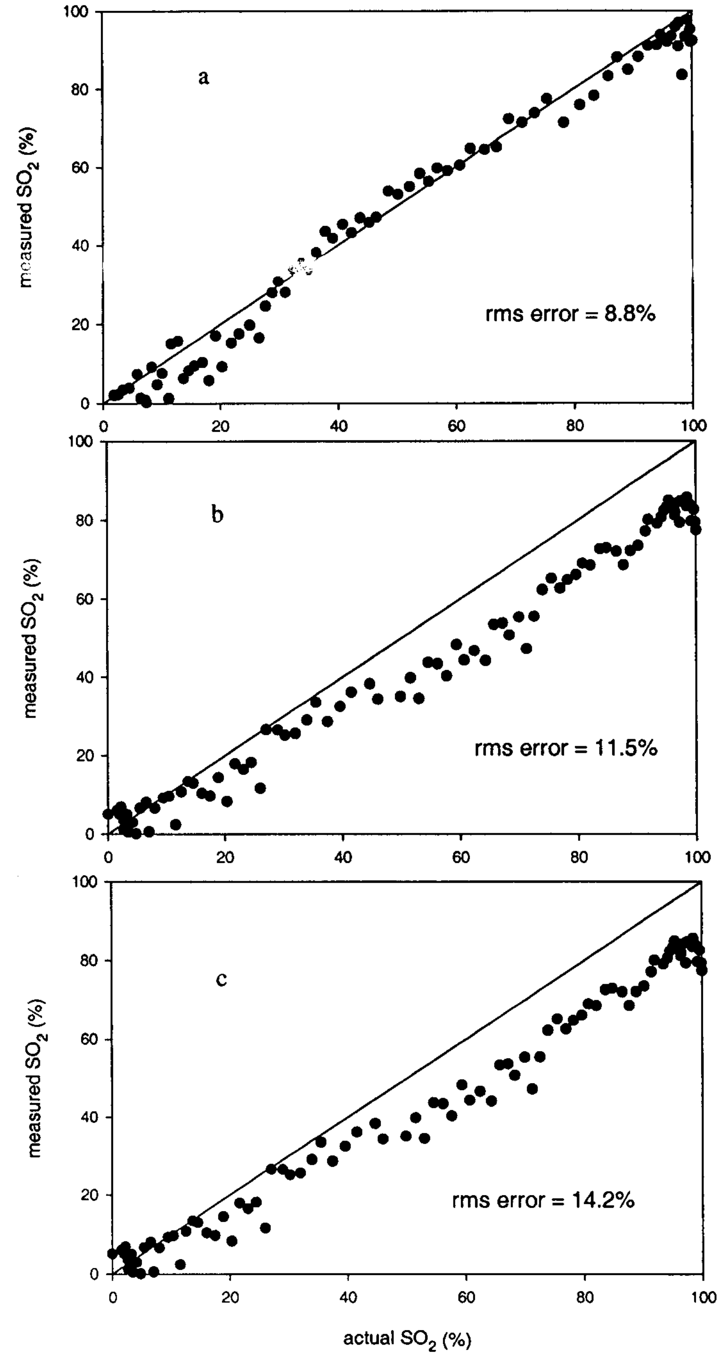

Figure 5.10: Measured hemoglobin saturation plotted against actual SO_2 for (a) 1.5 mm fat layer (b) 5 mm fat layer and (c) 10 mm fat layer. The rms error is also shown. Data were analyzed assuming background absorption equivalent to water.

analyzed assuming the background absorption was exactly that of water at each wavelength and the results are presented in Figure 5.10(a-c). In each case, the rms error increased when the background absorption was assumed to correspond to water. For the experiment simulating a 1.5 mm fat layer over muscle, the error increased from 4.9% to 8.8%. Similar changes were observed for the 5 mm layer (5.2% to 11.5%) and 10 mm layer (8.2% to 14.2%). In an *in vivo* experiment it would not be possible to measure the background absorption alone, so it may be necessary to add a third wavelength which would be used to provide a measurement of the background absorption. This would not only account for water absorption but any other chromophore that may be present, assuming the absorption spectrum of the chromophore was relatively featureless.

The time-resolved measurement system utilized in these experiments was able to recover hemoglobin saturation in the bottom layer of a two-layer system with an accuracy that depended on the nature and the thickness of the top layer. Errors greater than 10% were observed when the top layer was skin. For cases where fat was the overlying layer, the errors ranged from 5% to 8% as the fat layer thickness increased. The system was less successful in predicting total hemoglobin saturation; as fat layer thickness increased large errors were observed. These results depended on *a priori* knowledge of the background absorption, a condition not possible if the system is to be useful *in vivo*. In the next chapter, the use of this system for *in vivo* measurements was investigated.

6 IN VIVO MEASUREMENTS

In chapter 5, the ability of the measurement system to monitor oxygenation changes in a realistic two-layer phantom model was examined. Hemoglobin saturation in the bottom layer was successfully determined when the top layer was a thin fat layer. As the top layer thickness increased, the accuracy of the system decreased. The accuracy of the technique in determining hemoglobin concentration deteriorated more quickly than did the saturation accuracy. The final test of the time-resolved system is to investigate its performance *in vivo*. Measurements have been performed by other authors primarily on the skull and muscles in the extremities. The current measurement system is best suited to determining saturation in muscle or subcutaneous tumors. Unfortunately, a suitable comparative technique is not readily available. The system samples a finite tissue volume that encompasses both arteries and veins and hence, a pulse oximeter or sampling of blood would not provide an accurate measure of oxygenation. The *in vivo* experiments described here are only qualitative and will not be compared to other measurements.

In vivo measurements were performed on the anterior side of the forearm midway between the elbow and wrist. The forearm is an ideal location due to the fact that there is usually little fat in the area and occlusion experiments in the arm are possible. The combined top layer thickness (skin and fat) for these measurements was approximately 5 mm. The optical probe was fixed in place with a strap to limit motion artifacts and covered to prevent stray light from entering. Since the model assumed a homogeneous medium, care was taken to ensure the probe was not located near visible superficial blood vessels. The effect of vessels was investigated by Liu *et al.* (1995b) and found to be significant. The source-detector separation used was 20 mm and the collection time was typically 30 seconds. The index of refraction of tissue was assumed to be 1.4 and the boundary was assumed to be matched. Since a background measurement was not possible, it was assumed that the background was water, at a concentration of 70% in the tissue.

The first experiment was designed to estimate the stability of the measurement. Twenty consecutive measurements at 30 second intervals were performed on the forearm of a healthy human volunteer. Time-resolved reflectance at two wavelengths was fitted with the homogeneous diffusion model to provide estimates of the reduced scattering and the absorption coefficient. The average values from these measurements are reported in Table 10. These results are typical of other measurements performed in our lab. As expected, the scattering coefficient decreased with increasing wavelength.

	750 nm		810 nm	
	$\mu_a \pm \sigma(\mu_a)$ (mm^{-1})	$\mu_s' \pm \sigma(\mu_s')$ (mm^{-1})	$\mu_a \pm \sigma(\mu_a)$ (mm^{-1})	$\mu_s' \pm \sigma(\mu_s')$ (mm^{-1})
mean	0.028 (0.001)	1.16 (0.02)	0.030 (0.001)	1.12 (0.03)

Table 10: Optical properties from forearm of volunteer at two wavelengths.

The absorption coefficients estimated from the model were used to determine the hemoglobin saturation and concentration using the same method discussed previously. The results from this experiment are plotted in Figure 6.1. The average value of total hemoglobin concentration was 119 ± 4 μM and the average saturation was 77 ± 4 %. These results are similar to those reported by other researchers for example, Matcher and Cooper (1994) and Fantini *et al.* (1995).

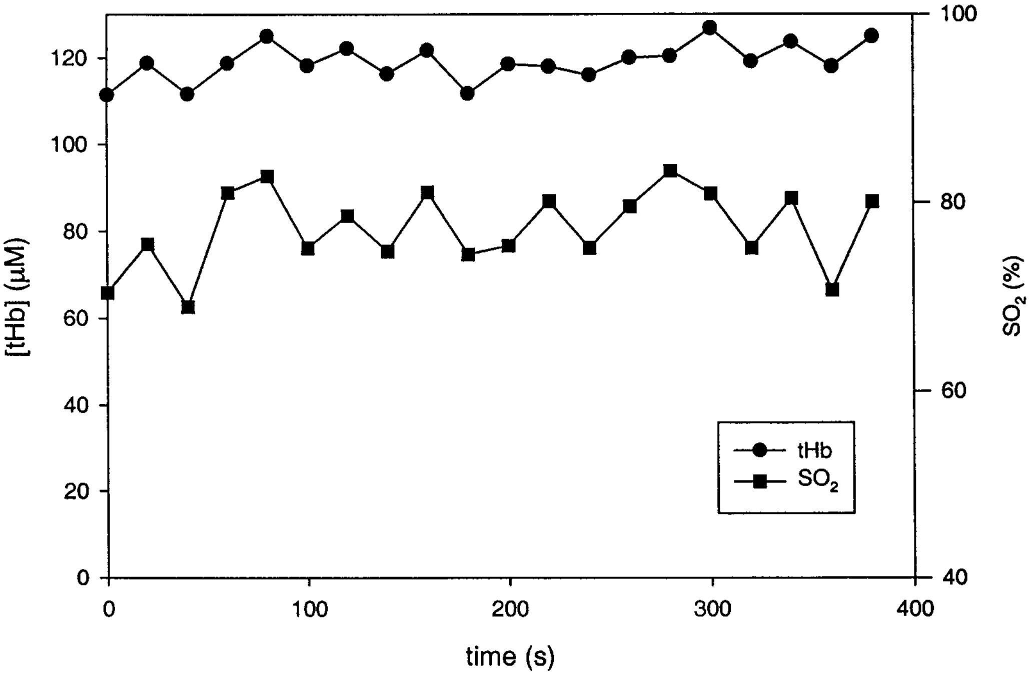

Figure 6.1: *Oxygenation parameters (tHb and SO_2) of the forearm over the course of 400 seconds.*

The above data set was analyzed assuming 70% water absorption as background and the maximum frequency fit was 0.66 GHz. These parameters were varied in order to see the effect they would have on the oxygenation properties returned by the fitting procedure. Figure 6.2 is a graph of SO_2 and [tHb] versus percent water background absorption and 6.3 shows the variation with maximum frequency fit.

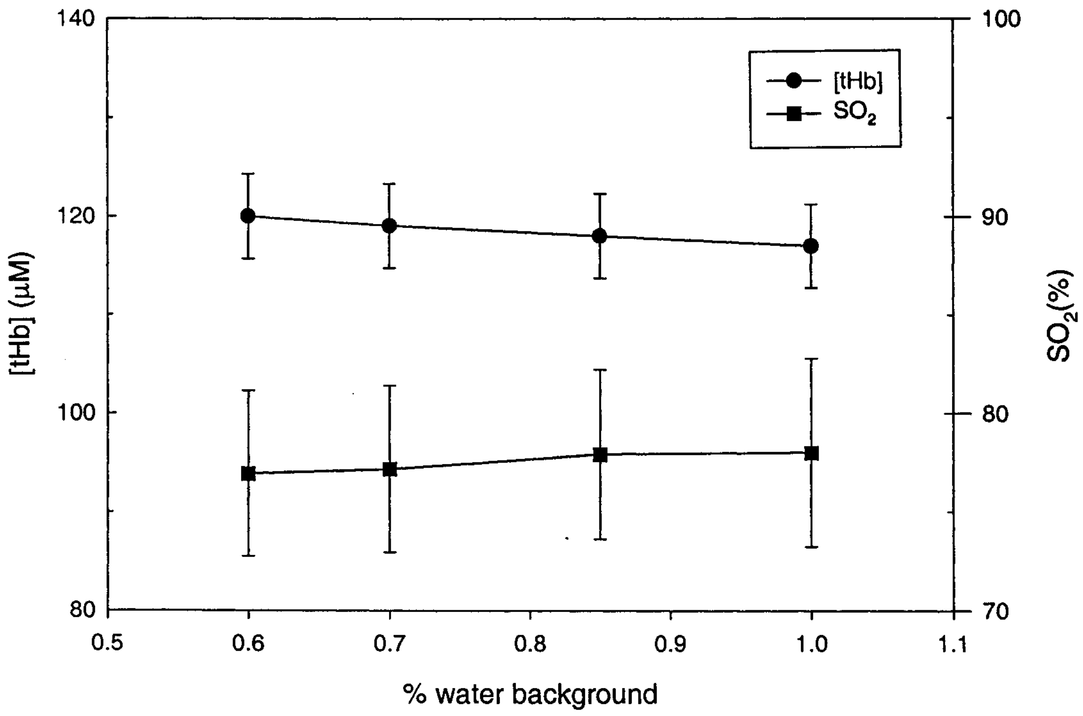

Figure 6.2: The effect of changing background absorption on SO_2 and [tHb].

Although as the percent water increased in Figure 6.2, the hemoglobin concentration decreased and the saturation increased, the changes were small and within the observed uncertainty. Similarly, there was a trend of decreasing SO_2 as higher frequencies were included in the fitting range in Figure 6.3, but the changes were not significant. The only significant change was in the hemoglobin concentration as a function of maximum frequency fit. As more high frequency information was omitted from the signal, the hemoglobin concentration increased. Limiting high frequency data should correspond to weighting towards photons that traveled deeper into tissue. Deeper penetration into tissue corresponds to examining the muscle layer more than either the skin or fat and the muscle layer has a higher hemoglobin concentration than the more superficial layers, so this results is reasonable. In general, the value of SO_2 estimated by this method does not depend on the background absorption assumed or the fitting range used, over the limits examined in these experiments.

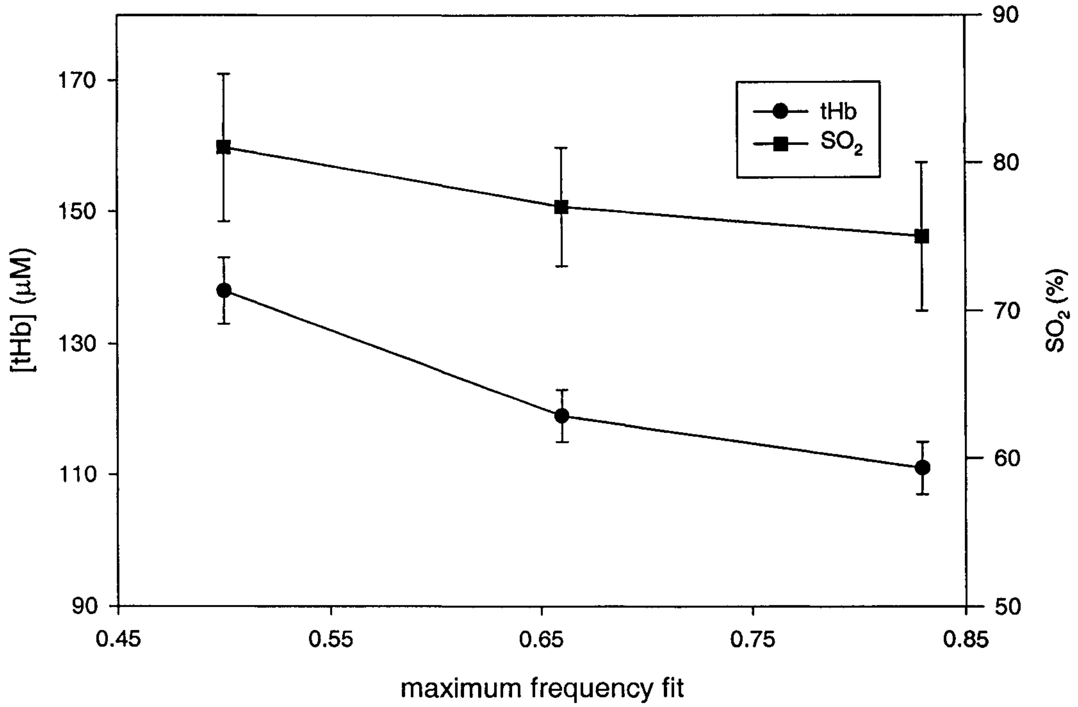

Figure 6.3: The effect of limiting the maximum frequency fit on the oxygenation parameters.

In order to demonstrate the ability of the system to monitor changes in oxygenation, occlusion measurements were performed. Measurements of tissue oxygenation were performed as described above before, during, and after arterial occlusion. The application of a blood pressure cuff on the upper arm inflated to a pressure of 220 mm Hg was used to block blood flow to the forearm. This should result in decreased hemoglobin saturation distal to the cuff as oxygen is consumed by the tissue. Release of the cuff allows for the return to normal oxygenation status. This experiment was performed on a healthy volunteer and the average baseline oxygenation parameters were $SO_2 = 63 \pm 8$ % and [tHb] = 102 ± 3 μM compared to $SO_2 = 36 \pm 7$ % and [tHb] = 106 ± 4 μM during occlusion. The change in hemoglobin saturation was significant ($p < 0.001$), while the change in concentration was not significant ($p > 0.01$). The concentration of hemoglobin should not change during the experiment, but the relative proportions of oxyhemoglobin and deoxyhemoglobin will change.

Two occlusion experiments were performed on the same volunteer, following the same protocol on different days. The results obtained were quite different; they are shown in Figure 6.4(a) and (b). The average hemoglobin concentration from Figure 6.4(a) was 111 ± 2 μM, while it was only 99 ± 2 μM in the second experiment. Although the pressure used in both experiments was the same and the duration of occlusion was similar, a much lower hemoglobin saturation value was obtained in the first experiment (30% compared to 50%) although the baseline SO_2 values were comparable in both cases (~70%). Following application of the cuff there was a decrease in saturation in both experiments, as expected. The fluctuations observed during the first experiment were larger than the second. Upon release of the cuff, there was a marked increase in saturation as normal blood flow resumed. Although no quantitative comparisons to a gold standard were made, the results obtained appear sensible and the induced oxygenation changes were detected.

The results can, however, be compared to the work of other authors. For example Casavola et al. (2000) performed measurements on the calf with a frequency domain, multi-distance, near-infrared spectrometer (ISS, Inc., Champaign, IL) and found the resting hemoglobin saturation to be about 75%. Ferrari et al. (1992) found the absorption coefficient of the forearm at 800 nm to be about 0.029 mm^{-1} under normal conditions. Sahlin (1992) conducted arterial occlusion measurements on the vastus lateralis muscle with NIRS, using a similar protocol and found that the SO_2 decreased with a half-time of 138 ± 12 s (n = 4) and restoration of blood flow occurred more rapidly with a half-time of 24 ± 2 s. For the two experiments shown in Figure 6.4 the half-time of saturation decrease was about 90 ± 10 s and recovery was about 20 ± 5 s. Although the recovery time observed was similar, the deoxygenation occurred more rapidly in the forearm than in the leg. This may be due to the fact the arteries are more superficial in the arm than they are in the leg, making them more readily occluded. Fantini et al. (1995) performed occlusion measurements in the arm and determined that hemoglobin saturation decreased from 80% to about 45% during arterial occlusion. Again, these results are comparable to the results obtained in this thesis.

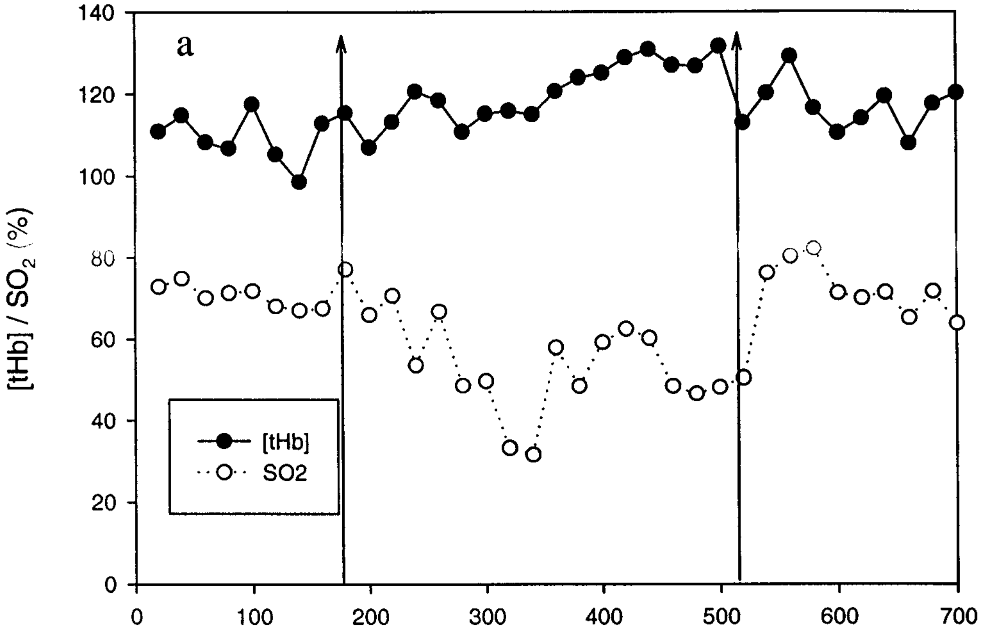

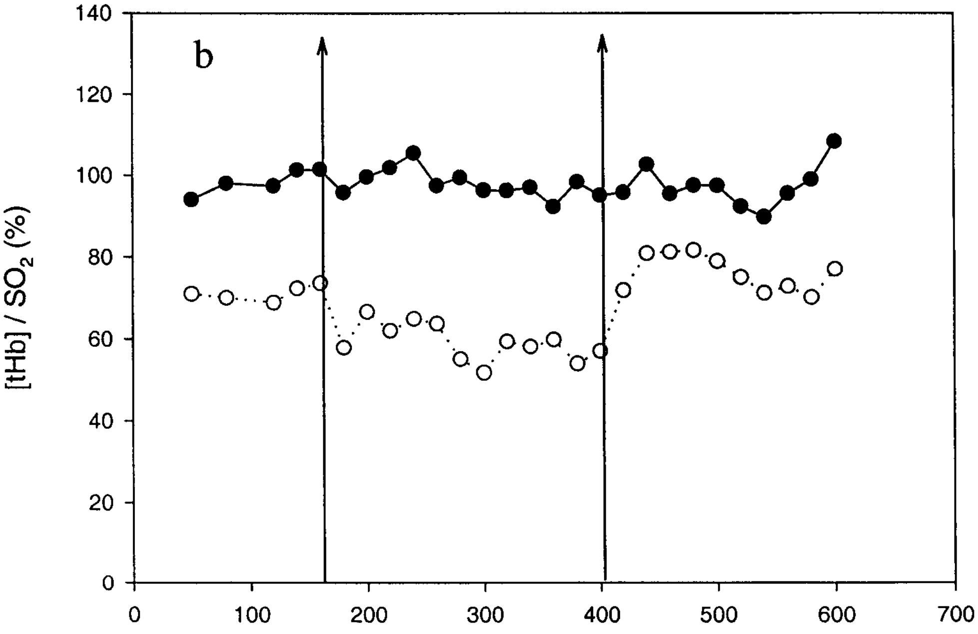

Figure 6.4(a,b): *Time traces of oxygenation parameters from two separate occlusion experiments performed on the forearm.*

These experiments were designed merely to show that the system is capable of detecting induced changes in oxygenation. The next step of this project could be to continue *in vivo* measurements. In order to make the system more feasible as a clinical device, some changes are necessary. Current technology allows for a significant reduction in the size of the electronics associated with the system – a bin of electronics can now be housed on a single card. The use of a notebook computer instead of a desktop would also increase portability. Following these changes, it would be interesting to use this system to investigate oxygenation in patients. Muscle oxygenation studies between diseased patients (peripheral vascular disease) and normal subjects, or the study of trained athletes could be conducted. It may also be interesting to study oxygenation changes during cancer treatments (PDT or radiation) and to observe whether the oxygenation status of tissue changes during the course of radiation therapy.

7 CONCLUSIONS

This thesis described the characterization of a system for the noninvasive determination of hemoglobin saturation in tissue. Determination of the optical properties of tissue provides knowledge regarding the physiological status of the sample. In the near infrared, light penetrates well into tissue, but undergoes both absorption and scattering. From the light that is scattered out of the tissue, the reflectance, it is possible to estimate the optical properties of the medium through the application of a suitable model. When measuring in turbid media, such as tissue, the diffusion approximation provides an adequately accurate model of the transport of light.

The time-resolved reflectance measurement system was used in these experiments to determine the optical properties of the samples investigated. The principle of time domain measurements is as follows: when a short, narrow pulse of light is incident on a turbid medium, it is broadened and attenuated due to scattering and absorption. The reflectance is collected and fit with the diffusion theory. It is assumed that the medium is homogeneous, semi-infinite and that there is no mismatch in the indices of refraction between the probe and the phantom. The fitted reflectance provides an estimate for the optical properties of the medium. By performing measurements at two wavelengths and exploiting the known differences in absorption between oxyhemoglobin and deoxyhemoglobin at those wavelengths, it is then possible to determine the hemoglobin saturation of the tissue. The hemoglobin saturation is the percentage of hemoglobin molecules that are bound to oxygen and is indicative of the oxygenation status of the tissue. The noninvasive determination of hemoglobin saturation has applications in monitoring cerebral oxygenation of neonates, patients with peripheral vascular disease and oxygen levels in the treatment site for both photodynamic therapy and radiation therapy.

Models of light transport in tissue typically assume that the medium being investigated is homogeneous which is not the case in tissue. Much effort has been put into developing models that account for the layered structure of tissue. However, for many applications it may not be necessary to recover the optical properties of the all the different tissue layers. A knowledge of the bottom layer absorption (and oxygenation) is the quantity of interest in many clinical applications, such as muscle oxygenation studies or studies of subcutaneous tumors. Using this time-resolved reflectance measurement system and a simple homogeneous diffusion model, it may be possible to determine bottom layer oxygenation, under certain conditions. The aim of this research was to investigate the limitations of this approach.

The time-resolved system used in these experiments differs from the standard time domain apparatus because it employs inexpensive pulsed diode lasers as light sources and uses a miniature photomultiplier tube to collect the reflectance. Previous researchers have used lasers which are large, expensive, complex, and hence not ideal for clinical use. Furthermore, the photomultiplier tube used in these studies is much less expensive than the standard tube. The diode lasers operate at 750 nm and 810 nm, wavelengths at which there are distinct absorption differences between oxyhemoglobin and deoxyhemoglobin. Their low power ensures that they are safe for *in vivo* use, yet they provide adequate signal for measurements to be possible. The system can be controlled such that they alternately irradiate the sample and hence simultaneous dual wavelength measurements can be performed.

Following system optimization, system performance was characterized by measuring samples with known optical properties. Oxygenation measurements were then performed in a homogeneous medium and compared to data from an oxygen electrode and an alternate optical technique. System performance in a two-layer geometry was studied through the use of diffusion theory calculations to simulate a deoxygenation experiment in a two-layer system and a simpler experiment using ink to simulate hemoglobin saturation changes in a two-layer tissue-simulating phantom. A direct test of system performance was demonstrated by comparing hemoglobin saturation and concentration measured by the time-resolved method to an alternate method. Finally, preliminary *in vivo* measurements of hemoglobin saturation were performed on human volunteers.

Time-resolved measurements of reflectance were fitted to the time-resolved semi-infinite diffusion model of light transport to provide estimates of the optical properties of the samples under investigation in the various experiments discussed throughout this thesis. To improve the speed of fitting, the Fourier transform of the data was fitted in the frequency domain. The differences between experimental and theoretical phase and modulation were iteratively minimized to provide a best estimate of the optical properties of the medium being investigated. From the absorption coefficient determined, it was then possible to calculate the concentrations of oxy- and deoxyhemoglobin in the sample which are used to calculate the hemoglobin saturation and concentration.

Since hemoglobin saturation is the primary quantity of interest, it is necessary to have another method of measuring this parameter. Initial measurements were compared to measurements from an oxygen electrode. This was an indirect technique as the data provided was pO_2 which was then converted to SO_2 using the accepted hemoglobin-oxygen dissociation curve. Due to this fact and other difficulties with the electrode measurements, an optical technique involving spectrally resolved white light reflectance was developed as a gold standard for comparison.

The time-resolved system was characterized by examining the effects of counting statistics on the results and measurement stability. A study to determine the optimum weighting factors used by the fitting routine for phase and modulation was performed. A relative weighting factor (modulation:phase) of 1000:1 for homogeneous measurements and about 200:1 for layered measurements was found to produce the most accurate results. Also, an investigation of the optimum data fitting range in a homogeneous geometry was undertaken. For these measurements, the best results were obtained when the data was fitted over a range of frequencies from 0 to 1 GHz. Measurements in layered phantoms revealed that a range of frequencies from 0 to 0.5 GHz provided the best estimates of the bottom layer optical properties.

System performance was characterized by the accuracy of the estimated optical properties returned. Changes in scattering were introduced by varying the concentration of Intralipid or polystyrene spheres in a liquid phantom. It was found that the scattering coefficient could be estimated to within about 10% for a wide range of μ_s' values (0.5 to 1.5 mm^{-1}). Measurements using increasing ink concentrations were performed to determine the accuracy of the system in estimating μ_a. A more accurate comparison was obtained from measurements using MnTPPS and it was found the system was quite accurate in measuring the absorption properties of a tissue-simulating phantom; errors were less than 10%.

Oxygenation measurements were then performed in a tissue-simulating phantom. The phantom was composed of a blood/yeast/Intralipid mixture which was heated, activating the yeast which consumed oxygen in the phantom. Measurements of time-resolved reflectance and pO_2 from an oxygen electrode were performed for the duration of the deoxygenation experiment. Time-resolved measurements of SO_2 were used to construct an experimental hemoglobin-oxygen dissociation curve. These curves (from three separate experiments) were then compared to the standard curve. The expected results were $p_{50} = 25.95 \pm 1.43$ mm Hg and $n = 2.46 \pm 0.05$ (Zwart *et al.* 1984) and the results from the data were $p_{50} = 23.6 \pm 3.5$ mm Hg and $n = 2.32 \pm 0.55$.

It would be preferable to compare to a direct measure of hemoglobin saturation, so the continuous wave method of determining hemoglobin saturation was used in all subsequent experiments. The validity of the simple Beer-Lambert model used in the analysis of the cw reflectance was first confirmed through the use of forward generated diffusion theory calculations of reflectance. The error introduced by this simple model was small, about 2% in SO_2. Time-resolved and cw measurements of hemoglobin saturation were found to be in good agreement. The rms error in SO_2 for the time-resolved system was only 4.2% when compared to the cw results in a homogeneous phantom.

After system performance was validated in a homogeneous geometry, it was necessary to extend the measurements to two-layer phantoms. Theoretical results show it should be possible to estimate bottom layer absorption in a two-layer system at a source-detector separation of 20 mm. By eliminating high frequency data from the fitting region, photons that have penetrated deeper into the tissue will contribute more to the collected signal.

Diffusion theory calculations of reflectance from a two-layered medium were analyzed with the simple homogeneous diffusion model to investigate the accuracy of the model in determining bottom layer hemoglobin saturation. Experiments where the absorption of the bottom layer of a two-layer phantom was increased to simulate changes in SO_2 by increasing the ink concentration were also undertaken to investigate the system performance. These two predictions of system performance were done for a range of effective SO_2 values from 0 to 100% for the specific conditions used in the actual deoxygenation experiments. The total hemoglobin concentration was chosen to match the experiments and the properties of the layers were identical as well. A direct test of system performance was conducted by measuring time-resolving reflectance through various top layers to determine bottom layer hemoglobin saturation and total concentration and comparing to the cw measurements made directly in the bottom layer of the phantom.

It was found that the accuracy of the system in estimating SO_2 was strongly dependent on the top layer properties. In all these experiments, the bottom layer was designed to simulate muscle of varying degrees of oxygenation. When the top layer was a thin skin layer, the rms error in the time-resolved measurements was 11.1% for the actual oxygenation experiment, higher than predicted from either simulated experiment. However, for a 1.5 mm fat layer, the rms error was only slightly larger than that observed in the homogeneous measurement; its value was only 4.9%. The rms error in SO_2 increased as the fat layer thickness increased to 5 mm (5.2%) and to 10 mm (8.2%). Except for the measurements through a 10 mm thick top layer, the simulated experiments and the direct oxygenation measurements were comparable. The simulated experiments with a 10 mm thick top layer showed poorer results than the actual experiment.

The system accuracy in measuring [tHb] was also studied. The best results were obtained with the 1.5 mm top layer, but the accuracy decreased rapidly as the top layer thickness increased. At 10 mm the hemoglobin concentration was underestimated by about 40%. Since the determination of SO_2 is based on the ratio of absorption coefficients, it is not surprising that it is more accurately determined that the [tHb] value which depends on the absolute value of μ_a determined from the time-resolved measurement.

Finally, the system's ability to measure hemoglobin saturation and total concentration was investigated *in vivo*. Although no quantitative comparisons to alternate measurement techniques were made, it was found that the system responded to oxygenation changes as expected. Induced deoxygenation through the use of a blood pressure cuff on the arm of a volunteer could be followed through the SO_2 determined by the time-resolved system. Results obtained from these experiments were comparable to those obtained by other researchers.

The next step in the development of this system should be to continue with *in vivo* measurements. In its current configuration, this system is not suitable to be used a clinical instrument. To make the system more practical as a clinical device, the system must be made more compact and portable. The size of the electronics associated with the system can be significantly reduced to a single computer card. The use of a notebook computer instead of a desktop would also increase portability. Once the system was made portable, it would be interesting to use this system to investigate hemoglobin saturation in patients. Muscle oxygenation studies of patients with compromised circulation, i.e. peripheral vascular disease or trained athletes could be undertaken. The efficacy of cancer treatments, PDT or radiation, may also be increased by studying oxygenation changes during the treatments time. The effectiveness of both treatments depends upon the presence of oxygen in the treatment region. A study of the oxygenation during the course of radiation therapy would also be an interesting venture. Studies of tumor oxygenation would be best applied to large, superficial tumors, such as head and neck cancers, due to the intrinsic limitations of the measurement system identified in this research.

8 REFERENCES

Aldrich, C.J., J.S. Wyatt, J.A. Spencer, E.O.R. Reynolds, and D.T. Delpy. 1994. The effect of maternal oxygen administration of human fetal cerebral oxygenation measured during labour by near infrared spectroscopy. *Br.J.Obstet.Gynaecol.* 101:509-513.

Aldrich, C.J., D. D'Antona, J.A. Spencer, D.T. Delpy, E.O. Reynolds, and J.S. Wyatt. 1996. Fetal heart rate changes and cerebral oxygenation measured by near-infrared spectroscopy during the first stage of labour. *Eur.J.Obstet.Gynecol.Reprod.Biol.* 64:189-195.

Alexandrakis, G.A., T.J. Farrell, and M.S. Patterson. 1998. Accuracy of the diffusion approximation in determining the optical properties of a two-layered turbid medium. *Applied Optics* 37:7401-7409.

Alexandrakis, G.A., T.J. Farrell, and M.S. Patterson. 2000. Monte Carlo diffusion hybrid model for photon migration in a two-layer turbid medium in the frequency domain. *Applied Optics* 39:2235-2244.

Boushel, R. and C.A. Piantadosi. 2000. Near-infrared spectroscopy for monitoring muscle oxygenation. *Acta Physiol.Scand* 168:615-622.

Bruulsema, J.T., J.E. Hayward, T.J. Farrell, and M.S. Patterson. 1997. Correlation between blood glucose concentration in diabetics and noninvasively measured tissue optical scattering coefficient. *Optics Letters* 22:190-192.

Casavola, C., L.A. Paunescu, S. Fantini, M.A. Franceschini, P.M. Lugara, and E. Gratton. 1999a. Application of near-infrared tissue oxymetry to the diagnosis of peripheral vascular disease. *Clin.Hemorheol.Microcirc.* 21:389-393.

Casavola, C., A. Paunescu, M.A. Franceschini, S. Fantini, L. Winter, J. Kim, D. Wood, and E. Gratton. 1999b. Near-infrared spectroscopy and the tilting table protocol: a novel method to study the blood flow and the oxygen consumption of tissue. *Proc.SPIE* 3597:685-692.

Casavola, C., L.A. Paunescu, S. Fantini, and E. Gratton. 2000. Blood flow and oxygen consumption with near-infrared spectroscopy and venous occulusion: spatial maps and the effect of time and pressure of inflation. *Journal of Biomedical Optics* 5:269-276.

Chance, B., S. Nioka, J. Kent, and K. McCully. 1988. Time-resolved spectroscopy of hemoglobin and myoglobin in resting and ischemic muscle. *Annals of Biochemistry* 174:698-707.

Chance, B., E. Anday, S. Nioka, S. Zhou, L. Hong, K. Worden, C. Li, T. Murray, Y. Ovetsky, D. Pidikiti, and R. Thomas. 1998. A novel method for fast imaging of brain function, non-invasively, with light. *Optics Express* 2:411-423.

Cheatle, T.R. and S.P. Coleridge. 1991. Pulse oximetry: a new non-invasive assessment of peripheral arterial occlusive disease. *Br J.Surg.* 78:889

Cheong, W.F., S.A. Prahl, and A.J. Welch. 1990. A Review of the Optical Properties of Biological Tissues. *IEEE J.Quant.Elect.* 26:2166-2185.

Conover, D.L., B.M. Fenton, T.H. Foster, and E.L. Hull. 2000. An evaluation of near-infrared spectroscopy and cryospectrophotometry estimates of haemoglobin oxygen saturation in a rodent mammary tumour model. *Phys.Med.biol.* 45:2685-2700.

Cope, M. The Development of a Near Infared Spectroscopy System and its Application for Non Invasive Monitoring of Cerebral Blood and Tissue Oxygenation in the Newborn Infant. 1991. Ph.D. Thesis, University College London.

Cubeddu, R., A. Pifferi, P. Taroni, A. Torricelli, and G. Valentini. 1999. Compact tissue oximeter based on dual-wavelength multichannel time-resolved reflectance. *Applied Optics* 38:3670-3680.

De Blasi, R.A., N. Almenrader, P. Aurisicchio, and M. Ferrari. 1997. Comparison of two methods of measuring forearm oxygen consumption (VO_2) by near infrared spectroscopy. *Journal of Biomedical Optics* 2:171-175.

Deiber, M.P., R.E. Passingham, J.G. Colebatch, K.J. Friston, P.D. Nixon, and R.S. Frackowiak. 1991. Cortical areas and the selection of movement: a study with positron emission tomography. *Exp.Brain Res.* 84:393-402.

Delpy, D.T., M. Cope, P. van der Zee, S.R. Arridge, S. Wray, and J.S. Wyatt. 1988. Estimation of optical pathlength through tissue from direct time of flight measurement. *Phys.Med.biol.* 33:1433-1442.

Du Plessis, P.A. 1995. Near-infrared spectroscopy for the in vivo study of cerebral hemodynamics and oxygenation. *Curr.Opin.Pediatr.* 7:632-639.

Duderstadt, J.J. and L.J. Hamilton. 1976. Nuclear Reactor Analysis. John Wiley & Sons, New York.

Fantini, S., M.A. Franceschini, J.S. Maier, and S.A. Walker. 1995. Frequency-domain multichannel optical detector for noninvasive tissue spectroscopy and oximetry. *Optical Engineering* 34:32-42.

Farrell, T.J., M.S. Patterson, and B.C. Wilson. 1992. A diffusion theory model of spatially resolved, steady-state diffuse reflectance for the non-invasive determination of tissue optical properties *in vivo*. *Medical Physics* 19:879-888.

Farrell, T.J., M.S. Patterson, and M. Essenpreis. 1998. Influence of layered tissue architecture on estimates of tissue optical properties obtained from spatially resolved diffuse reflectometry. *Applied Optics* 37:1958-1972.

Ferrari, M., R.A. De Blasi, P. Bruscaglioni, M. Barilli, L. Carraresi, M. Gurioli, E. Quaglia, and G. Zaccanti. 1991. Near infrared time-resolved spectroscopy and fast scanning spectrophotometry in ischemic human forearm. *Proc Soc Photo-Opt Instrum* 1431:276-283.

Ferrari, M., Q. Wei, L. Carraresi, R.A. De Blasi, and G. Zaccanti. 1992. Time-resolved spectroscopy of the human forearm. *J.Photochem.Photobiol.B: Biol.* 16:141-153.

Franceschini, M. A., Paunescu, A., Fantini, S., Pratesi, S., Maier, J. S., Donzelli, G. P., and Gratton, E. 1998. Frequency-Domain Optical Measurements *in vitro* on Two- and Three- Layered Tissue-Like phantoms, and *in vivo* on Infant Heads. 1998. *Optical Society of America. Technical Digest: Advances in Optical Imaging and Photon Migration.* 15-17.

Gray, L.H., A.D. Conger, M. Ebert, S. Hornsey, and O.C.A. Scott. 1953. The concentration of oxygen dissolved in tissues at the time of irradiation as a factor in radiotherapy. *Br .J.Radiol* 26:638-648.

Hale, G.M. and M.R. Querry. 1973. Optical Constants of Water in the 200-nm to 200-μm Wavelength Region. *Applied Optics* 12:555-563.

Hall, E.J. 1988. The Oxygen Effect and Reoxygenation. In Radiobiology for the Radiologist. S.M. Gay and S. Robinson, editors. J.B. Lippincott Co., Philadelphia. 137-160.

Haskell, R.C., L.O. Svaasand, T. Tsay, T. Feng, M.C. McAdams, and B.J. Tromberg. 1994. Boundary conditions for the diffusion equation in radiative transfer. *Journal of the Optical Society of America A* 11:2727-2741.

Henderson, B.W. and T.J. Dougherty. 1992. How does photodynamic therapy work? *Photochem.Photobiol.* 55:145-157.

Hicks, A., S. McGill, and R.L. Hughson. 1999. Tissue oxygenation by near-infrared spectroscopy and muscle blood flow during isometric contractions of the forearm. *Can.J.Appl.Physiol.* 24:216-230.

Hielscher, A.H., H.L. Liu, B. Chance, F.K. Tittel, and S.L. Jacques. 1996. Time-resolved photon emission from layered turbid media. *Applied Optics* 35:719-728.

Hirth, C., H. Obrig, J. Valdueza, U. Dirnagl, and A. Villringer. 1997. Simultaneous assessment of cerebral oxygenation and hemodynamics during a motor task. A combined near infrared and transcranial Doppler sonography study. *Adv.Exp.Med.Biol.* 411:461-9.:461-469.

Homma, S., T. Fukunaga, and A. Kagaya. 1996. Influence of adipose tissue thickness on near-infrared spectrascopic signals in the measurement of human muscle. *J.Biomed.Opt.* 1:418-424.

Hull, E.L., M.G. Nichols, and T.H. Foster. 1998. Quantitative broadband near-infrared spectroscopy of tissue-simulating phantoms containing erythrocytes. *Phys.Med.biol.* 43:3381-3404.

Hull, E.L., D.L. Conover, and T.H. Foster. 1999. Carbogen-induced changes in rat mammary tumor oxygenation reported by near-infrared spectroscopy. *Br.J.Cancer* 79:1709-1716.

Hunter, R. J. Dual wavelength time resolved reflectance measurements for the determination of hemoglobin oxygenation in tissue. 1998. M.Sc. Thesis, McMaster University.

Hyde, D.E., T.J. Farrell, M.S. Patterson, and B.C. Wilson. 2001. A diffusion theory model of spatially resolved fluorescence from depth-dependent fluorophore concentrations. *Phys.Med.Biol.* 46:383

Isobe, K., T. Kusaka, Y. Fujikawa, M. Kondo, K. Kawada, S. Yasuda, S. Itoh, K. Hirao, and S. Onishi. 2000. Changes in cerebral hemoglobin concentration and oxygen saturation immediately after birth in the human neonate using full-spectrum near infrared spectroscopy. *Journal of Biomedical Optics* 5:283-286.

Jacques, S.L. and S.T. Flock. 1991. Effect of surface boundary on time-resolved reflectance: measurements with a prototype endoscopic catheter. *Proc.Soc.Photo-Opt.Instrum.Eng.* 1431:12-20.

Jobsis, F.F. 1977. Non-invasive infra-red monitoring of cerebral and myocardial oxygen sufficiency and circulating parameters. *Science* 198:1264-1267.

Kienle, A. and R. Hibst. 1995. New optical wavelength for treatment of portwine stains? *Phys.Med.biol.* 40:1559-1576.

Kienle, A. and M.S. Patterson. 1997. Improved solutions of the steady-state and time-resolved diffusion equations for reflectance from a semi-infinite turbid medium. *Journal of the Optical Society of America* 14:246-254.

Kienle, A., M.S. Patterson, N. Dognitz-Utke, R. Bays, G. Wagnieres, and H. van den Bergh. 1998. Noninvasive determination of the optical properties of two-layered turbid media. *Applied Optics* 37:779-791.

Kienle, A. and T. Glanzmann. 1999. In vivo determination of the optical properties of muscle with time-resolved reflectance using a layered model. *Phys.Med.biol.* 44:2689-2702.

Levy, W.J., S. Levin, and B. Chance. 1995. Near-infrared measurement of cerebral oxygenation. *Anesthesiology* 83:738-746.

Liu, H., D.A. Boas, Y. Zhang, A.G. Yodh, and B. Chance. 1995a. Determination of optical Properties and blood oxygenation in tissue using continuous NIR light. *Phys.Med.biol.* 40:1983-1993.

Liu, H., B. Chance, A.H. Hielscher, S.L. Jacques, and F.K. Tittel. 1995b. Influence of blood vessels on the measurement of hemoglobin oxygenation as determined by time-resolved reflectance spectroscopy. *Medical Physics* 22:1209-1217.

Liu, H.L., Y. Song, K.L. Worden, H. Jiang, A. Constantinescu, and R.P. Mason. 2000. Noninvasive investigation of blood oxygenation dynamics of tumors by near-infrared spectroscopy. *Applied Optics* 39:5231-5243.

Madsen, S.J., M.S. Patterson, and B.C. Wilson. 1992. The use of India ink as an optical absorber in tissue-simulating phantoms. *Phys.Med.biol.* 37:985-993.

Matcher, S.J. and C.E. Cooper. 1994. Absolute quantification of deoxyhaemoglobin concentraion in tissue near infrared spectroscopy. *Phys.Med.biol.* 39:1295-1312.

McBride, T.O., B.W. Pogue, E.D. Gerety, S.B. Poplack, U.L. Osterberg, and K.D. Paulsen. 2001. Spectroscopic diffuse optical tomography for the quantitative assessment of hemoglobin concentration and oxygen saturation in breast tissue. *Applied Optics* 38:5480-5490.

McCully, K.K. and T. Hamaoka. 2000. Near-infrared spectroscopy: what can it tell us about oxygen saturation in skeletal muscle? *Exerc.Sport.Sci.Rev.* 28:123-127.

McCully, K.K., C. Halber, and J.D. Posner. 1994. Exercise-induced changes in oxygen saturation in the calf muscles of elderly subjects with peripheral vascular disease. *J.Gerontol.* 49:B128-B134

McCully, K.K., L. Landsberg, M. Suarez, M. Hofmann, and J.D. Posner. 1997. Identification of peripheral vascular disease in elderly subjects using optical spectroscopy. *J.Gerontol.A.Biol.Sci.Med.Sci.* 52:B159-B165

Meek, J.H., M. Firbank, C.E. Elwell, J. Atkinson, O. Braddick, and J.S. Wyatt. 1998. Regional hemodynamic responses to visual stimulation in awake infants. *Pediatr.Res.* 43:840-843.

Mosca, F.A., M. Colnaghi, M. Lattanzio, M. Bray, S. Pugliese, and M. Fumagalli. 1997. Closed versus open endotracheal suctioning in preterm infants: effects on cerebral oxygenation and blood volume. *Biol.Neonate.* 72:9-14.

Nioka, S., Rosenthal, D., Ma, H. Y., and Chance, B. 2000. The effect of radiation on oxygen concentration in metastatic cancer. *Optical Society of America. Technical Digest: Advances in Optical Imaging and Photon Migration*, 292-293.

Niwayama, M., L. Lin, J. Shao, T. Shiga, N. Kudo, and K. Yamamoto. 2000. Quantitative measurement of muscle oxygenation by NIRS: Analysis of the influence of a subcutaneous fat layer and skin. *Proc.SPIE* 3597:291-298.

Nossal, R., J. Kiefer, G.H. Weiss, R.F. Bonner, H. Taitelbaum, and S. Havlin. 1988. Photon migration in layered turbid media. *Applied Optics* 27:3382-3391.

Ntziachristos, V., Ma, X. H., Schnall, M., Yodh, A. G., and Chance, B. 1998. Concurrent multi-channel time-resolved NIR with MR mammography: Instrumentation and initial clinical results. *Optical Society of America. Technical Digest: Advances in Optical Imaging and Photon Migration.* 143-145.

O'Connor, D.V. and D. Phillips. 1984. Time-correlated Single Photon Counting. Academic Press, London.

Obrig, H., C. Hirth, J.G. Junge-Hulsing, C. Doge, R. Wenzel, T. Wolf, U. Dirnagl, and A. Villringer. 1997. Length of resting period between stimulation cycles modulates hemodynamic response to a motor stimulus. *Adv.Exp.Med.Biol.* 411:471-80.:471-480.

Patterson, M.S., B. Chance, and B.C. Wilson. 1989. Time resolved reflectance and transmittance for the non-invasive measurement of tissue optical properties. *Applied Optics* 28:2331-2336.

Patterson, M.S., J.D. Moulton, B.C. Wilson, K.W. Berndt, and J.R. Lakowicz. 1991. Frequency-domain reflectance for the determination of the scattering and absorption properties of tissue. *Applied Optics* 30:4474-4476.

Peebles, D.M., J.A. Spencer, A.D. Edwards, J.S. Wyatt, E.O. Reynolds, M. Cope, and D.T. Delpy. 1994. Relation between frequency of uterine contractions and human fetal cerebral oxygen saturation studied during labour by near infrared spectroscopy. *Br.J.Obstet.Gynaecol.* 101:44-48.

Pham, T., T. Spott, L.O. Svaasand, and B.J. Tromberg. 2000. Quantifying the properties of two-layer turbid media with frequency-domain diffuse reflectance. *Applied Optics* 39:4733-4745.

Pogue, B. W., Testorf, M., Osterberg, U. L., and Paulsen, K. D. 1998. Quantitative imagingin frequency-domain diffuse optical tomography for breast cancer detection. *Optical Society of America. Technical Digest: Advances in Optical Imaging and Photon Migration.* 110-112.

Pogue, B.W., K.D. Paulsen, C. Abele, and H. Kaufman. 2000. Calibration of near-infrared frequency-domain tissue spectroscopy for absolute absorption coefficient quantitation in neonatal head-simulating phantoms. *Journal of Biomedical Optics* 5:185-193.

Robertson, C.S. and B. Chance. 1997. Use of near infrared spectroscopy to identify traumatic intracranial hematomas.. *Journal of Biomedical Optics* 2:31-41.

Sahlin, K. 1992. Non-invasive measurements of O_2 availability in human skeletal muscle with near-infrared spectroscopy. *Int.J.Sports.Med.* 13:S157-S160

SPIE Proceedings. *Optical Tomography and Spectroscopy of Tissue IV.* 4520. 2001.

Steinbrink, J., H. Wabnitz, H. Obrig, A. Villringer, and H. Rinneberg. 2001. Determining changes in NIR absorption using a layered model of the human head. *Phy.Med.Biol.* 46:879-896.

Stryer, L. 1995. Biochemistry. W. H. Freeman and Company, New York.

Szmedra, L., J. Im, S. Nioka, B. Chance, and K.W. Rundell. 2000. Hemoglobin /myoglobin oxygen desaturation during Alpine skiing. *Med.Sci.SportsExerc. 232*:232-236.

TOPS Conference Proceedings. *Advances in Optical Imaging and Photon Migration.* 21. 1998.

Toronov, V., M.A. Franceschini, M. Filiaci, S. Fantini, M. Wolf, A. Michalos, and E. Gratton. 2001. Near-infrared study of fluctuations in cerebral hemodynamics during rest and motor stimulation: temporal analysis and spatial mapping. *Medical Physics* 27:801-815.

van de Hulst, H.C. 1980. Light Scattering by Small Particles. Dover, New York.

van Staveren, H.J., C.J.M. Moes, J. van Marle, S.A. Prahl, and M.J.C. van Gemert. 1991. Light scattering in Intralipid-10% in the wavelength range of 400-1100 nm. *Applied Optics* 30:4507-4514.

Villringer, A. and B. Chance. 1997. Non-invasive optical spectroscopy and imaging of human brain function. *Trends.Neurosci.* 20:435-442.

Wray, S., M. Cope, D.T. Delpy, J.S. Wyatt, and E.O. Reynolds. 1988. Characterization of the near-infrared absorption spectraof cytochrome aa_3 and haemoglobin for the non-invasive monitoring of cerebral oxygenation. *Biochimica et Biophysica Acta* 933:184-192.

Yang, Y., H. Liu, X. Li, and B. Chance. 1997. Low-cost frequency-domain photon migration instrument for tissue spectroscopy, oximetry and imaging. *Optical Engineering* 36:1562-1569.

Zwart, A., G. Kwant, B. Oeseburg, and W.G. Zijlstra. 1984. Human whole-blood oxygen affinity: effect of temperature. *Journal of Applied Physiol.* 57:429-434.